INTRAVASCULAR LASER INDUCED CAVITATION: A STUDY OF THE MECHANICS WITH POSSIBLE DETRIMENTAL AND BENEFICIAL EFFECTS.

By

Ralph de la Torre

Harvard-M.I.T. Division Of Health Sciences and Technology

Submitted in partial fulfillment of the Requirements for the M.D. Degree and in partial fulfillment of the Requirements for the Sc.M. Degree

February, 1992

Area of Concentration: Cardiovascular/Renal/Respiratory
Project Advisor: R. Rox Anderson
Prior Degrees: B.S.E. (Biomedical Engineering)

I have reviewed this thesis. It represents work done by the author under my guidance/supervision.

Thesis Advisor

PREFACE

The Harvard-MIT Division of Health Sciences and Technology was created over fifteen years ago to educate physicians and scientists alike. Their goal was to achieve a better avenue of communication between these two often divided fields. They seek to train the scientist with an understanding of medicine and medical needs as well as to train the physician with an understanding of science and the scientific method.

It was with these goals that I enrolled in the Division of Health Science and Technology four years ago and began pursuing both research interests and scholastic training. It is the incorporation of science and medicine that forms the substance to this research. It seeks to explore the science behind a medically relevant problem and then to incorporate this understanding into both the development of a new medical device as well as the modification of an existing one.

Many people have significantly contributed to this work as well as to the development of my career. I wish to thank Dr. Kenton Gregory who first brought me to Wellman labs; he was not only the initial impetus and guide behind my research, he was also my friend. I also wish to thank Dr. R. Rox Anderson for all the guidance and help he has given me. Five minutes with Rox is worth days of research. I wish to thank Dr. Scott Prahl for teaching me physics and for always being available and willing to help. I would like to finish by thanking Drs. Abelman and Mark, for guiding me and for making HST what it is today. I hope to make you proud as I continue my career.

INTRODUCTION

Andreas Gruntzig's use of percutaneous transluminal coronary angioplasty (PTCA) to treat cardiac ischemia marked a turning point not only in cardiology but in medicine itself.[1] It represented a revolutionary step towards minimally invasive therapeutic modalities, and changed the way physicians and scientists viewed the fragility of the human body. If a balloon could be inflated to over 10 atmospheres of pressure within a fragile coronary artery, what were the therapeutic limits? Following Gruntzig, cardiologists, vascular surgeons, and engineers alike have been searching for other mechanical methods of treating high grade symptomatic stenoses. Various modalities of coupling mechanical energy into plaque removal have been attempted. These include rotoblative devices (such as the Kensey catheter and the Wooley wire), thermal devices (such as the "hot tip" laser, a laser heated device), and an assortment of other tools, such as Simpson's atherectomy catheter.[2] These mechanical devices, however, have been unable to improve upon the outcome seen with PTCA. Compared to PTCA, these devices all appear plaqued with an increased re-stenosis rate, an increased rate of perforation as well as being expensive, difficult to use, and requiring additional training.

As the search for improved methods of mechanically removing plaque progressed, it was inevitable that the use of lasers would be explored. Lasers have been used in medicine almost since the

creation of the ruby laser in the 1960's. They have revolutionized ophthalmology

Theoretically, lasers pose several advantages over more traditional dynamic angioplasty modalities. By controlling the wavelength, pulse length, and delivery mechanism the extent of damage to the arterial wall could be minimized.[3] Hence, restenosis rate, the incidence of dissection, and the incidence of perforation might all be improved. Furthermore, flexible fiber optic delivery systems made the treating total and distal occlusions a theoretical possibility. To this ends, holmium, pulsed dye, carbon dioxide, and ultraviolet pulsed lasers have been used both experimentally and clinically in the treatment of atherosclerosis. Unfortunately, the theoretical advantages offered by these systems have not resulted in clinical successes. Their use has been limited by several factors: cost, difficulty in manipulating delivery systems, no improvement in restenosis rate over conventional PTCA, and an increased risk of perforation. Recent studies have shown the six month restenosis rate following excimer laser angioplasty to be 40-50%, and the risk of perforation, approximately1-2%.[4] Until recently, the lack of flexible but large-lumen laser angioplasty catheters has necessitated the use of adjunct PTCA, further increased the risk of restenosis.

As is often the case, medical trials preceeded controlled scientific investigations. As excimer, holmium, and pulsed dye laser systems entered clinical trials, scientific tissue ablation studies were just begining. Furthermore, despite the fact that all laser angioplasty is currently done with blood completely surrounding both the catheter and the targeted plaque, it was not until recently that laser

light/blood interaction has been investigated. It is this interaction that I wish to address in this work.

When laser light encounters an absorber, energy is deposited within that absorber. If enough energy is deposited within a given volume a phase change occurs. In the case of a liquid absorber this phase change can yield an unstable vapor bubble known as a cavitation bubble. In the past, researchers have often used lasers as a means of creating cavitation bubbles. These bubbles could then be studied without the encumbrances of the device that created them.[5] With the exception of ophthalmologic lasers, the interrelationship between laser parameters, absorbing media, method of delivering the laser light, and the dynamics of the resulting vapor cavities has not been studied.

Laser induced cavitation within medical applications differs somewhat from the vapor bubbles created by Q-switched lasers to study cavitation; laser fiber delivery, inhomogeneous absorption media, and different laser parameters are but some of the confounding factors in the study of cavitation. For example, it is currently not feasible to use pulses shorter than several hundred nanoseconds for laser angioplasty because of damage to the optical delivery fiber. Therefore, pulse durations of a microsecond or longer are used, which means that laser energy continues to be delivered during the early formation of cavitation. This differs greatly from the nanosecond domain pulses used to create cavitation in ophthalmic surgery. Also, with Q-switched laser cavitation, formation of a plasma is the initial event.[6] In this microsecond domain study, thermal excitation and expansion initiates the cavitation event. Furthermore,

blood is an inhomogeneous optical medium, and at wavelengths absorbed by hemoglobin, microsecond domain pulses should cause transient high temperatures in erythrocytes, which may become a nidus for cavitation.

In this work, I explored the impact of various laser parameters and delivery systems have on cavitation within the context of a blood field. Following these studies, an in vivo perforation study was performed. Together, these studies suggest improvements in current laser angioplasty. Furthermore, in the course of this work, it became evident that laser induced cavitation can be used to reverse arterial vasospasm. Hence, in the final section , I show how cavitation can be created in a controlled fashion to potentially treat a devastating malady, cerebral vasospasm; and I will report the results of in vivo animal studies showing the feasability of this treatment.

The first chapter discusses the phenomenon of cavitation, starting with a brief review of cavitation bubble dynamics. Subsequently, the effect varying laser and blood parameters has upon the bubble dynamics is explored.

The second chapter presents experimental data for cavitation in a blood field. In all cases, my study of cavitation is confined to vapor cavities following laser light delivery via fiber optic systems. The first part of the study deals with the effect absorption coefficients have upon cavitation. Then the influence media homogeneity has upon cavitation will be investigated. Here, varying absorption coefficients for whole blood and lysed blood will be investigated with regards to the size of the ensuing cavitation

bubbles. The third section deals with the acoustic transient generated upon bubble collapse and how distance and varying laser systems impacts upon them. I will then explore how pulse length affects cavitation in whole blood and lysed blood. In the fifth section, I will investigate how various multi-fiber delivery systems impact the formation of vapor bubbles and how their shapes affect acoustic transient generation. Also, at the end of this section, I will briefly explore a phenomena linked to but not part of cavitation, that of the initial acoustic transient.

In the third chapter the focus shifts to vascular injury. The relationships between intravascular cavitation, perforation, and intravascular damage are explored. Having made these observations, I offer an analytic viewpoint on how to make the procedure of laser angioplasty safer.

Finally, in the last chapter, I show how cavitation can be used to treat a currently untreatable and often fatal phenomenon. I will describe the development of a new medical device, based on cavitation, which could be in clinical trials in hte near future.

INTRODUCTION: CAVITATION BUBBLE DYNAMICS

The first mention of cavitation came from Sir Isaac Newton in a 1704 paper entitled "Optics". In this work, Newton says:

> "When the water was between the glasses, if I pressed the upper glass variously at its edges to make the rings move nimbly from one place to another, a little white spot would immediately follow the center of them, which upon creeping in of the ambient water into that place would presently vanish."

Newton then goes on to explain:

> "Its appearance was such as interjacent air would have caused, and it exhibited the same colors. But it was not air, for were any bubbles of air were in the water, they would not vanish. The reflection must have rather been caused by a subtiler medium, which could recede through the glasses at the creeping in of the water."[7]

As we now know, this phenomenon was air coming out of solution under the direct action of reduced pressure. Before we continue, it is important to delineate what is meant by the word "bubble" so as to avoid the confusion encountered by Newton himself. We will begin by differentiating bubbles according to their content. One form of bubble, that which contains mostly gas, can expand via several methods: 1) through diffusion of dissolved gas from the liquid into the bubble, 2) through a reduction in pressure outside of the bubble or 3) through a rise in temperature.[8] Another type of bubble containing mostly vapor, can appear when the ambient pressures is reduced sufficiently at constant temperature.

This pressure reduction causes explosive vaporization into cavities, and hence, the traditional definition of "cavitation". In this context, "vapor" describes gas arising from a phase change, whereas "gas" represents an entity in solution. Lauterborn and Young have divided cavitation into four basic groups based on how the cavitation bubbles originated.[9]

The first, hydrodynamic cavitation, is due to pressure variations in a flowing liquid secondary to the geometry of the system. This is a form of cavitation commonly encountered in ship's propellers, in which the low pressure immediately behind the blade creates a bubble which upon collapse pits the blade, a phenomenon that harasses shipping companies and keeps propeller companies forever in business.[10]

The second form of cavitation is acoustic cavitation. In acoustic cavitation the sound waves produce pressure variations which give rise to cavitation bubbles. When the pressure variation is great enough to lower the pressure to or below vapor pressure, cavitation ensues.

Particle cavitation is cavitation produced by an elementary particle, as a proton rupturing in liquid.

The fourth type, which is the focus of this paper, is optical cavitation. This comes from photons of high intensity light rupturing a liquid.

In a scheme presented by Lauterborn, cavitation can be classified as two essentially different phenomena. The first is tension cavitation which is caused via a drop in pressure and includes hydrodynamic and acoustic cavitation. The second is energy

deposition cavitation and includes optical or particle-induced cavitation.

The complex physics of cavitation has perplexed students for many years. Factors which contribute to the complexity are: 1) the unknown ratio of gas and condensable vapor in the cavity; 2) the energy losses involved are difficult to monitor. These include, heat conduction, viscosity, compressibility, surface tension, mass transfer, diffusion, and temperature discontinuity at the phase interface.[8]

For many years, the study of cavitation bubbles was encumbered by the devices and the geometries involved in their creation. It was not until the advent of lasers that empirical studies could effectively measure the creation and collapse of cavitation bubbles. Work by Lauterborn, Vogel and others proceeded to this end. Much of this work has actually come to support early cavitation dynamics theory.

LASER LIGHT DEPOSITION

As light passes through a material with absorption coefficient, μ_a, parallel energy is deposited according to Beer's law, given as:

$$E(x) = E_0 e^{-\mu_a x} \qquad \text{Equation 1.1}$$

E(x) = the total energy remaining
x= distancelight has travelled within the absorber
μ_a= the absorption coefficient of the material

This energy can then meet one of two fates. If the energy deposited within a given volume is sufficient, a phase change ensues. If the deposited energy is not sufficient, then heat dissipation occurs

through convection, conduction, and radiation, with radiation playing a larger role in small mechanistic length scales. In this analysis photochemical effects will be neglected. This is supported by the scarcity of photochemical interactions at the wavelengths being investigated (λ>300 nm). We will now confine our discussion to a liquid absorber in which the deposited energy is sufficient to cause a phase change.

Absorbed energy can be modeled according to the simplified equation:

$$E_{pulse} = E_{cavitation} + E_{SW\ /AT} + E_{lost} \qquad \text{Equation 1.2}$$

were the total energy given in a single laser pulse is given by E_{pulse}, the energy contained in a cavitation bubble is given by $E_{cavitation}$, the energy contained in the transmitted shock wave/acoustic transient is given by $E_{SW\ /AT}$, and the energy lost to scattering, thermal dissipation, and other processes is given by E_{lost}. This equation introduces the shock wave/acoustic transient phenomenon which will be treated later. This phenomenon describes transient heating that produces a pressure disturbance propagated at either sonic (acoustic transient) or supersonic (shock wave) velocities. Furthermore, the shock wave exists only in the near field, with the near field for comparable investigations being on the order of 10um.[11] Beyond the near field, the shock wave becomes an acoustic wave. Hence, even in the case of an energy concentration sufficient to produce a shock wave (usually above plasma threshold), these phenomena can be treated as a continuum with the shock wave becoming an acoustic wave.

In equilibrium, the energy contained in a cavitation bubble follows from simple physics:

$$E_{cavitation} = \frac{4}{3}\pi r^3 \Delta P \qquad \text{Equation 1.3}$$

where ΔP is the pressure difference between the vapor in the bubble and the fluid vapor, and r is the bubble radius.[12] Likewise, the energy of an acoustic transient, travelling as a spherical wave, is given as:

$$E_{AT} = \frac{4\pi r^2}{\rho c}\int P^2(t)dt \qquad \text{Equation 1.4}$$

were ρ is the density of the liquid, c is the speed of sound for the given media, r is the distance from the acoustic source, and P(t) is the pressure-time profile.[12] Armed with a rudimentary understanding of how a laser pulse can create a cavitation bubble we will now explore how the dynamics of such a bubble can be modeled.

A SPHERICAL BUBBLE

We will discuss the dynamics of spherical bubble expansion and collapse (independent of the initiating event) using Young's analysis of Besant's equation.[8] Consider an empty spherical bubble that is either expanding or collapsing. If R is the bubble radius and r is a distance from the bubble center, then the velocity of a particle at a distance r from the bubble center be related to the velocity for a bubble radius R by assuming a constant volume expansion with time:

$$\frac{d\left(\frac{4}{3}\pi r^3\right)}{dt} = \frac{d\left(\frac{4}{3}\pi R^3\right)}{dt}$$

$$r^2 \frac{dr}{dt} = R^2 \frac{dR}{dt} \quad \text{and hence } \dot{r} = \frac{R^2 \dot{R}}{r^2}$$

and the velocity potential, u, is :

$$u = -\int_r^{\infty} \dot{r} dr = \frac{\dot{R} R^2}{r}$$

This analysis assumes: 1) the cavity is purely spherical, 2) the fluid is incompressible, 3)motion is irrotational, and 4) constant volume increase with time. The first two assumptions are only approximately valid and will be corrected for later.

We can now use the Bernoulli equation to derive a relation between wall velocity and the liquid pressure. Let $P_l(t)$ be the pressure in the fluid just beyond the interface of the wall and P_∞ be the pressure at an infinite distance. In an open liquid system P_∞ is equal to the atmospheric pressure, hence the simplification P_∞=0.

$$\frac{P_l - P_\infty}{\rho} + \frac{\partial u}{\partial t} + \frac{1}{u^2} = 0$$

$$\frac{P_l - P_\infty}{\rho} = \frac{2RR'^2 + R^2 R''}{r} + \frac{R^4 R'^2}{2r^4}$$

If we wish to follow the motion of the wall we set r=R,

$$\frac{P_l(t)}{\rho} = R\ddot{R} + \frac{3}{2}\dot{R}^2 \qquad \text{Equation 1.5}$$

This equation, first mentioned by Besant in 1859, is called by Young the fundamental equation of bubble dynamics. The same relation is obtained using conservation of energy and neglecting viscous and surface tension effects. This equation, however, is inappropriate for high velocity bubble wall expansion because the assumption of an incompressible liquid surrounding the bubble does not hold. Flynn relaxed the incompressability constraint by considering a constant sound velocity in the medium.[13] With this assumption it follows that:

$$\frac{\partial P}{\partial \rho} = c^2$$

c= velocity of sound in the medium
ρ= density of the liquid

The fundamental equation of bubble dynamics becomes:

$$R\ddot{R} + \frac{3}{2}\dot{R}^2 = \frac{1}{\rho}\left[P_L + \frac{R}{c}\left(1 - \frac{\dot{R}}{c}\right)\dot{P}_L - P_\infty\right] \quad \text{Equation 1.6}$$

This equation, first derived by Flynn, assumes: 1) the wall velocity is significantly smaller than the velocity of sound, and 2) the cavity is empty and not filled by a gas. Treating the liquid as compressible is important especially in the final stages of collapse, as the velocity of the wall increases. In underwater explosions the cavity will grow rapidly until its pressure equals that of the surrounding water. At this stage, the growth continues due to the inertia of the expanding bubble. Upon collapse, an incompressibile fluid theory predicts an oscillating cavity of constant frequency and amplitude. In treating the fluid as compressible in the terminal stages of collapse, Keller and Kolodner have shown mathematically a resulting damped

oscillation is expected.[8] We will now shift our focus to the collapse of a spherical cavity that has grown to a given dimension. The equations of bubble dynamics explained above will be used in the next section to explore the dynamics of a collapsing bubble. For us, this phenomena takes on increased significance for various reasons. First of all, the damped oscillations seen in the experiments that follow will be explained using the Rayleigh analysis detailed below. Furthermore, the analysis will be used to calculate and subsequently predict bubble diameters.

RAYLEIGH AND THE COLLAPSING CAVITY

We will now use these equations of bubble dynamics to explore the dynamics of a collapsing bubble. These dynamics are important since the Rayleigh analysis detailed below will be used to calculate and predict maximum bubble diameters.[14,8]

If we let R be the radius of the bubble at time t and r be a radial distance from the center, then, by assuming continuity:

$$\dot{r}r^2 = \dot{R}R^2$$

The kinetic energy of the liquid with a density, ρ, can then be given by:

$$KE = \frac{1}{2}mu^2 = \frac{1}{2}\rho\int_R^\infty 4\pi r^2\dot{r}^2 dr$$

m= mass of fluid displaced
u= velocity of fluid

Whose solution can be found as follows:

$$= 2\pi\rho \int_{R}^{\infty} r^2 \dot{r}^2 dr$$

$$2\pi\rho \left| \frac{-R^4 \dot{R}^2}{r} \right|_{R}^{\infty} = 2\pi\rho \dot{R}^2 R^3$$

Using conservation of energy and setting the kinetic energy solution found above equal to the work done by hydrostatic pressure, we generate a description of the bubble dynamics for the collapse phase of the cavity:

$$\frac{4}{3}\pi P_{R\max}\left(R^3_{\max} - R^3\right) = 2\pi\rho \dot{R}^2 R^3 \qquad \text{Equation 1.7}$$

R= radius of the bubble
$P_{R\max}$= pressure inside the cavity at maximum radius
$R_{\max}$= maximum cavity radius

Simplifying:

$$\dot{R}^2 = \frac{2P_{R\max}}{3\rho}\left(\frac{R^3_{\max}}{R^3} - 1\right)$$

Therefore:

$$dt = dR\left(\frac{3\rho R^3}{2P_{R\max}\left(R^3_{\max} - R^3\right)}\right)^{\frac{1}{2}}$$

This derivation assumes both isothermal compression as well as an incompressible fluid surrounding the cavity. From here we easily find the time of total collapse(R=0) from the maximum radius:

$$\tau = 0.915 R_{\max}\sqrt{\frac{\rho}{P_{R\max}}} \qquad \text{Equation 1.8}$$

If the cavity is not empty but filled with vapor at the equilibrium pressure, then the Rayleigh equation above becomes:

$$\tau = 0.915 R_{max} \sqrt{\frac{\rho}{P_{R\max} - P_{V.R\max}}} \qquad \text{Equation 1.9}$$

$P_{V.R\max}$= vapor pressure at equilibrium, ie at maximum radius

This equation 1.9 will be used to calculate the maximum radius based upon the cycle time. Before relying on this equation, we will attempt to assess the validity of our assumption of an incompressable liquid.

As a cavity begins to collapse, an area of increasingly high pressure forms just outside the bubble wall. As the collapse continues, the area of high pressure moves closer to the bubble wall, increases in magnitude, and decreases in thickness. Eventually, near the end of the collapse phase, the bubble is surrounded by a very thin shell of very high pressure fluid. Rayleigh and Neppiras used conservation of momentum to estimate how the pressure of this thin layer varies during collapse. Numerical solutions as calculated by Neppiras are given below in figure I.1(from Young, Cavitation). The maximum pressure can be calculated, according to this model :

$$P_{MAXIMUM} = 4^{\frac{-4}{3}} \left(\frac{R_{MAX}}{R} \right)^3 P_0 \qquad \text{Equation 1.10}$$

$P_{MAXIMUM}$= maximum pressure in the thin shell outside the wall

P_0= initial pressure

Furthermore, the peak pressure exists at a distance $4^{\frac{1}{3}}R$ from the wall of the bubble. It is this thin layer of high pressure fluid that

serves as the source of a propagated acoustic transient. We will later use this acoustic transient to detect the collapse of a cavitation bubble.

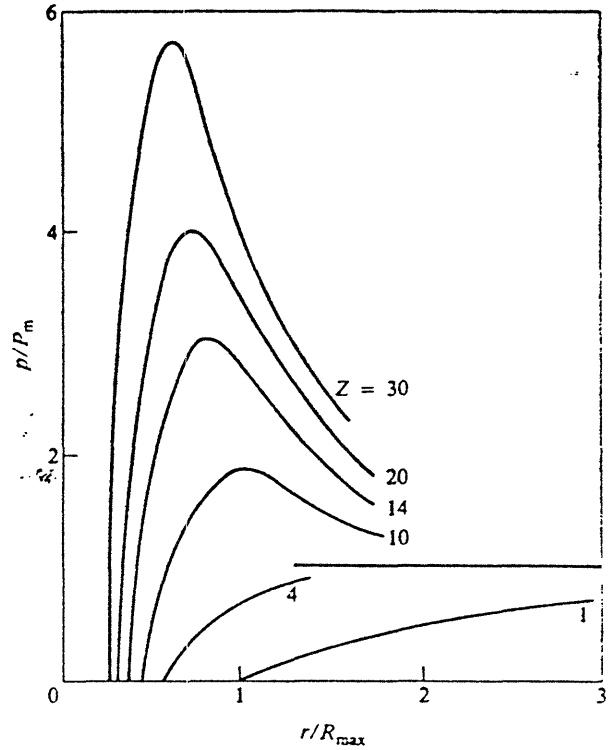

Pressure developed in the liquid surrrounding a cavity. Z is the volume compression ration. (From Young, ref 8).

The approximation derived above is based on an incompressible fluid model. This is not the case during the terminal stages of a bubble's collapse, as the wall velocity increases and approachs the speed of sound. Several models of cavitation dynamics have incorporated a compressible fluid media. One such model, the Herring-Trilling model, simply assumes a constant sound velocity and a constant ambient pressure. In this model for the wall velocity:

$$\dot{R}^2 = \frac{2P_0}{3\rho}\left[\left(\frac{R_{MAX}}{R}\right)^3 - 1\right]\left(1 - \frac{4\dot{R}}{3c}\right)^{-1} \qquad \text{Equation 1.11}$$

c= speed of sound in the liquid medium

As $\dot{R}/c$ approaches zero in this model, Rayleigh's solution is obtained. In figure I.2 below (from Young, Cavitation) a comparison of cavity wall velocities for the models described above, as well as the Gilmore model (which also allows a compressible liquid), is made to experimentally derived velocities. As one can see, there is little difference in predicted velocity except in the final stages of collapse, after $\frac{R_{MAX}}{R}$=0.01. Since this represent less than 1% of the total collapse time the Rayleigh equations derived above should yield adequate values for the maximum radii calculated using collapse time.

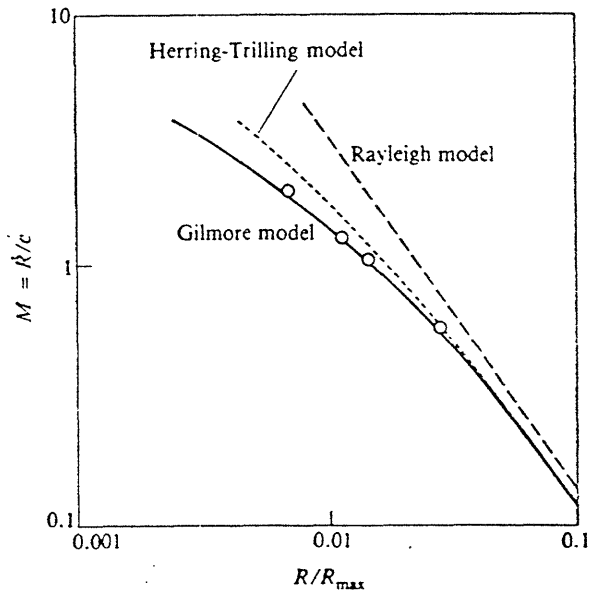

Figure 2. Cavitation bubble wall velocity for various models as the radius approaches zero. From Young, Cavitation.

CHARACTERIZATION OF LASER-INDUCED CAVITATION

I will now set out to characterize laser-induced cavitation for parameters applicable to intravascular lasers. This does not include a detailed investigation of cavitation bubble/vessel wall interaction; although this subject is touched upon in this work, a detailed investigation is beyond the scope of this thesis. Instead, the primary intent of this chapter is to describe laser induced cavitation within a blood field.

As reviewed in the introduction, cavitation is a well studied phenomenon. Recently, pulsed lasers have made the study of cavitation much simpler. They have provided a way to initiate cavitation without mechanically infringing upon the bubble's environment. These studies have been done by tightly focusing a short pulse laser beam within a homogeneous transparent medium, with a laser induced plasma initiating the cavitation.[6] This set up, while providing great insight into cavitation mechanics, has done little to elucidate how various laser parameters and characteristics affect the creation of cavitation within specific medical applications, especially when a plasma is not induced.

My studies of cavitation are confined to vapor cavities forward using laser light delivered via a fiber optic system. The first part of the study deals with the effect of absorption coefficients upon cavitation. This relationship bears great significance not only because of the varying wavelengths used clinically but also because of the varying hematocrits which may be encountered.

The influence of media homogeneity upon cavitation was investigated next. Whole blood is a heterogeneous absorber in which

red blood cells are suspended in plasma, and lysed blood as a homogeneous absorber with hemoglobin distributed throughout the plasma.

The third section deals with the acoustic transients generated by cavity collapse, and how distance, prior bubble dynamics, and laser pulse parameters affect these acoustic transients.

The fourth part explores how pulse length affects the cavitation process in whole blood and lysed blood. Finally, I investigated how multi-fiber versus single fiber delivery systems affect the formation of vapor bubbles, and how different bubble shapes alter acoustic transient generation. These studies are presented below.

I. Effects of absorption coefficient (μ_a) upon the relationship between laser energy and bubble diameter.

Methods

The experimental set up described below is the foundation for all experimentally derived results in this chapter. All modifications to the apparatus or protocol are delineated in the specific sections that follow.

A. Lasers:

A Candela one microsecond pulsed dye laser operating at a wavelength of 480 nanometer (using coumarin dye) and an Advanced Interventions Systems (AIS) excimer laser with a pulse length of 0.2 microseconds and an output wavelength of 308 nanometers (Xenon/Chloride) were used to generate laser pulses of varying energy. These pulses were then focused into a solid silica fiber with a diameter of 320 micron. The distal tip of the fiber consisted of a flat, fire polished

finish possessing no convergent or divergent properties. The output of this system was calibrated prior to and immediately after all measurements using a Scientech 320 power meter.

B. Hydrophone Measurements

The laser fiber was inserted into a Styrofoam cube measuring 15 cm on side (see figure 1). A needle hydrophone, mounted on a Micronta XYZ stage with 0.03 mm resolution, was placed with its face perpendicular to the acoustic transient. Three hydrophones were used to measure the generated acoustic transients. A Whilst Medsonics hydrophone was used in many of the measurements involving cycle time, but due to its slow rise time and inconvenient harmonics, was not used to measure the acoustic transient itself. All measurements of the acoustic transients as well as many cycle time measurements were done using either one of two Imotec PVDF piezoelectric needle hydrophone with rise times of 50 - 70 nanoseconds and a sensitivity of 0.250 pC/bar and 0.310 pC/bar, respectively. Transducer capacitances and impedances were 241pF and 238pF and >100Mohm. Hydrophone outputs were measured using either a LeCroy 7435 180MHz oscilloscope or a Tektronix DSA 602A oscilloscope triggered with a photodiode located within the laser cavity.

For each cavitation event, at least two acoustic transients were measured, one on generation of the cavitation event and one generated upon cavity collapse. Several measurements displayed the multiple acoustic transient patterns seen with an oscillating bubble. The cavity's lifetime was therefore measured as the time between two successive acoustic peaks; this was defined as the cycle time. The collapse time was

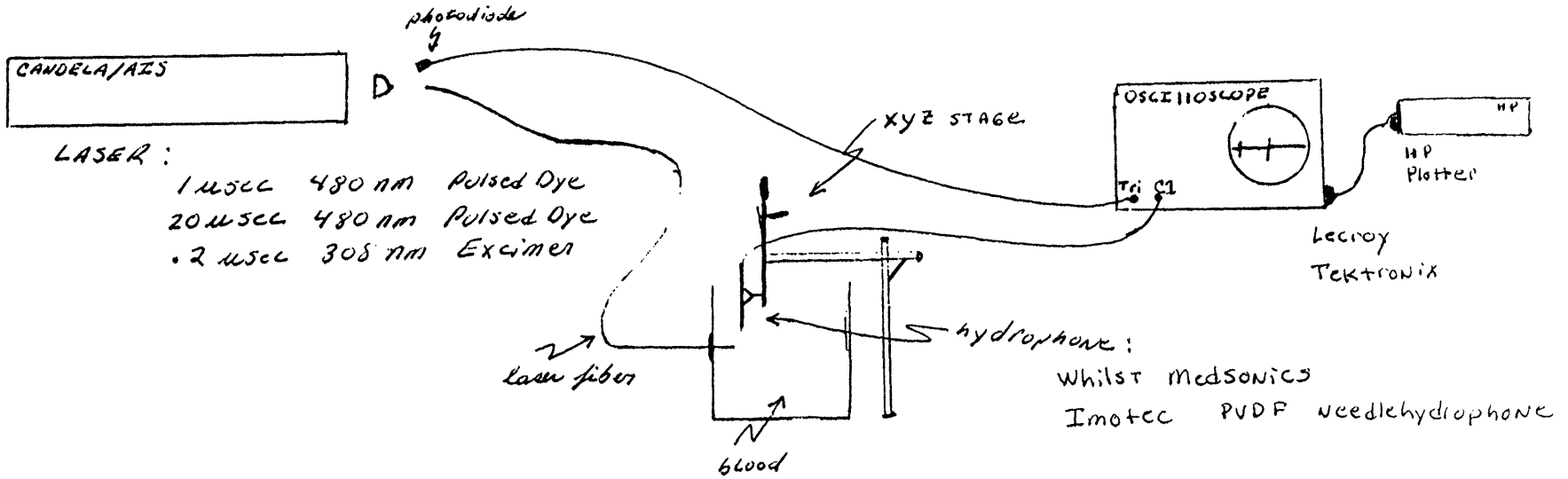

Figure 1. Apparatus used for detection of cavitation cycle time and acoustic transients.

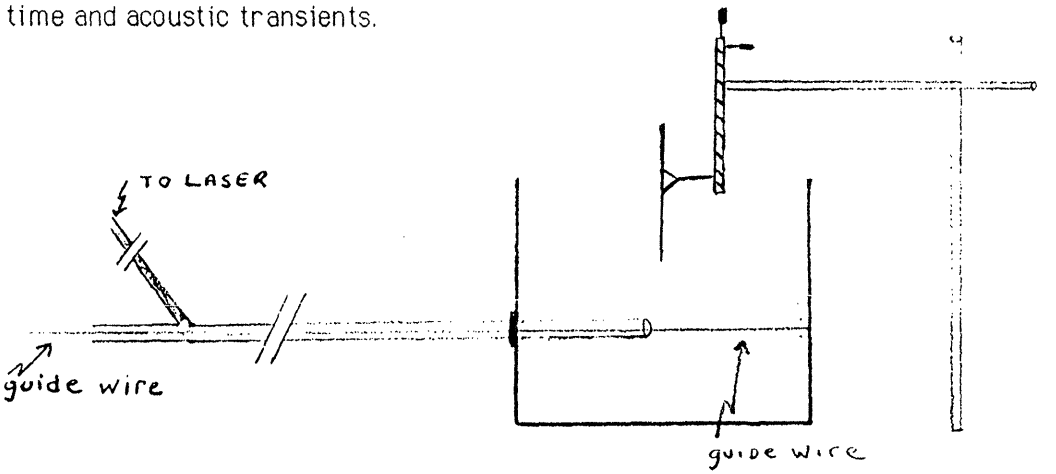

Figure 2. Set up for multi-fiber system placement. Guidewire is pulled taut and catheter passed over the wire to a midpoint in the apparatus.

defined as 2/5 of the cycle time, based on the calculations outlined above. Bubble diameters were calculated using the Rayleigh equation derived in the introduction (eq 1.7).

C. Blood

Outdated, heparinized human whole blood, of any blood type, obtained from the Massachusetts General Hospital Blood Bank was used. The blood was placed within the apparatus and intermittently stirred. Hematocrit (Hct) and hemoglobin (Hgb) were measured.

Pulse energies of 5, 10, 15, 20, 30 and sometimes 40, and 50 mJ/ pulse were used to create cavitation bubbles. Three to five measurements were made at each energy. The cycle time was determined from the oscilloscope trace and bubble radius calculated. Three separate absorption coefficients (132, 62.5, and 31 cm^{-1}) were obtained by diluting the whole blood with saline. One absorption coefficient was obtained for the excimer system (250 cm^{-1}). Hematocrit and hemoglobin were measured after each dilution. A plot of absorption coefficient as a function of wavelength and Hct is given in the appendix.

Results & Discussion

The effect of the absorption coefficient on the relationship between pulse energy and maximum cavitation bubble radius is shown in figure 3. The radius of the bubble obeys an approximate relationship with the cube root of the laser pulse energy (log plot given in figure 4). This relationship is expected since the energy stored by a cavity varies

with its maximum volume, and hence the cube of its maximum radius (equation 1.2 above). This relation, however, is not valid at lower energy levels when the delivered laser energy is significantly different from the energy in the cavity. As shown in equation 1.1, the delivered laser energy has three possible destinations: the formation of an acoustic transient (AT); the formation of a vapor cavity; and "insensible" other losses, e.g. thermal. Only when the energy going into cavity formation is approximately equal to the pulse energy does equation 1.2 hold, ie:

$$E_{LASER} \cong E_{CAVITATION} >> E_{AT} + E_{INSENSIBLE}$$

At lower energy levels, a greater proportion of the pulse energy is lost to heating prior to vaporization. In this simplified model, this energy does not contribute directly to the acoustic transient or the bubble formation and is classified as insensible. Interestingly, the theoretical threshold thermal excitation, the minimum amount of energy/unit volume required for cavitation is approximately 300 J/cc, with the majority of energy going to raising the temperature from 20° Celsius, room temperature, to 100° Celsius. The empirically determined threshold of 2.0 mJ with an absorption coefficient of $130 cm^{-1}$, however, translates to a deposited energy density of approximately 260 J/cc . Therefore, virtually all of the threshold energy goes into raising the liquid to the point of vaporization. Why the threshold energy for cavitation is slightly less than that needed to bring the fluid up to the point of vaporization at 1 atmosphere pressure is explained below.

As shown in figure 3, the threshold energy increases with decreases in absorption coefficient. Although expected, the threshold

energies increase much less than expected in the case of whole blood (a heterogeneous absorber). Decreasing the absorption coefficient from 135 to 62.5 to 31 cm^{-1} increased the threshold energy rise of less than 1 mJ, respectively. If the heat of vaporization and the specific heat are constant, the threshold energy should vary with absorption coefficient as follows:

$$\Phi_v = E_{th}\mu_a = \Delta T \rho c + H_v \qquad \text{Equation 2.1}$$

Φ_v = energy per unit volume necessary to vaporize a media (J/cc)
E_{th} = the threshold fluence (J/cm^2)
μ_a = absorption coefficient (cm^{-1})
ΔT= phase transition temperature-initial temperature
ρc= specific heat capacity
H_v= heat of vaporization

Hence the threshold energy should increase proportionally for a given decrease in absorption coefficient. However, empirically, variations in absorption coefficient have a small effect on threshold energy. The discrepancy between expectation and experiment is most likely caused by the heterogeneity of whole blood as an absorbing medium. In essence, erythrocytes are the sites of absorption whereas the absorption coefficient reported for whole blood are average values over a given volume. If a number of finite volumes are taken and their absorption coefficients determined, a distribution of values is obtained. Hence, the absorption coefficient is more accurately described by an average and a distribution. I will employ such a characterization to explain some of the phenomenon observed in this investigation.

Hence, we will begin by defining a volume whose concentration of absorber we will model. The critical volume is defined as the minimum volume that will form a cavitation if the energy necessary for a phase change is deposited. This volume can be estimated from the minimum cavitation bubble dimension measured, a radius of 0.25mm. Using a 1500 fold critical volume increase following a phase change, a liquid volume of $4.4 \times 10^{-5}\ mm^3$, representing a cube 35 um on a side, is calculated. Based on this volume and the heat of vaporization, assumed to be equal to water, we can then calculate the concentration of absorber based upon the measured threshold energy. This calculation for whole blood with a Hct of 44% yields approximately 530 red blood cells per critical volume, corresponding to a Hct of 53% within the critical volume.

We are then left with a distribution of the number of red cells contained in a critical volume. Given that the maximum number of red cells is in a volume depends on the size of the volume, we have as the upper limit of the number of cells:

$$\Psi \to 0, \text{ as } \frac{V_{RBC} * RBC_{V_{critical}}}{V_{critical}} \to 1$$

Ψ= number of critical volumes with a given number of red cells
V_{RBC}= volume of a red blood cell
$RBC_{V_{critical}}$= number of red blood cells in a given critical volume

The most likely number of red cells is given by our average number of red cells in a critical volume, $RBC_{average}$,, as:

$$RBC_{average} = \frac{Hct * V_{critical}}{V_{RBC}}$$

and the distribution given diagramatically:

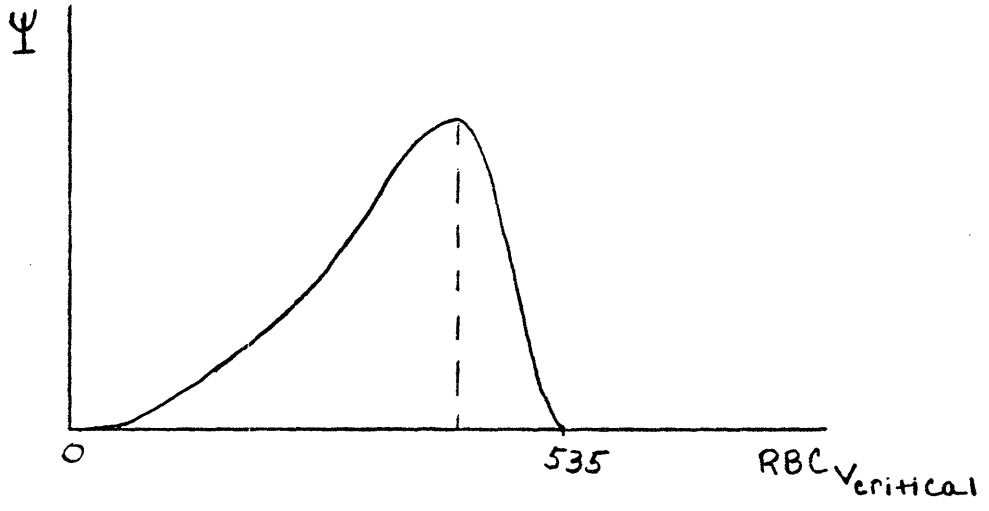

This curve can be used as a probability distribution. Saying a minimum probability must exist for a given concentration to exist then equation 2.1 above is modified:

$$\Phi_v = E_{th}\mu_a(P_{critical})$$

where $\mu_a(P_{critical})$ is the maximum absorption coefficient with a probability of existing greater than the critical probability. Hence, the absorption coefficient, with respect to threshold, is a function of the distribution function. In the case of whole blood with a normal hematocrit, approximately 44%, the intra-red blood cell distance is roughly one cell diameter and the width of the distribution function about the maximum is small. If, however, serial dilutions increase the

intracellular distance the probability function Acquires the shape shown above. Subsequent dilutions not only shift the probability curve but also increases the width about the maximum value. Hence, incident light does not necessarily encounter the average absorption coefficient of the entire volume.

Another unexpected finding was the effect blood dilution (change in absorption coefficient) has upon the laser energy/ bubble radius relationship, independent of its effect upon threshold. Figure 5 shows the cycle time vs. normalized laser energy. The laser energy is normalized by subtracting the threshold energies and shifting the curves accordingly. Hence, variation in slope is emphasized while compensating for threshold energy. The curves fan out at higher laser energies implying a source of insensible loss dependent upon absorption coefficient for which we have not accounted.

We will begin by exploring the theoretical effect absorption coefficient (and, hence, threshold energy) has upon bubble size. Assume two absorption coefficients, μ_{a_1} and μ_{a_2}, in which μ_{a_1} is greater than μ_{a_2}. Sketch A represents the fluence, E(x), as a function of x, the penetration depth. The penetration depth is defined as the distance, measured linearly parallel to the incident light rays, from the surface of the absorber into the media. If one now looks at the thermal excitation, $\Phi(x)$, given, as the product of fluence and absorption coefficient, we are left with Sketch B.

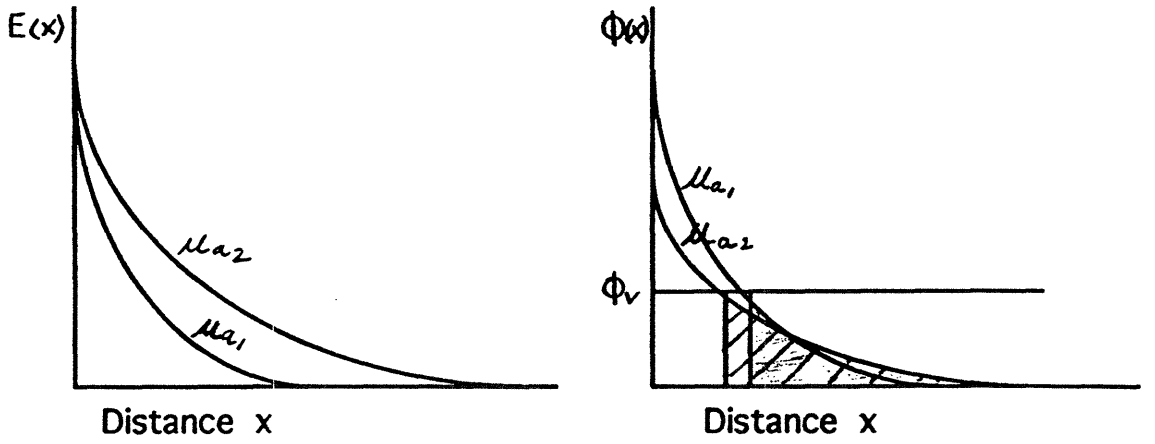

If E(x) obey Beer's Law, we are left with the equations shown below. Assuming a constant heat of vaporization, as a greater amount of energy is deposited within a given volume, a greater amount of vaporization occurs. Since the fluence trails off exponentially with distance, beyond a certain distance, X_{th}, there will not be enough energy to elicit a phase change. Hence we can represent the heat needed to vaporize a given volume liquid media as being a function of the penetration depth, since this our only volumetric variable. This threshold, $\Phi(x_{th})$, can be represented as shown in Sketch B. Then, the shaded area represents energy that is lost due to sub threshold thermal excitation. As discussed in the introduction, this would represent insensible loss. Solving the system of equations, where the lost energy (given in fluence) is labeled E_{lost}, we see that the energy available for transfer into a cavitation bubble is a function not only of the incident energy itself, E_0 , but also of the threshold energy. More importantly, we see that the amount of energy available for cavity formation is simply the incident energy minus the energy necessary to achieve threshold.

Hence, we would expect that by subtracting the threshold energy (shifting the curves) the bubble radius/ laser energy relationships would superimpose. The same result is obtained when the approach is taken from the launch point to the threshold distance (also shown below). Here E_{used} is the energy deposited in the region prior to the threshold penetration distance. This energy is available for cavity formation, both, by raising the temperature of the absorber as well as by inducing a phase change directly.

$$E_{lost} = \int_{x_{th}}^{\infty} \Phi(x)dx = \int_{x_{th}}^{\infty} E_0 e^{-\mu_a x} \mu_a dx$$

$$= E_0 \alpha \left| \frac{e^{-\mu_a X}}{\alpha} \right|_{x_{th}}^{\infty} = E_0 e^{-\mu_a X_{th}} = E(X_{th}) \quad \text{Equation 2.3}$$

alternately: $$E_{used} = \int_0^{x_{th}} \Phi(x)dx = E_0 - E(X_{th}) \quad \text{Equation 2.4}$$

As shown in figure 4, however, the curves do not superimpose but fan out, implying some additional dependence between lost energy and incident energy, a dependence modified by absorption coefficient. As usual, a model's failures lie in the assumptions that have been made. We will begin with the assumption that penetration distance was the only volumetric variable.

OPTICAL DIVERGENCE PHENOMENON

We will begin by looking at a characteristic peculiar to optical fiber delivery systems. In Figure X, a fiber system with beam divergence, θ, is depicted.

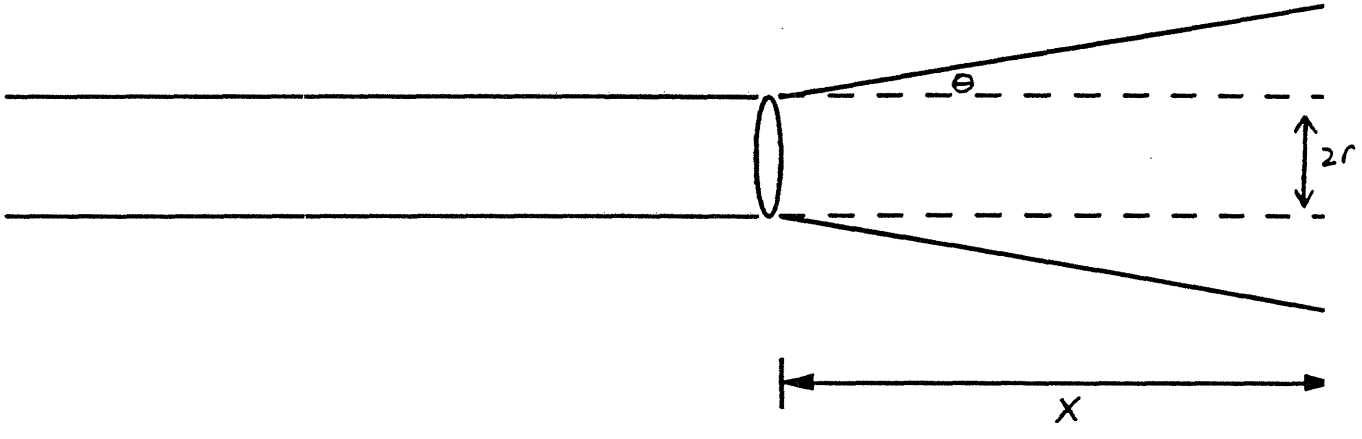

Because of the beam divergence, a geometrical factor accounting for loss of optical intensity with distance must be included. We will now make an argument similar to that made in equation 2.2 and 2.3 above and calculate the energy lost to sub threshold excitation. Here we will use P(x) as the total incident energy (Joules) at a distance x within the media. Hence $\Phi(x)$ as defined above is given as the product of P(x) and μ_a divided by cross sectional area of the beam profile at distance x, with the area calculated as shown.

$$\Phi(x) = \frac{P(X)\mu_a}{A(X)} \qquad \text{Equation 2.5}$$

with $P(X) = P_0 e^{-\mu_a x}$ we are left with:

$$\Phi(x) = \frac{P_0 e^{-\mu_a x}\mu_a}{\pi(r + x\tan\theta)^2} \qquad \text{Equation 2.6}$$

We can now integrate $\Phi(x)$ to find energy lost.

$$E_{lost} = \int_{x_{th}}^{\infty} \frac{P_0 e^{-\mu_a x}\mu_a}{\pi(r + x\tan\theta)^2} dx$$

Using the following integration:[16]

$$\int_u^{\infty} \frac{e^{-\mu x}}{(x+s)^2} = e^{-\mu u}\mu e^{s u} Ei[-(u+s)\mu]$$

and defining these variables as follows:

$$a = \tan\theta$$

$$B = \frac{P_0\mu_a}{\pi}$$

we are left with the solution, given here:

$$E_{lost} = B\int_{x_{th}}^{\infty} \frac{dx}{e^{\mu_a x}(r + ax)^2} \qquad \text{Equation 2.7}$$

$$E_{lost} = \frac{B}{a^2\left(e^{-\mu_a x_{th}}\right)\mu_a\left(e^{\frac{-r\mu_a}{a}}\right)} Ei(\delta) \qquad \text{Equation 2.8}$$

$$\delta = -\left(x_{th} + \frac{r}{a}\right)\mu_a$$

Hence the lost energy is given above for the case were significant divergence has taken place. This has been derived since it is a case

peculiar to optical fibers and hence noteworthy as a phenomenon one may encounter with intravascular laser use. In this way, one can explain the dependence of the lost energy upon pulse energy and absorption coefficient. Extrapolating this relationship, where bubble radius depends on bubble energy and bubble energy is a function of laser energy minus threshold, or lost energy. In simple terms, the lower the absorption coefficient, the more energy diverges and hence the greater the proportion of energy that is lost and not available for cavitation.

Another source of error comes from the assumption that energy deposited in the supra threshold region contributes to the phase change phenomenon. Even if this may be the case in a homogeneous media, if it is certainly not the case in our media of isolated absorbers. As previously discussed, whole blood is an inhomogeneous optical media. As such, there are areas in which small amounts of absorber are contained. These volumes of fluid, having a sub-critical concentration of absorber with respect to the fluence at that particular penetration depth, will absorb energy and subsequently dissipate this energy as heat. Hence, these areas will act as energy sinks. The shielding effect of this inhomogeneous distribution will have greater significance at lower absorption coefficients were the distance between absorbers is greater and the media is more heterogeneous.

We therefore have two possible explanations for the increased insensible loss seen as a function of absorption coefficient and energy, i.e. the fanning out phenomenon. Numerical analysis indicates that beam divergence plays a very small role at these absorption coefficients, with cone angles less than 10% and path lengths between one fourth and one

fiber diameter in size. The relative contribution of the inhomogeneous media is difficult to quantitate without more data. The relative contribution of each will become clearer in the sections that follow. If beam divergence is the major contributor to this phenomenon, then changing the homogeneity and the pulse length should have little effect.

II. Influence of media homogeneity on cavitation bubble formation: A comparison of whole blood and lysate.

Methods

The experimental apparatus described above was used to measure cavitation cycle times for lysed blood of varying Hgb concentrations. Packed red blood cells were diluted using non isotonic saline (to increase lysis) and then further lysed by placing them in an ultrasonicator for 15 minutes. Three to five measurements were made at each of the following laser pulse energies: threshold, 5 10, 15, 20, and 30 mJ/pulse. The lysate was then diluted to 1/2 and subsequently 1/4 the original Hgb concentration and the above measurements repeated. Blood chemistry was performed to document Hgb levels as well as degree of lysis at each interval. Technical calibrations were as above.

Results and Discussion

Chemistry data showed that significant, but incomplete, lysis had taken place. With hematocrit (Hct) approximately 1/2 that expected for given Hgb. Normal, half normal, and quarter normal hemoglobin/hematocrits

were found to be: 11.6/26.2, 6.8/9.3, and 2.9/4.1, respectively. This represents lysis of slightly more than 50% of all red cells. Nevertheless, the media containing the lysed red blood cells behaved differently from the inhomogeneous media (whole blood) described above. Figure 6 shows the cavity cycle time vs. laser pulse energy for lysed blood with the three parameters delineated above. Since only the homogeneity of the media has been affected, the average absorption coefficients are the same as those for whole blood.

Unlike that seen in whole blood, the threshold energy's dependence upon absorption coefficient is now quite dramatic, as expected. With subsequent μ_a's of 132, 61.5 and $32 cm^{-1}$, thresholds of approximately 2.5, 5.0, and 7.5 mJ/pulse were seen. This further substantiates the argument made above that single erythrocytes can provide a nidus for cavitation. Since the lysate has a fairly equal distribution of hemoglobin the probability profile of finding a given concentration of absorber approaches that of a homogeneous media, i.e. a delta function. So

$$\frac{\Phi_v}{E_{th}} = P(\mu_a)$$

is simplified by setting the probability equal to the average value, $P(\mu_a) = \mu_a$, and yields:

$$\Phi_v = E_{th}\mu_a$$

As above Φ_v is the minimum thermal excitation necessary for cavitation, E_{th} represents the fluence at threshold, and μ_a represents the absorption coefficient of a homogeneous absorber. The threshold for cavitation in the lysate deviated from the theoretical expectations only at the lower absorption coefficient of $31 cm^{-1}$. Calculating the thermal excitation for the absorption coefficients of 132 and $61.5 cm^{-1}$, we find a

theoretical energy of approximately 2.5 and 5.0 mJ necessary to bring the liquid from 80°C to 100°C (assuming specific heat of water). The energy contribution from the heat of vaporization is virtually negligible given the small volume vaporized compared to the large volume heated. At threshold, the amount of energy going into vaporization is on the order of 0.1 mJ.

Plots 7, 8, and 9 show both lysate and whole blood of a given hemoglobin concentration plotted together. As can be seen, once the threshold energy is accounted for there appears to be little difference between the curves. They still follow the cube root seen with the whole blood curves. These curves, however, do appear to deviate from the their whole blood counterparts at higher energy levels.

The component of laser energy lost did not follow the same relationship it did for whole blood. Figure 10 shows cycle times for the three absorption coefficients of lysed blood plotted against the adjusted laser pulse energy, as used above to delineate slope. Hence, the fanning out phenomenon seen with whole blood is decreased but still present. This is further exemplified in Figure 11, which plots the difference in cycle time for different absorption coefficients at various laser pulse energies. Here we see that for the whole blood medium the difference increases with increasing energy. For the lysate, however, this difference is constant. This shows a pulse energy and absorption coefficient dependent correction factor that appears almost constant in the realm plotted. The value of this relatively horizontal line, approximately 60 usec, represents the threshold cycle time (the cycle time of the cavitation bubble initiated by a laser pulse of threshold energy). This implies, as was derived above, that the energy available

for cavitation bubble formation is simply the laser energy minus the threshold energy. Hence, our source of insensible loss is now gone, as is the inhomogeneity of the media.

III. Acoustic transients generated by bubble collapse: dependence on bubble radius and distance of observation.

Methods

A 1 usec, 480nm, 40 mJ pulse was used to create a relatively constant bubble with an approximate cycle time of 475 usec and 2.2 mm radius in whole blood as the target (Hct of 44%). The Imotec hydrophone described above was placed perpendicular to the fiber tip and moved independently in the x and y directions in increments of 1mm (tolerance 0.03mm). The magnitude of the acoustic transient and the cycle time of the cavitation bubble were recorded at each position. The magnitude of the acoustic transient as a function of distance was then plotted for a constant cycle time.

In the second part of this experiment, the dye laser was used at energies of 5, 10, 15, 20, 30, 40, and 50 mJ/pulse and the excimer at energies of 5, 10, 15, and 17 mJ/pulse to generate cavitation bubbles of various sizes. The acoustic transients generated upon bubble collapse were then measured and normalized with respect to distance from the fiber tip.

Results and Discussion

In Figure 12, the magnitude of the acoustic transient is plotted vs. distance from the fiber tip. The magnitude of the acoustic transient varies inversely with the distance from the fiber tip in both the vertical

and horizontal directions. As stated in equation 1.4, the energy contained in an acoustic transient can be calculated as follows:

$$E_{AT} = \frac{4\pi r^2}{\rho c} \int P^2(t) dt$$

Since the acoustic transient propagates radially from the bubble center, its energy is contained within an expanding surface area. If one assumes its energy is conserved, i.e. it is an elastic pressure wave, the pressure of the acoustic transient diminishes as the surface area increases, manifesting an inverse relationship with the square of the distance from the bubble center.[12] The relationship between the magnitude of the acoustic transient, i.e. the absolute pressure, and the distance from the bubble center, r, can be rewritten:

$$\frac{E_{AT}}{4\pi r^2} = \frac{1}{\rho c} \int P^2(t) dt$$

and, hence,

$$|P| \propto \frac{1}{r} \qquad \text{Equation 2.9}$$

Using equation 1.4 to calculate the total energy contained in an acoustic transient formed when a cavity of 200 usec cycle time collapses (a 10 mJ 1usec pulse in a whole blood field), we find it to contain approximately) 0.3 mJ.

Figure 13 plots acoustic transients, as a function of bubble cycle time and includes both cavitation bubbles created by excimer laser pulses as well as by one microsecond dye laser pulses. As shown, the magnitude of the acoustic transient generated on the bubble collapse does not depend upon the laser source, but varies almost linearly with the radius, reflected as the bubble cycle time. In essence, these cavitation bubbles have no "memory" of the type of laser that created

them. Once a bubble collapses the energy which had previously been contained in that bubble is redistributed. This can be written as follows:

$$E_{CAV.BUBBLE.1} = E_{AT.COLLAPSE} + E_{CAV.BUBBLE.2} + E_{LOST} \qquad \text{Equation 2.10}$$

It is important to remember that the response of the hydrophone (approximately 50 ns rise time) is comparable to the rise time of the generated acoustic transient and may underestimate the measured peak pressure. Therefore, whereas the relative relationship between magnitudes is not affected, the absolute values may be dampened. Unlike Q switched lasers that generate an initial shock wave following plasma formation, the acoustic transient generated on bubble collapse is greater than that generated initially.[12] This will be discussed in section VI of this chapter.

As was discussed in the introduction, a significant component of the energy contained in a cavity dissipates due to fluid compression. A larger cavity, owing to the interdependence between the maximum radius and the attained velocity, will transfer a greater amount of energy to fluid compression. Hence, if we assume a constant coupling between the primary bubble and the acoustic transient generated upon its collapse, i.e.:

$$E_{AT} = KE_{CAV} = K\frac{4\pi R^3 \Delta P}{3}$$

the relationship between bubble and acoustic transient should be on the order of the radius to the three halves, as shown below:

$$E_{AT} \propto P^2(T) = K'R^3$$
$$P_{MAX} = K''R^{3/2} \qquad \text{Equation 2.11}$$

As written above, R is the maximum bubble radius. K', K'', and K are all constants of proportionality and pressure is given in bar*mm (divide by radial distance to obtain actual pressure). Using plot 13 we can estimate this value to be $K''=0.286$ bar/$mm^{3/2}$

We can further explore the transfer equation given above by plotting the cycle time, once again analogous to radius, of the cavitation bubble generated upon collapse as a function of the cycle time of the preceding bubble. This plot is given in figure 14. The primary cavitation bubbles were generated by 1usec and 20usec pulsed dye lasers as well as by 0.2usec excimer. Whole blood as well as lysate data are also intermixed on the plot. Reflected in the data is a linear relationship showing a transference of 58%(correlation coefficient> 0.97). In other words, 58% of the energy contained in cavitation bubble one is transferred to cavitation bubble two. This finding correlates well with the oscillating damped cavity predicted by the Gilmore model described in the introduction.

IV. Effect of pulse duration upon cavitation.

Methods

A Candela tunable pulsed dye laser with 480nm coumarin dye and a pulse duration of 20 usec was used at varying energies to establish a relationship between energy and cavitation bubble size. Plots were obtained showing cycle time and acoustic transient magnitude for threshold, 5, 10, 20, and 30 mJ pulses. These studies were undertaken using normal, 1/2 normal, and 1/4 normal Hct. The

results were then compared to those for the 1usec pulse duration laser using an identical wavelength (480 nm).

Results and Discussion

Figure 15 shows the measured cycle times for the 20 usec laser pulses described above. Once again a correlation with the cube root of the energy is noted, as observed by the slope of the log plot.. Threshold for cavitation, however, behaved quite differently. For a given absorption coefficient, a 20 usec pulse length necessitated an increase in threshold energy as compared to the 1 usec pulse length. These threshold values were actually very similar to those of the 1usec pulses in lysate of comparable absorption coefficient. A Hct of 21 required a threshold energy increase of approximately 6 mJ and a HCT of 13 required 10 mJ. This finding is not surprising. The probability-based threshold model developed above assumed that a critical concentration of absorber was contained within a definable finite volume. Implicit in this assumption is that the deposited energy would also be confined to this volume. In the case of a homogeneous absorber the energy is deposited evenly throughout the volume irradiated. In the case of a prolonged pulse, however, the energy is deposited within a small volume but is able to diffuse out into the entire volume. This argument is identical to that made for selective photothermolysis. With pulse durations equal to or larger than the thermal relaxation time for the absorber both the absorber and an area surrounding the absorber are heated. The thermal relaxation is here defined as the time necessary for 50% of the energy to be lost from a given absorber. Numerical analysis have been found this to be 15 usec for a red blood cell. Hence, with a 20 microsecond pulse there is enough time for significant thermal diffusion to have

taken place. This can be calculated by adapting models based upon pulsed photothermolysis.[16]

Assume that energy is deposited equally throughout the pulse duration. Then energy deposition can be modeled by:

$$\frac{dQ'}{dt} = f I_0 \mu_a \qquad \text{Equation 2.12}$$

where : $\frac{dQ'}{dt}$ is the rate of heating given in an energy per unit volume per time; f is a transfer coefficient, for whole blood with erythrocytes as the only absorber we can set this value to 1; I is the incident irradiation and can be set equal to the fluence energy delivered divided by the pulse duration.

If we assume the red blood cell behaves as a point source, then the energy contained within a given red cell is modeled according to the following:[17]

$$E(t,r) = \int_0^t f I_0 \mu_a - \int_0^t \frac{1}{8\left[\pi\kappa(t-\tau)\right]^{\frac{3}{2}}} e^{\frac{-r^2}{4\kappa(t-\tau)}} d\tau \qquad \text{Equation 2.13}$$

And therefore, the amount of heat lost during energy transfer is given by the solution to equation 2.13 above; numerically calculated, a red blood cell loses approximately one third of the incident energy during a 20usec pulse.

The increased pulse length also impacted the slope of the energy/bubble size curves, shown in Figures 15. It appears to have

decreased the "fanning out" phenomenon described in the first section of this chapter. This decrease is compatible with decreased inhomogeneity due not to a lack of spacial inhomogeneity but a lack of temporal homogeneity. As explained above, sub threshold concentrations of absorbers actually acts as a heat sink by diverting energy deposition away from bubble formation. However, with pulse durations longer than the thermal relaxation of the red cell, heat transfer to the medium occurs. Red cells that had been acting as independent absorbers no longer do as there is sufficient time for heat transfer to take place and hence for the cell to interact with the environment. Figure 15 plots the difference in cycle time for two absorption coefficients (different by 50%), as a function of the respective energies. Unlike the 1 usec plot of this type, we see that the energy lost is relatively constant for a given absorption coefficient. Furthermore, the value of this relatively horizontal line, approximately 60 usec, represents the threshold cycle time (the cycle time of the cavitation bubble initiated by a laser pulse of threshold energy). This implies, as was derived above, that the energy available for cavitation bubble formation is simply the laser energy minus the threshold energy.

V. Effect of a multi-fiber delivery system upon cavitation bubble dynamics and acoustic transient generation.

Methods

The Advanced Intravascular Systems (AIS) excimer laser system described above was used in conjunction with the three clinical laser fiber systems of diameters 1.3mm, 1.6mm, and 2.0mm. These fiber

systems consisted of several hundred (>200) individual optical fibers arranged circumferentially around a central guidewire port. A standard 0.16 guide wire was incorporated, as shown in figure 2, into the experimental set up. In the first set of experiments, cavitation was created using three clinically relevant energy levels for each fiber system-1.6 mm: 8.6 mJ (35 mJ/mm^3), 21mJ (50mJ/mm^3), and 25.5 mJ (60mJ/mm^3); 2.0mm: 24 mJ (35 mJ/mm^3), 29 mJ (40 mJ/mm^3), and 34 mJ (49 mJ/mm^3). The cycle time as well as the magnitude, pressure time profile, and total energy (measured as the product of the square of the pressure and the time) of the acoustic transient generated on initial bubble expansion were recorded.

The second set of experiments recorded the pressure time profile, magnitude, and total energy of the acoustic transients generated upon bubble collapse with regards to the preceding cycle time.

Results and Discussion

Plot 17 shows the relationship between cycle time and pulse energy for two multi-fiber systems as compared to that for a single fiber excimer system. As is seen, the multi-fiber systems prod cavitation events with decreased cycle times as compared to single fiber systems when comparable energies are used. A cavitation bubble size has not been calculated since spherical geometry can not be assumed, and is likely, not present. Multi-fiber systems generated cavitation bubbles whose cycle times were somewhat less, albeit not by a large margin, than that for single fiber systems. The energy/cycle time curves are well behaved, however, and closely parallel those seen with single fiber systems. On a log plot they continue to have a cube root relationship between the cycle time and delivered energy. Hence, the

cycle time appears related to the energy of the cavitation bubble as if traditional spherical geometry were present.

Figure 18 shows how the acoustic transient created on cavity collapse varies with cycle time within the context of a multi fiber system. As is evidenced by the cluster of 1.3 mm data at cycle times of 115 and 150 usec as well as by the cluster of 1.6 mm data at 240 usec there appears to be more consistent acoustic transients at lower cycle times, and hence, lower energy levels. At longer cycle times, the acoustic transients vary greatly from bubble to bubble. This variation has not been seen in traditional, spherical bubbles. Furthermore, the time profile of the acoustic transients generated on collapse of a multi fiber system created cavitation bubble indicates a multifocal collapse, see figure D.2. In contrast to single fiber systems give acoustic transients with a smooth temporal profile, multi-fiber systems generate complex acoustic transients which appear to be a summation of various smaller acoustic transients. One possible explanation entails an asymmetrical bubble, possibly toroidal in nature, whose cycle time is governed by the total volume but whose collapse is governed by its geometry. Although the magnitude of the acoustic transients generated by the collapse of aspherical cavitation bubbles are significantly less than those created by the collapse of spherical cavitation bubbles, they are still of significant magnitude. As is seen on plot 18, AT's of up to 80 and 160 bar can be extrapolated at 1mm and 0.5mm, respectively, from the bubble focus.

VI. Acoustic transients generated on initiation of cavitation.

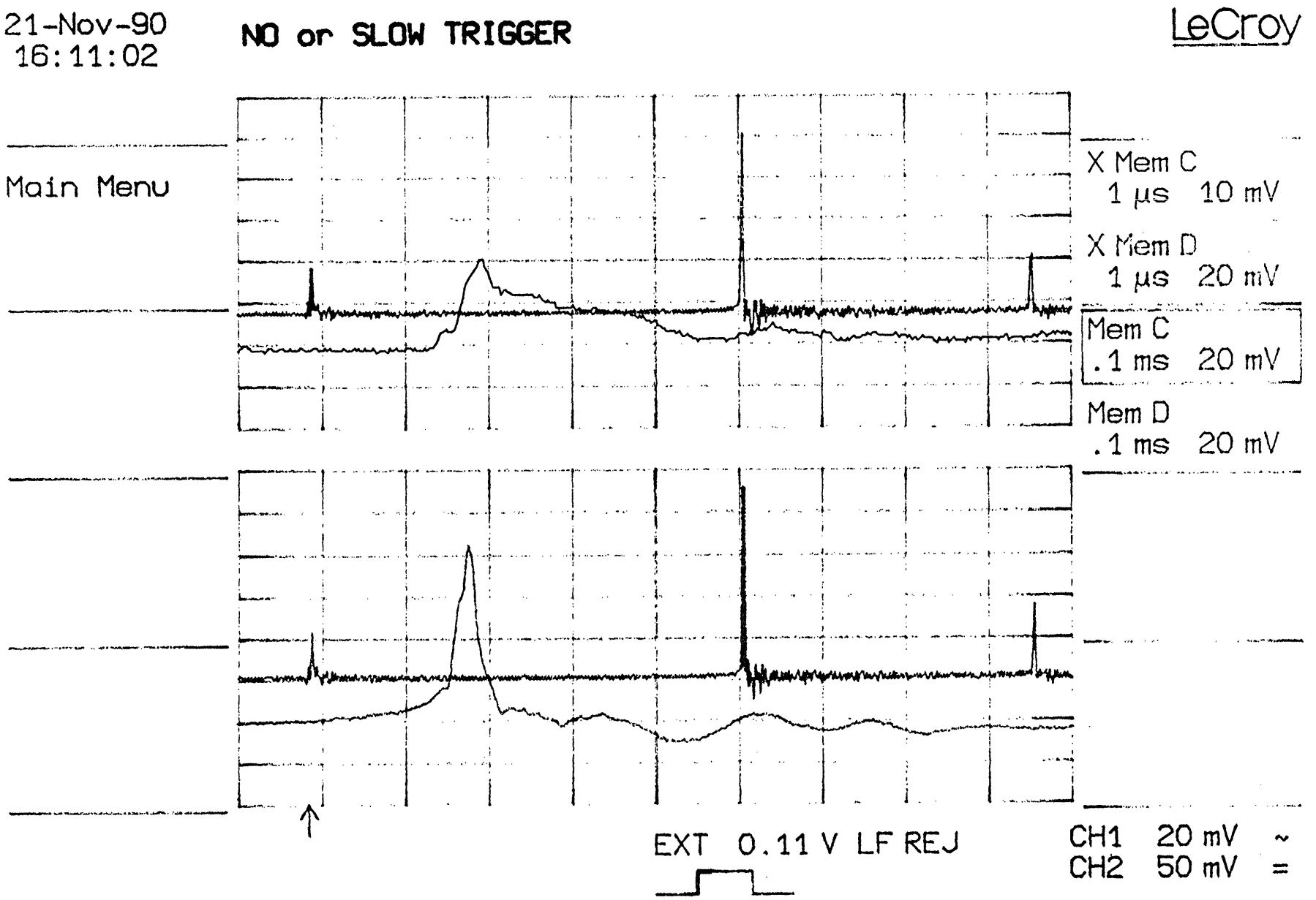

Figure D.1 Shown is a plot obtained from an oscilloscope reading. Here one can clearly see an initial acoustic transient, an acoustic transient generated on collapse, as well as a third acoustic transient generated upon a second collapse.

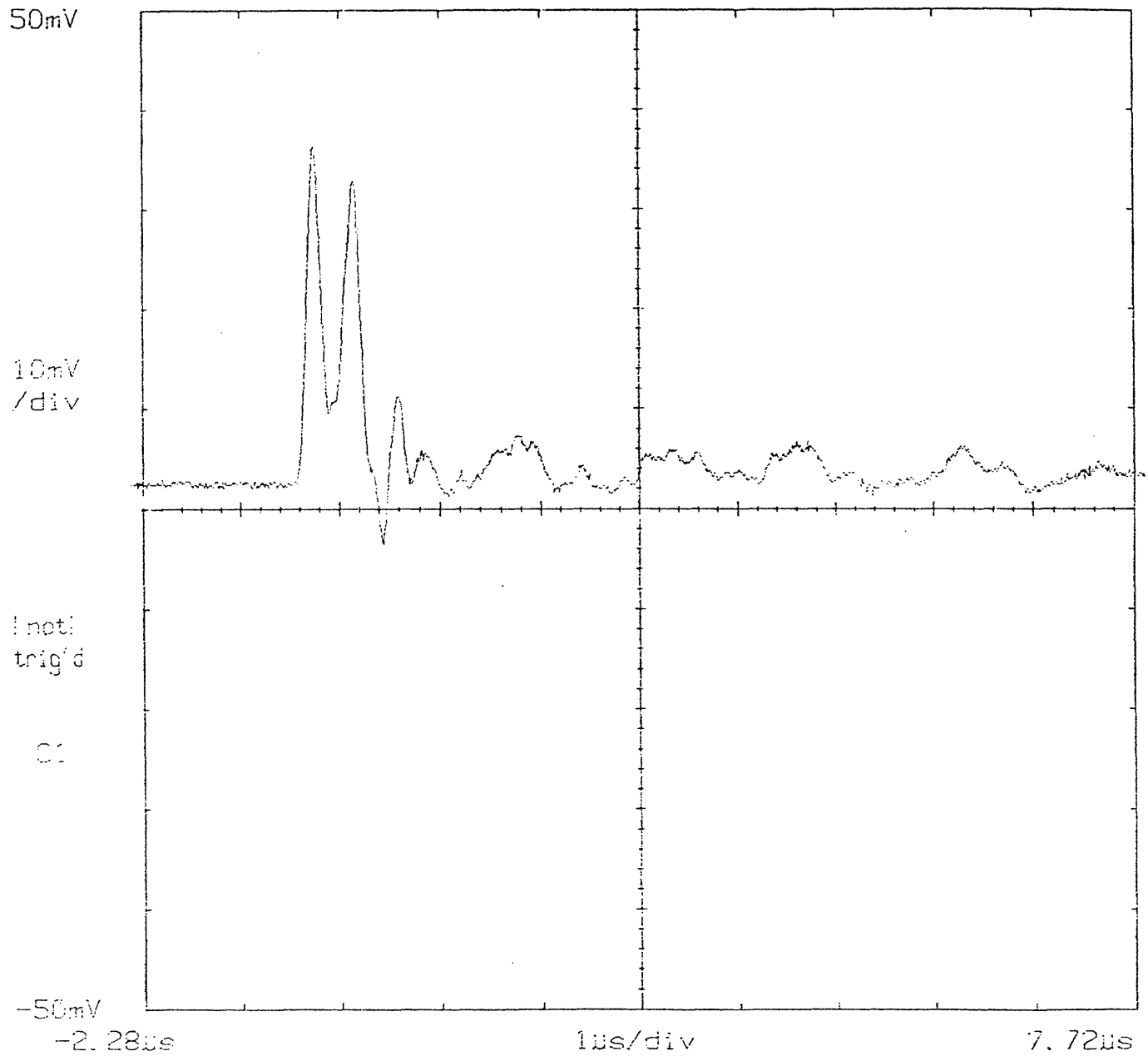

Figure D.2 Shown is a plot obtained from an oscilloscope reading of an acoustic transient generated upon collapse of bubble created using a multi fiber system. Notice the multiple peaks

Methods

Initial acoustic transients generated using the 1 usec, 480 nm, 320 micron fiber system as well as the 1.3 mm, 1.6 mm, and 2.0 mm AIS excimer multi-fiber systems were measured using the afore mentioned apparatus. Their magnitude and temporal profile were then compared to the acoustic transients generated upon bubble collapse. Their magnitude was also compared to the cycle time of the ensuing bubble in an attempt to generate a coupling coefficient.

Results

Magnitude of the initial acoustic transients were found to vary almost linearly with the pulse energy. These transients are shown in plots 19 and 20 for the 320 micron fiber pulsed dye and the 1.6mm and 2.0mm excimer laser systems, respectively. Initial acoustic transients for the pulsed dye system were found to be significantly less than those generated upon bubble collapse at a given energy. Excimer acoustic transients generated were found to be statistically comparable to their counterparts generated upon collapse. Magnitude of the initial transients ranged up to approximately 105 bar and 95 bar at 1 mm for pulsed dye and excimer systems, respectively.

Discussion

In all cases studied, initial acoustic transients were found to be less than those generated upon bubble collapse. This differs greatly from the ophthalmologic literature in which the opposite was found to be true. At the pulse durations and pulse energies investigate here we are well below the threshold for plasma generation. Hence, we do not see intense energy deposition leading to shock waves. This translates into a decreased component of laser energy transferred to formation of

the shock wave/acoustic transient phenomena. For example, a 10 mJ pulse transfers less than 0.2 mJ into the formation of the initial acoustic transient. Although these acoustic waves have a high peak pressure they are not comparable to shock waves. Lauterborn's investigations, for example, have cited as much as 80% of the energy contained in a Q-switched laser as being transferred into the formation of a shock wave.[18]

Since much of the laser angioplasty literature has focused on shock waves and their role in perforation, we will in the next chapter investigate perforation as a result of a cavitation interaction.

SUMMARY OF PULSED LASER INDUCED CAVITATION IN A BLOOD FIELD.

As detailed in the preceding sections, pulsed laser induced cavitation of a blood field substantially differs from previously studied cavitation. The threshold energy for cavitation depends strongly on the media inhomogeneity and pulse duration, as well as the absorption coefficient. The absorption coefficient, with respect to threshold, is better characterized as a distribution of absorption coefficients within a given volume. This spatial distribution is important where a localized concentration of absorber can serve as a nidus for supra threshold energy deposition. It is important temporally where the thermodynamic interaction between the absorber and its surroundings can confine or transfer the deposited energy, depending upon the pulse duration thermal relaxation of the absorber, and distance between absorption sites. The media inhomogeneity also increases the proportion of laser

energy dissipated as unused heat. The areas of sub threshold absorber concentration function as heat sinks dissipating energy deposited. With lysis of the blood media, variations in threshold due to pulse duration, and variations in lost energy, due to pulse energy and pulse duration disappear.

The optical divergence seen with fiber delivery of light does not significantly affect cavitation in blood. The high absorption coefficients prevent a vast change in incident light beam diameter. Subsequently, thermal excitation, within a path length, is not greatly affected. A decreased absorption coefficient would, however, increases the dependence of threshold on the absorption coefficient, lowering the threshold more than if non fiber delivery methods were used.

We have also shown that the acoustic transients generated initially are significantly less than those generated by the collapse of a bubble. The collapse generated transients while much less than those generated with laser systems that initiate plasmas and shock waves, are still of a very high pressure. The collapse of the bubble follows the compressible fluid models of bubble dynamics quite well, with compression of the fluid leading to a pressure wave and decreasing the size of the subsequent bubble (we have shown approximately 60% of the energy goes into the subsequent bubble).

Multi-fiber systems are also an interesting phenomenon. Although the cycle time of their cavitation bubbles are determined by the total volume of the bubble, and hence energy, the spherical geometry necessary for maximum acoustic transient generation makes the acoustic transient dependent on the shape of the bubble. Hence, multi-

fiber systems generate lower pressures on collapse than single fiber systems.

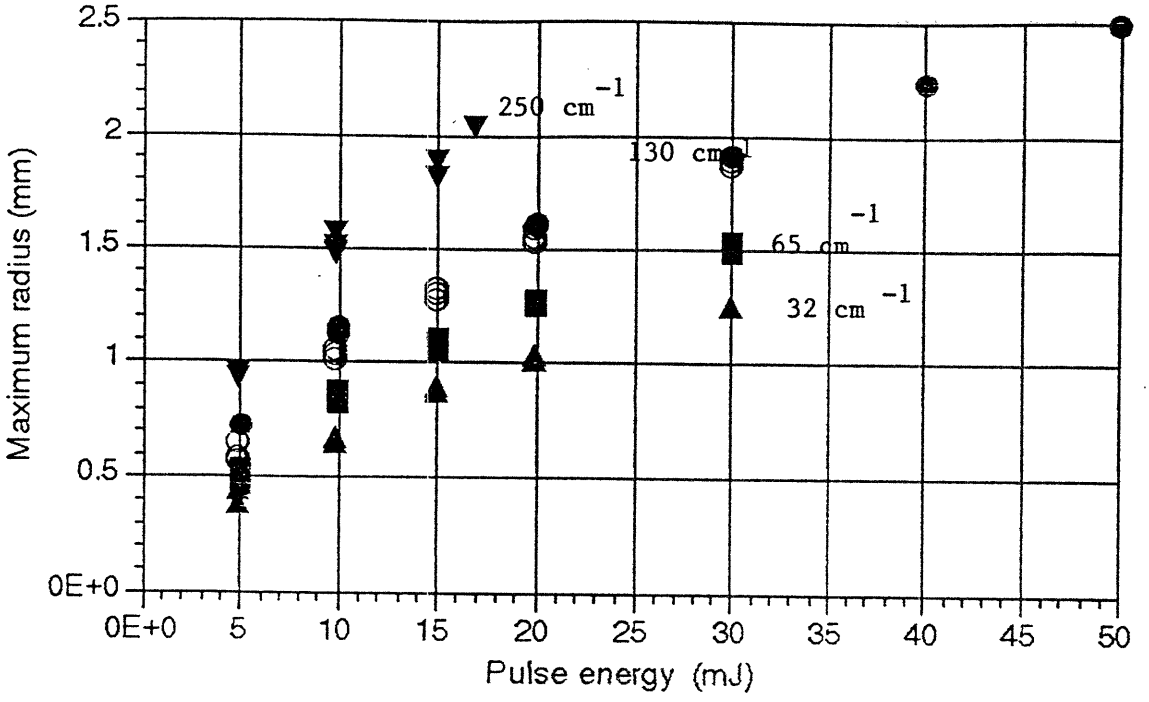

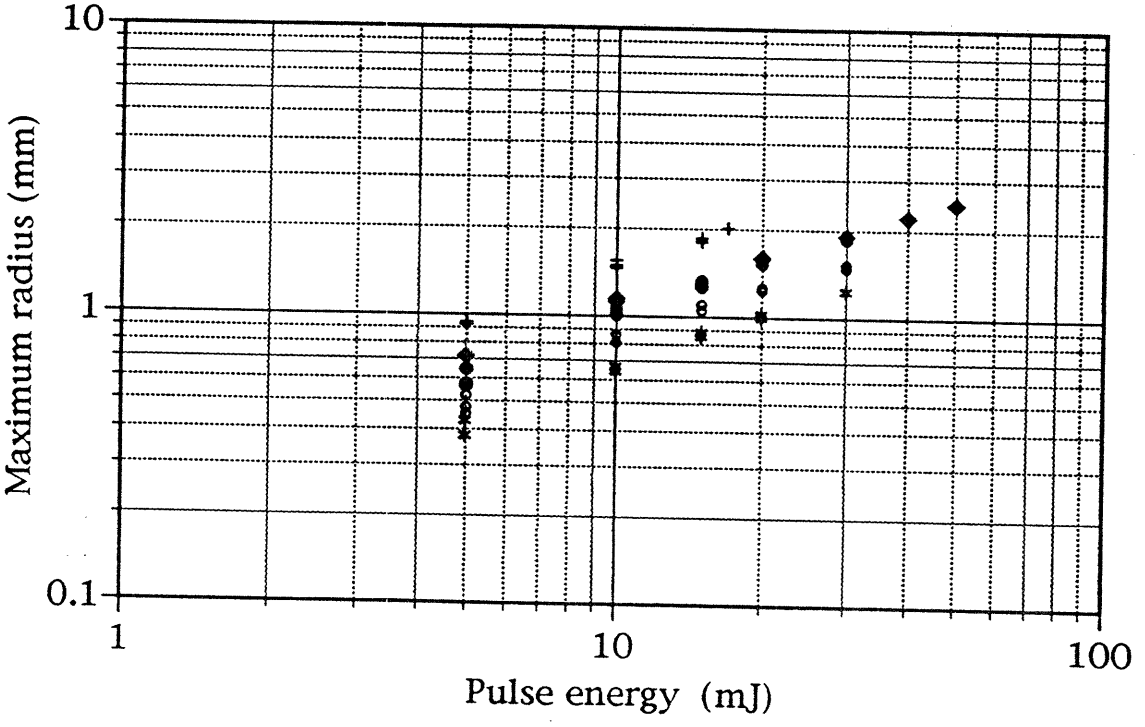

Figure 3. Radius of the cavitation bubble versus pulse energy for excimer laser, XeCl (inverted triangle), and pulsed dye systems in three HCT's: 42%, circles; 21%, squares; 11%, triangles. Plotted on a log scale below to show the cube root dependence.

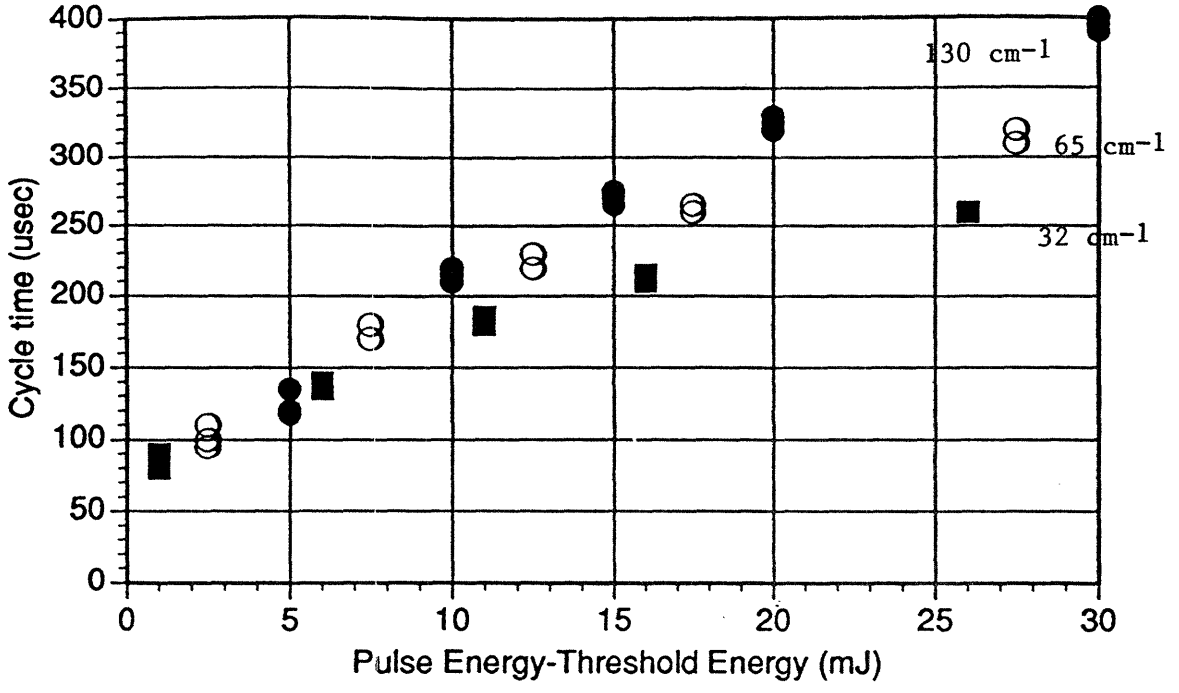

Figure 5. Cycle time as a function of pulse energy minus threshold energy for three absorption coefficients.

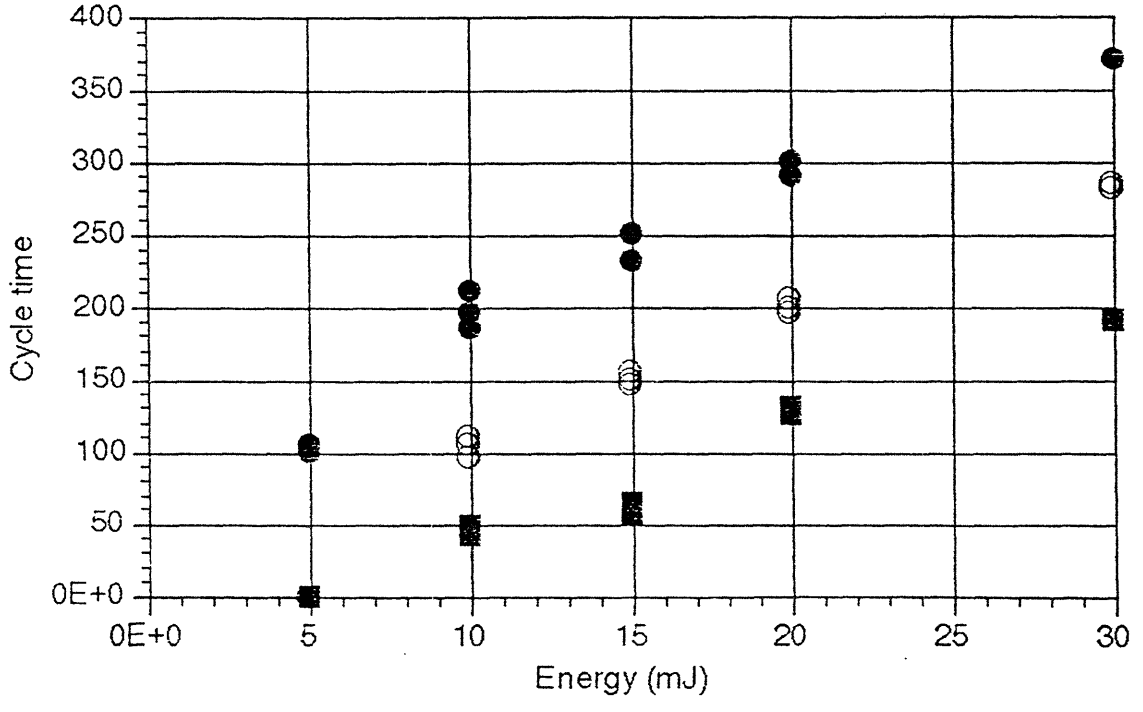

Figure 6. Cycle time as a function of pulse energy. Represented are three absorption coefficients, 120, 60, and 30 cm, for lysed blood.

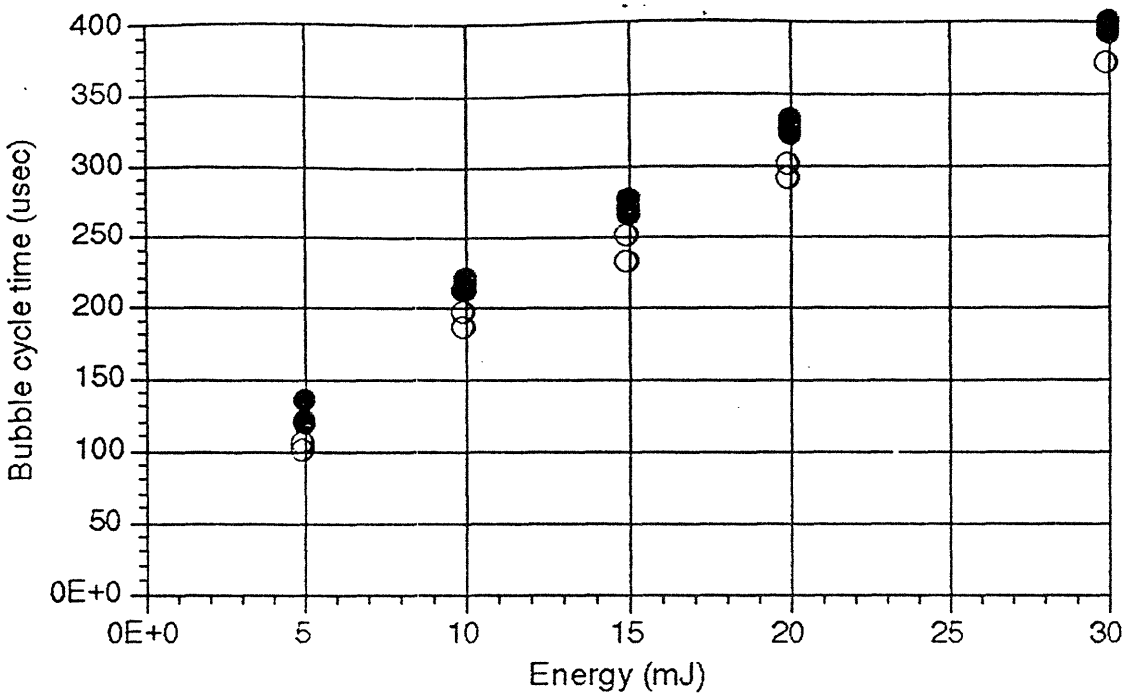

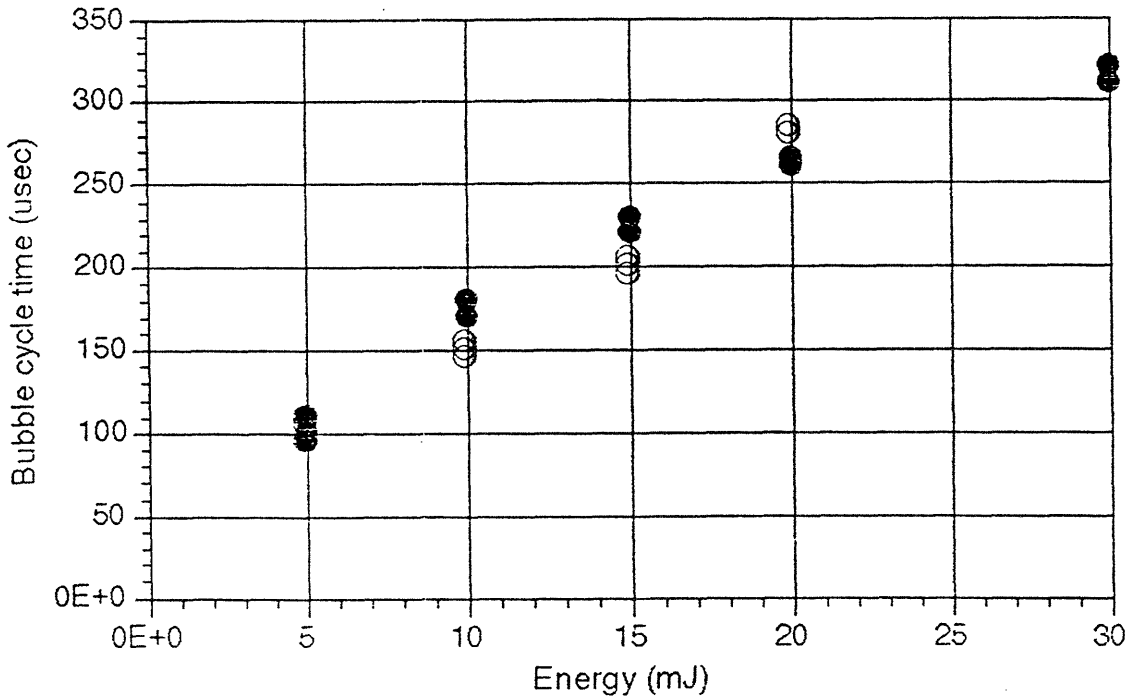

Figure 7 and 8. Represented is bubble cycle time as a function of pulse energy for whole blood (dark circle) and lysate (open circle). Hgb concentrations are equal in both media. Absorption coefficient = 120 cm in the top set of curves and 60 cm in the bottom. The bottom set of curves has been normalized to accentuate slope.

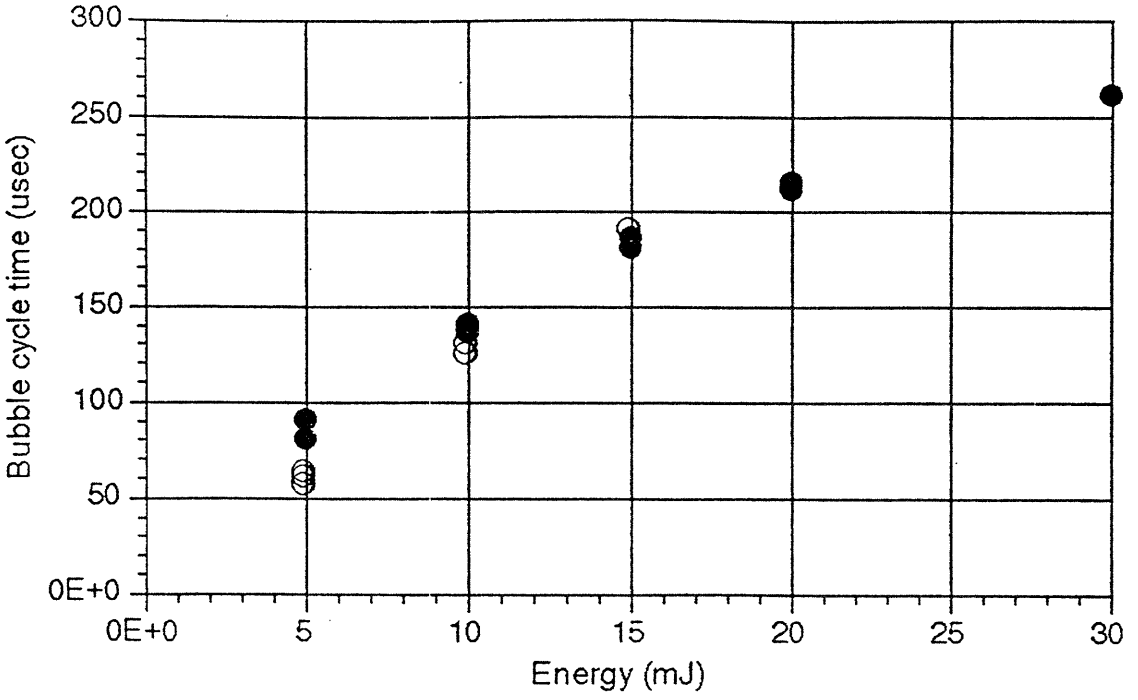

Figure 9. Represented is bubble cycle time as a function of pulse energy for whole blood (dark circle) and lysate (open circle). Hgb concentrations are equal in both media. Absorption coefficient = 30 cm. Curves have been normalized to accentuate slopes.

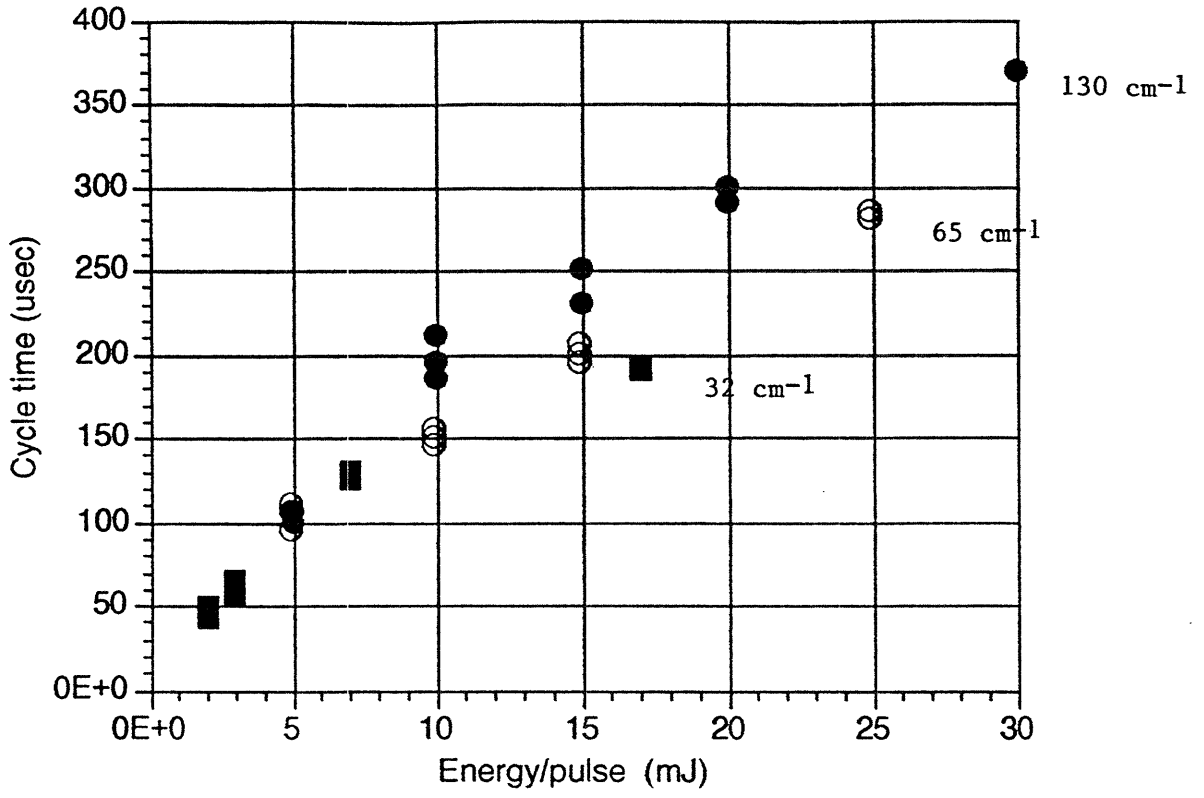

Figure 10. Bubble cycle time versus laser pulse energy minus threshold. Once again, this is done to demonstrate differences in slope.

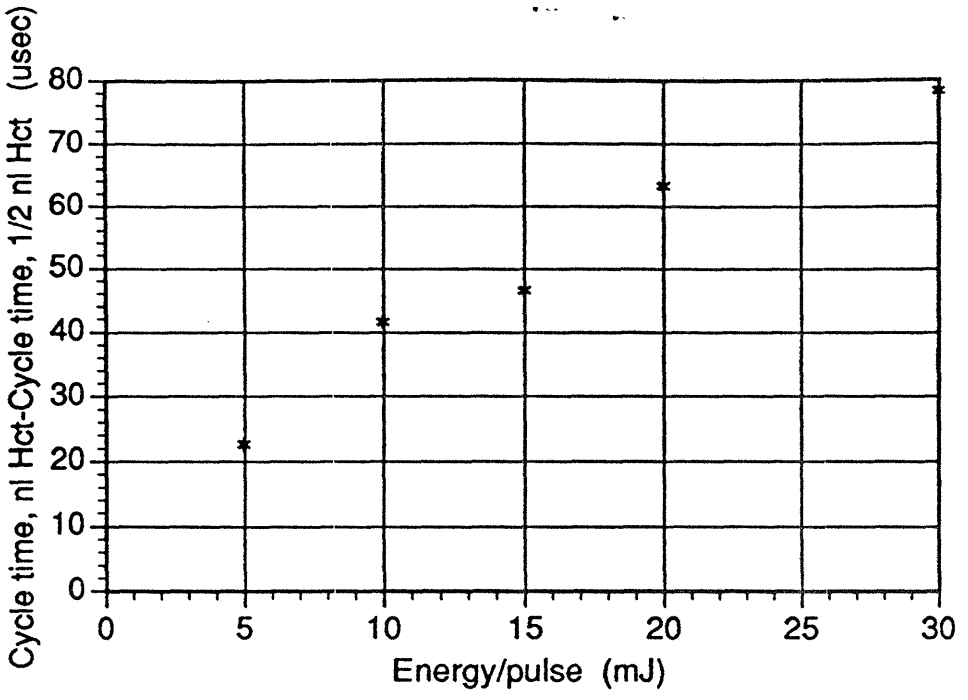

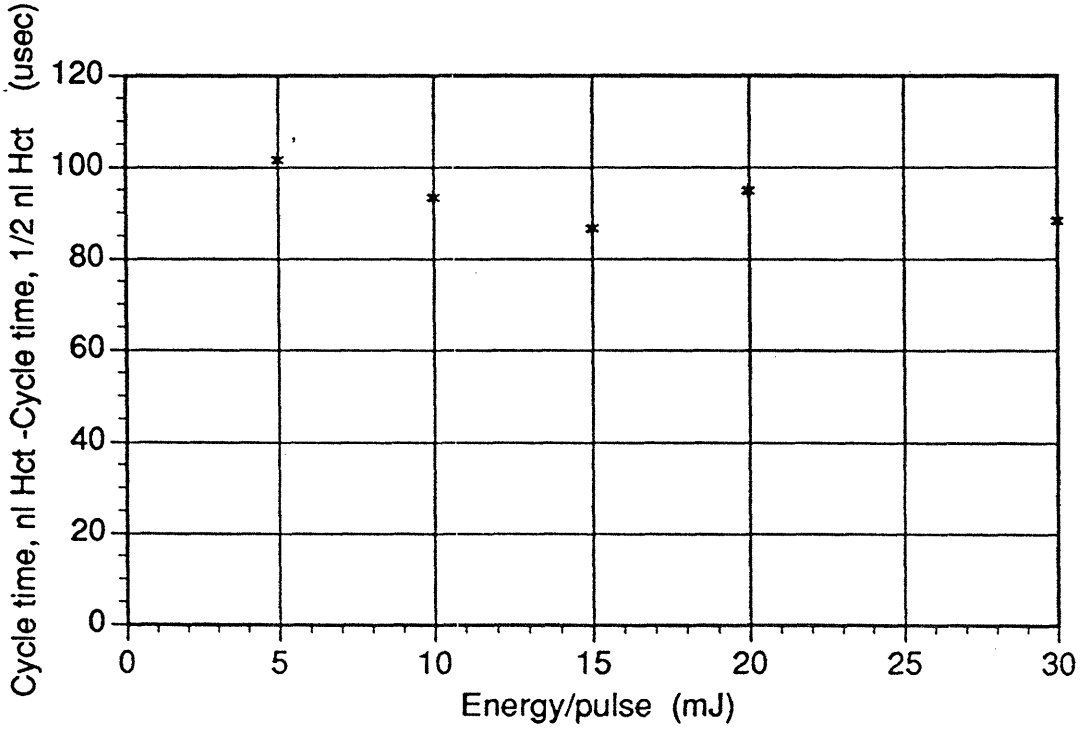

Figure 11. These plots represent the difference in cycle time between two hematocrits, hence two absorption coefficients, as a function of energy. The top plot represents whole blood the bottom lysed blood.

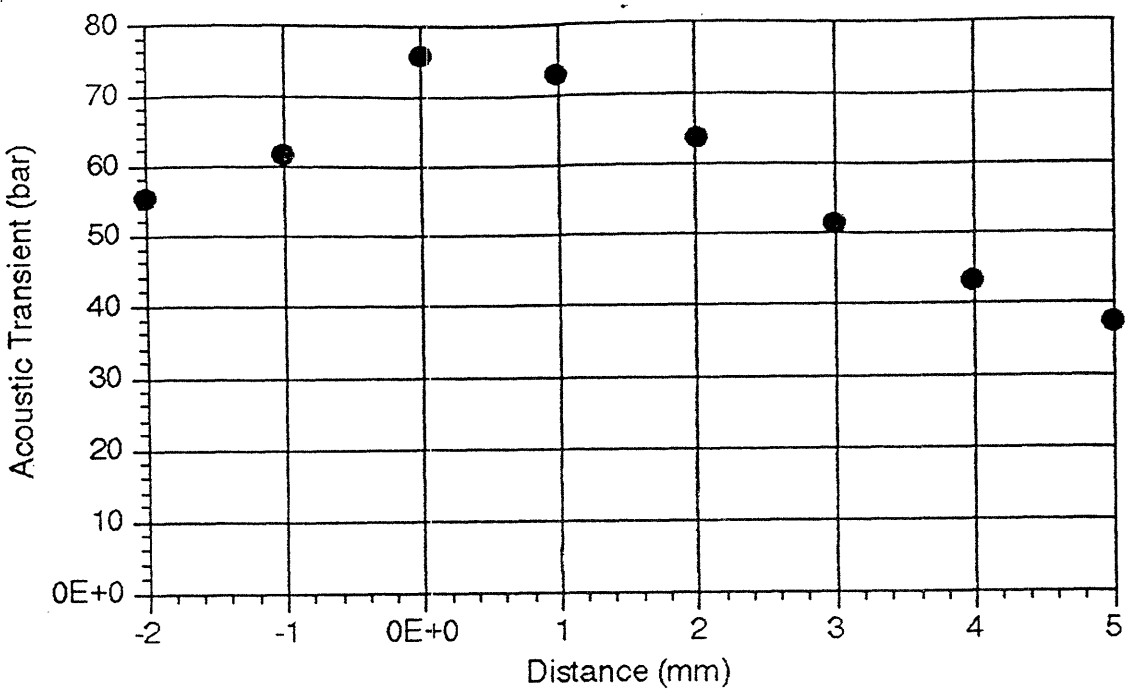

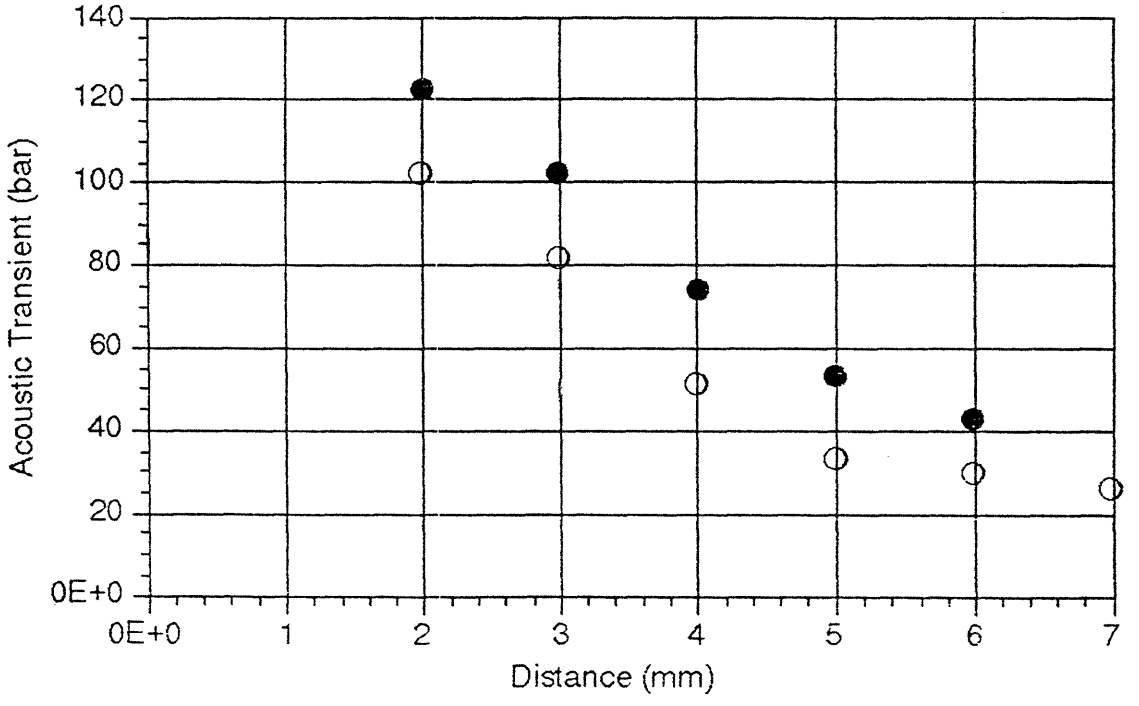

Figure 12. The magnitude of the acoustic transient is represented as a function of distance from the bubble collapse center. The top figure represents y direction whereas the bottom represents x direction.

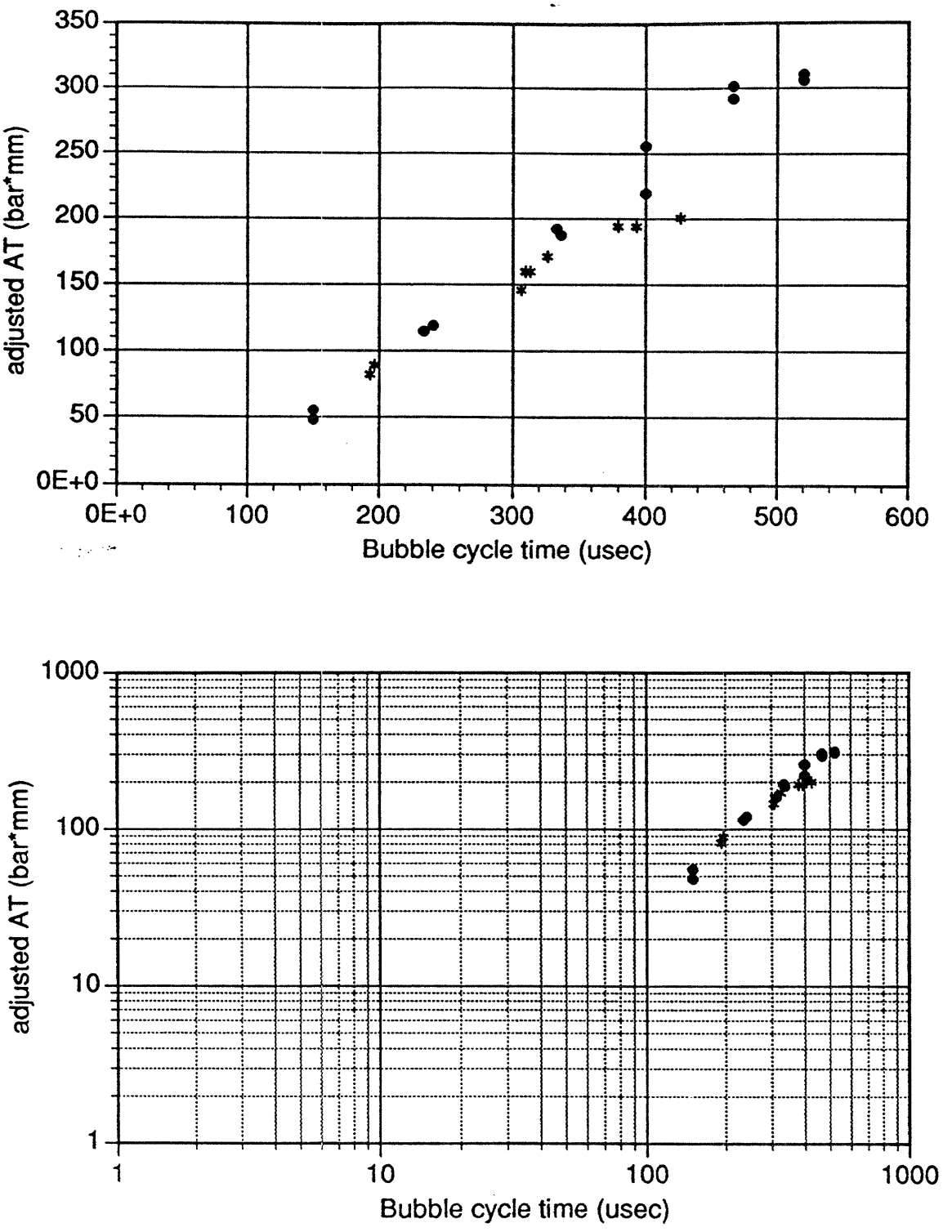

Figure 13. Acoustic transient generated upon bubble collapse, in bar*mm, vs. the cycle time of the preceding cavity. Dark circles are points created using a pulsed dye system, stars were created using an excimer laser. The bottom plot is on a log scale to showing a slope of 3/2.

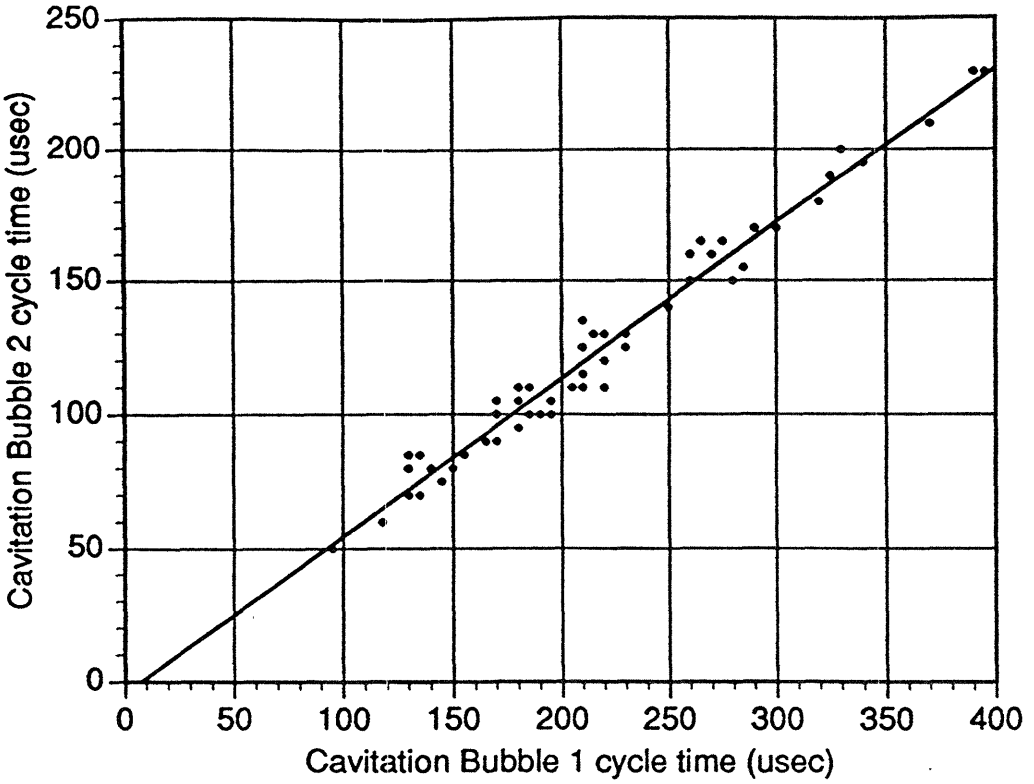

Figure 14. The cycle time of the cavitation bubble created on the collapse of the first bubble is shown as a function of the cycle time of the first bubble. All laser single fiber systems are plotted together.

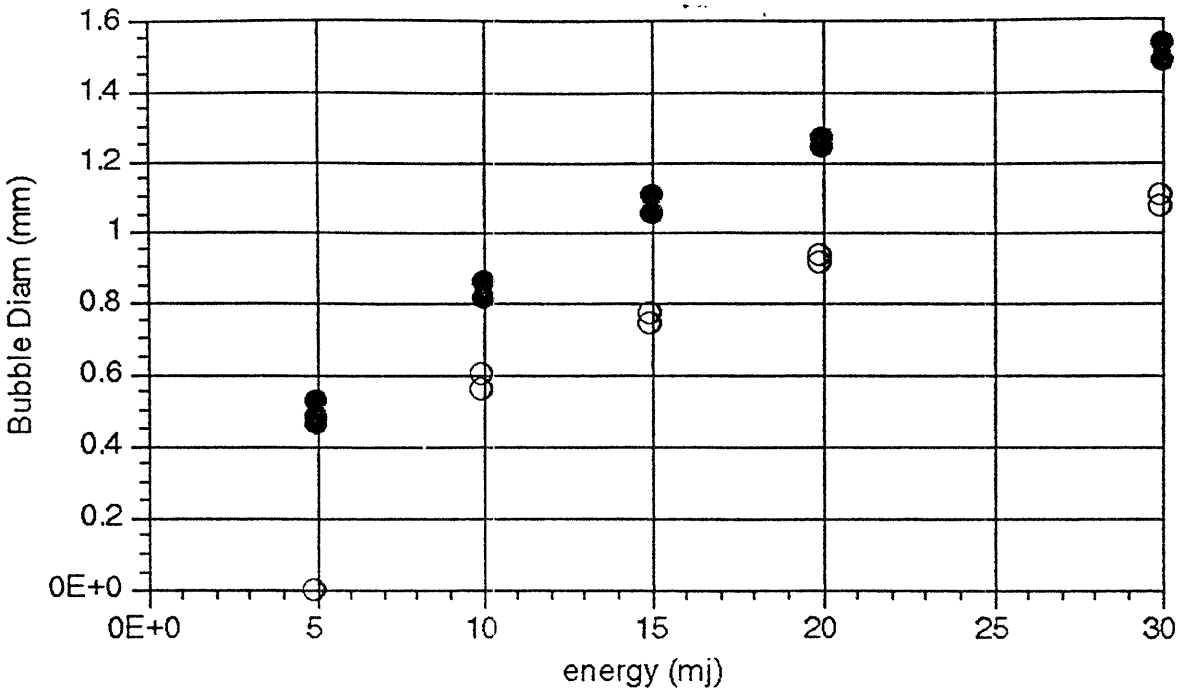

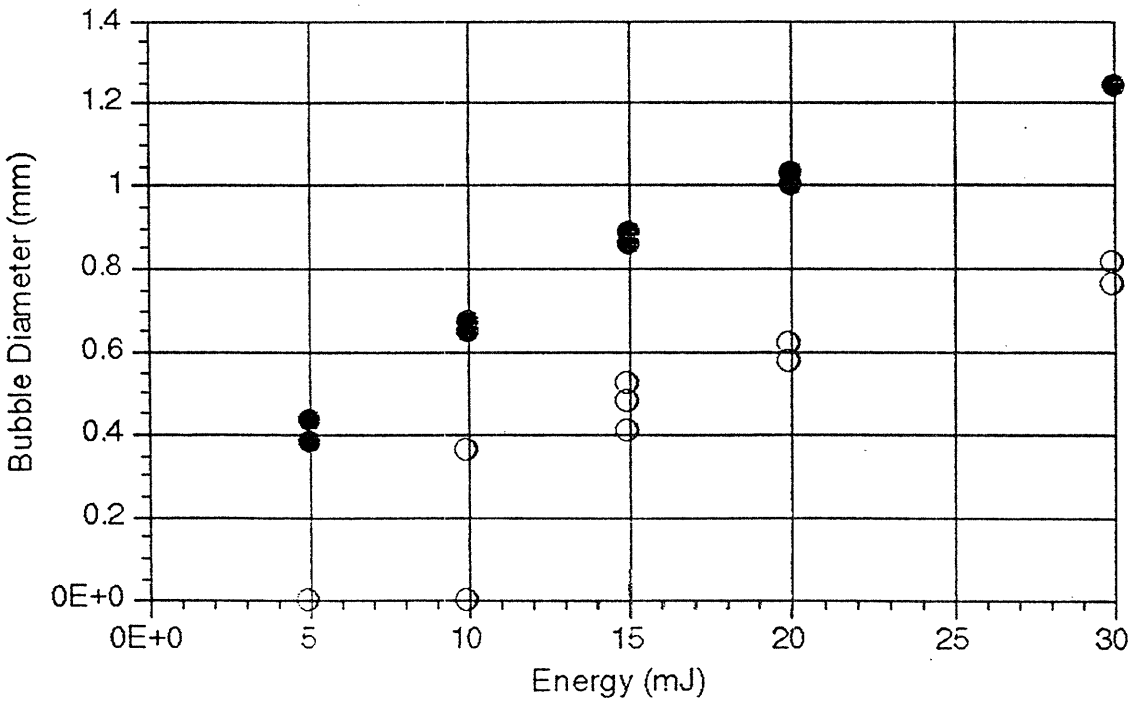

Figure 15. Bubble diameter as a function of laser energy comparing a 1 usec laser pulse, dark circle, and a 20 usec laser pulse, open circle. The top plot represents a whole blood media with HCT = 21%, the bottom a whole blood media with HCT = 11%.

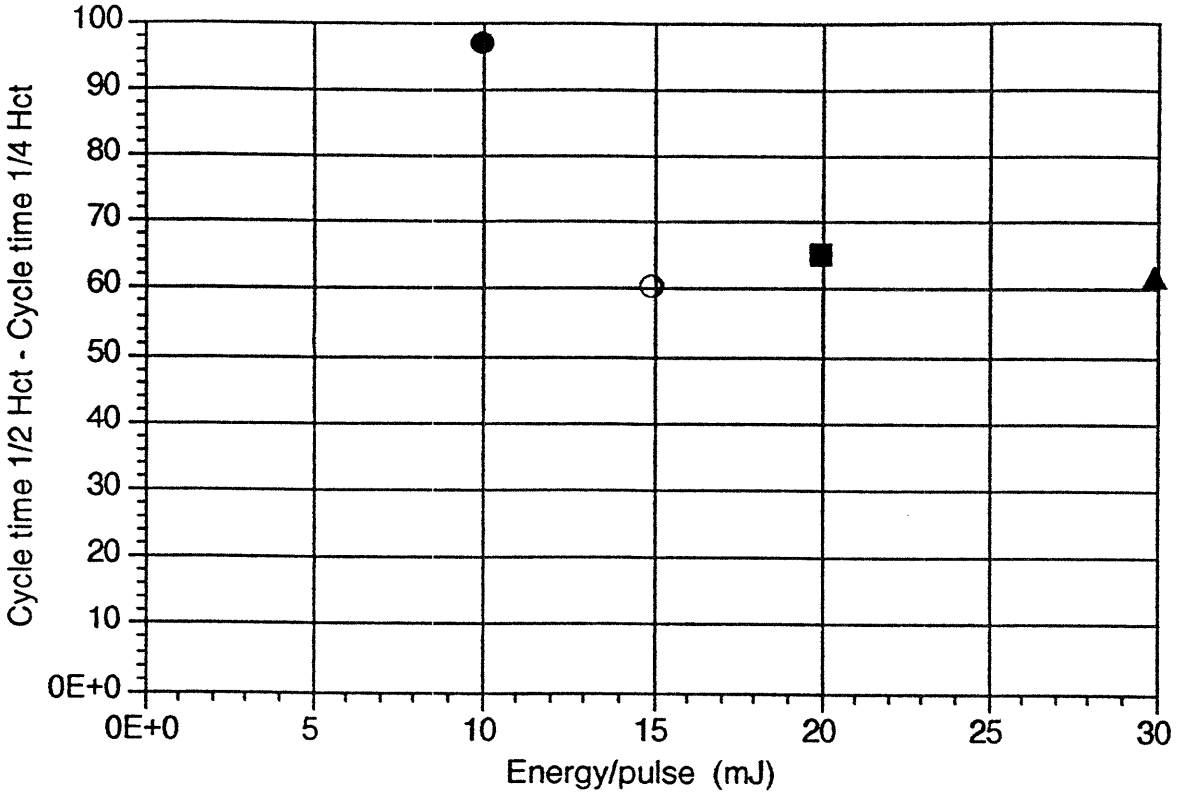

Figure 16. Plotted is the difference in cycle time for two hematocrits versus laser pulse energy for a 20 usec laser pulse. Unlike the 1 usec laser, the difference here is relatively constant. The first point reflects that the 1/4 Hct system was subthreshold at that energy.

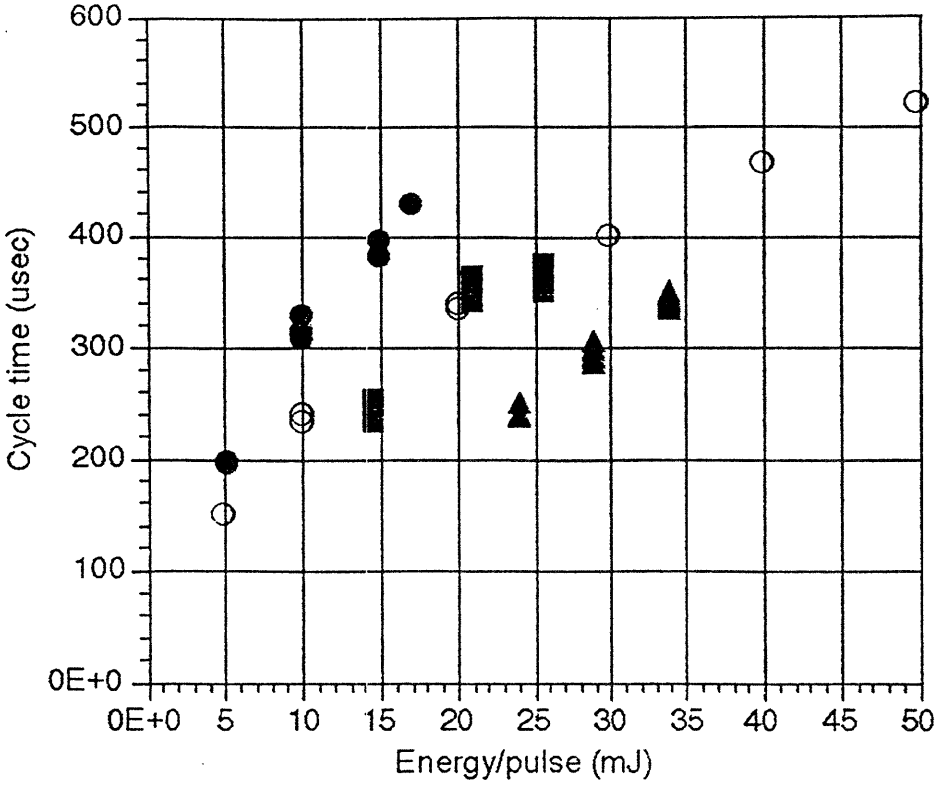

Figure 17. The relationship between cycle time and pulse energy for various laser systems is shown. Darkened circle represents the solid fiber excimer (XeCl), open circle the solid fiber pulsed dye laser, the box represents the 1.6mm multi-fiber system and the triangle represents the 2.0mm multi-fiber system.

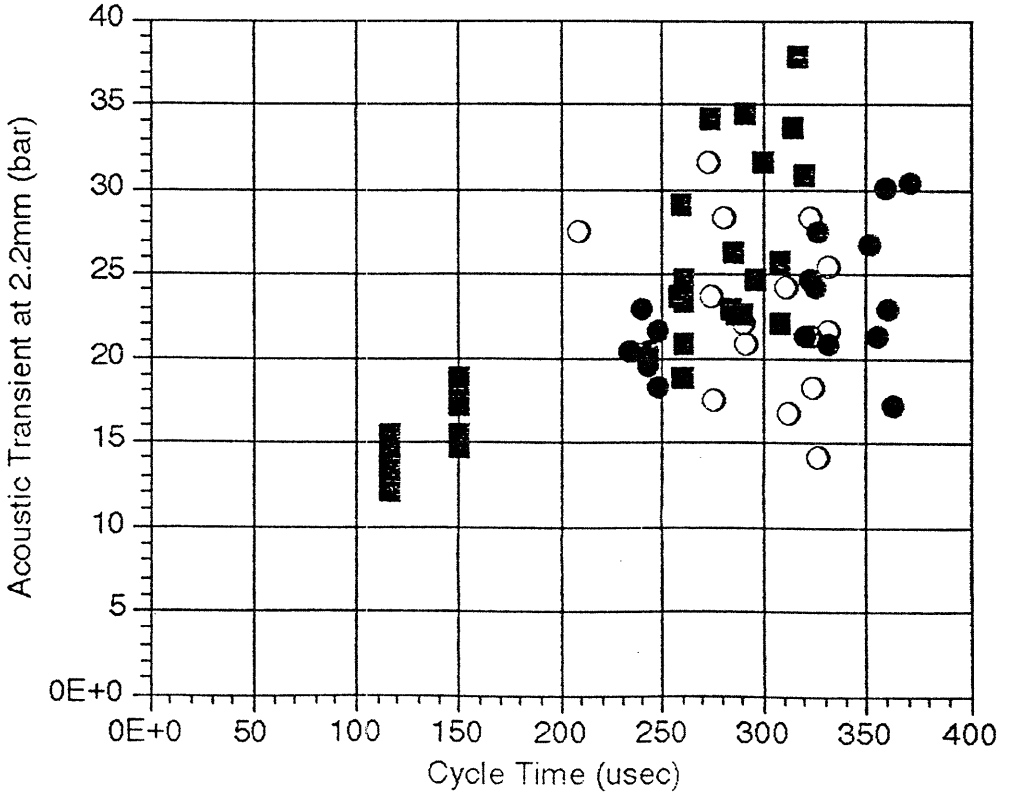

Figure 18. The acoustic transient generated upon bubble collapse measured 2.2mm from the tip of the fiber system. Boxes represent the 1.3mm excimer system, dark circles represent 1.6mm excimer system, and open circles the 2.0mm excimer system.

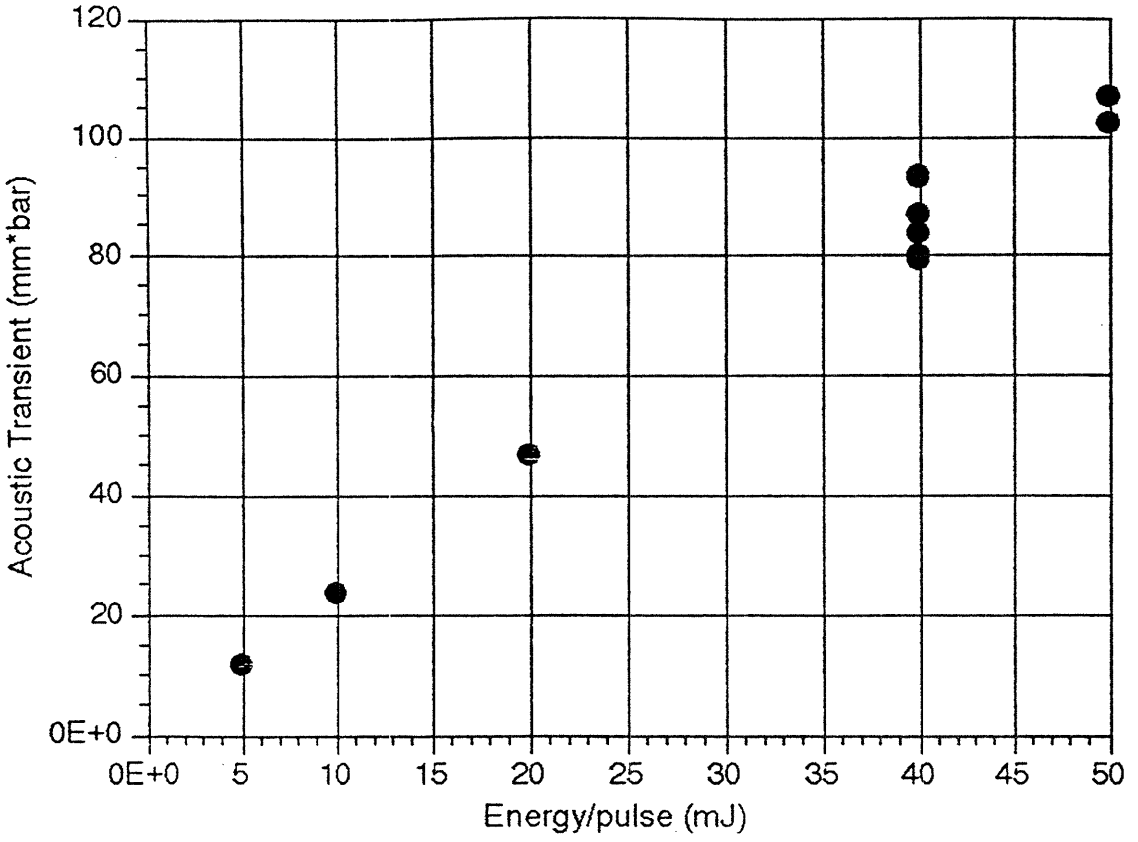

Figure 19. Shown is the initial acoustic transient as a function of laser pulse energy for the 1 usec solid fiber system.

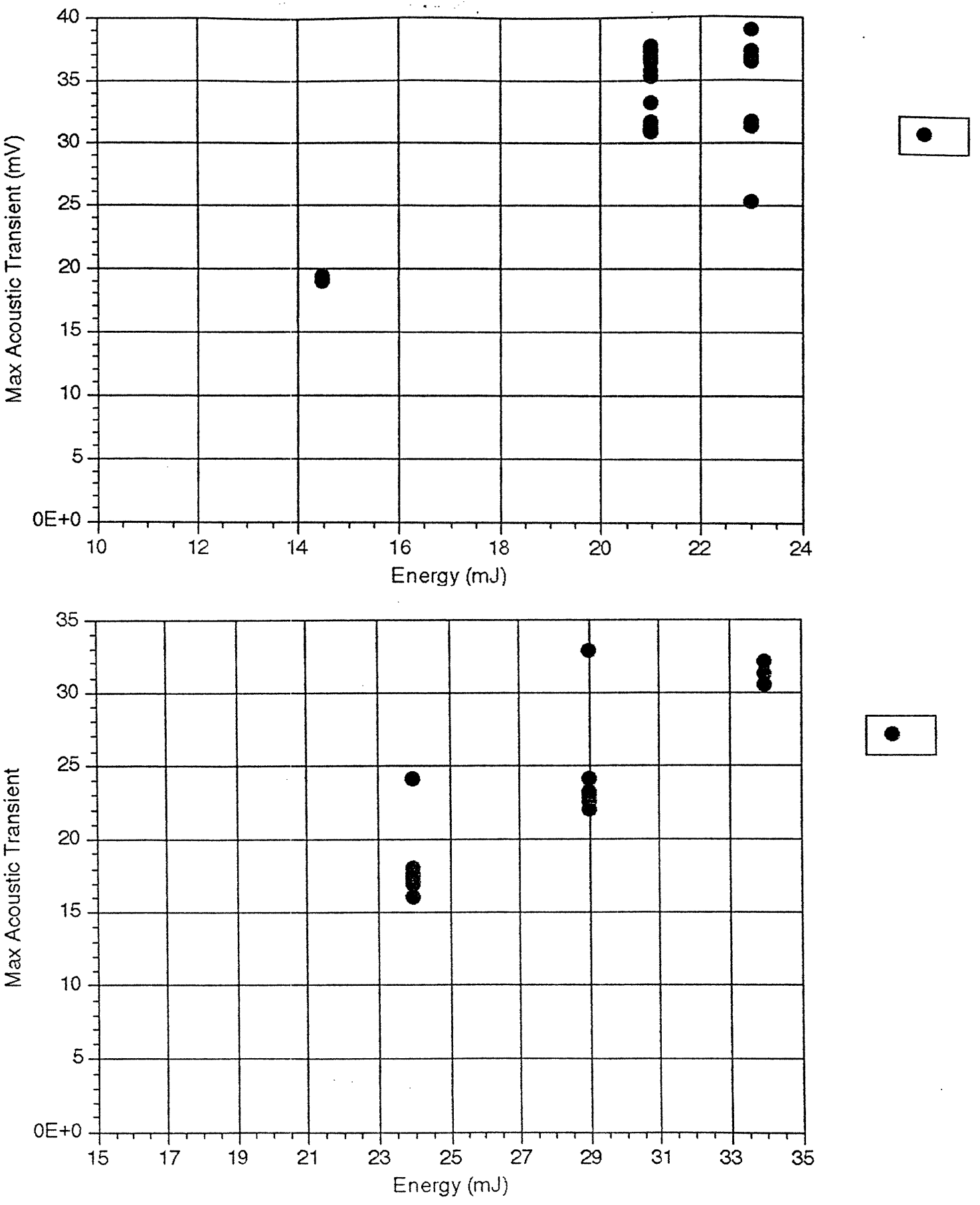

Figure 20. Shown is the initial acoustic transient as a function of laserpulse energy for the 1.6 mm (above), and the 2.0 mm AIS excimer multi fiber systems.

Cavitation induced perforation

Shock waves, laser vaporization of vessel walls, and/or mechanical trauma interaction are often blamed for the 1-2% risk of perforation seen in coronary laser angioplasty.[19] Shock waves and light incident on tissue, however, may not be significant components in the pulsed dye and excimer systems studied. Shock waves require a laser pulse intensity greater than that seen with these systems and laser/tissue interaction leading to perforation is difficult to imagine with a coaxial fiber surrounded by blood, a potent absorber. Laser induced cavitation, however, is a formidable phenomenon within this context. Cavitation-caused perforation, although never studied, can be postulated from clinical antedotes. The second pass phenomenon relates an increased risk of perforation when a second pass is made through a stenosis that has already been traversed once. Hence, this study addresses the question: Is laser induced cavitation sufficient to cause perforation.

Methods

Five New Zealand white rabbits were induced and maintained anaesthetized using 2:1 Xylazine:Ketamine im titrated to a corneal reflex. A ventral midline incision was used to expose both common carotid arteries. All loose areolar and connective tissue was then removed by sharp dissection. Double loop O silk was used to gain both proximal and distal control. A twenty-one gauge angiocath with

attached connector was then inserted as proximal as possible but distal to the control loop. A 320 um laser fiber was then introduced via the angiocath to a midpoint in the isolated carotid segment. The fiber was manipulated in an attempt to place it in the center of the carotid lumen. In six carotid arteries, blood flow was undisturbed, and in two carotids the blood field was cleared using saline flush. The carotid artery was maintained moist through the application of extravascular saline. Lasers pulses were then applied in a step wise fashion: using 5, 10, 15, 20, 25, 30 mJ pulses from a 1 usec pulsed dye laser with a wavelength of480 nm at an approximate repitition rate of 1 Hz. Ten pulses were applied at each energy level. If no perforation was noted the energy per pulse was increased and the application repeated. The laser fiber was not repositioned. Perforation was determined at the point of blood extravasation.

Results

Initial common carotid artery diameter was found to be on average 2.16, with a range of 2.0 -2.2. In all cases of a blood filled lumen (n=6), clear and visible extravasation of blood occurred at a pulse energy of 20 mJ and within 5 pulses of initiating exposure at that energy. In several rabbits, blood was seen to splatter through the arterial wall at energy levels that did not induce perforation, ie no blood was seen to extravasate when lasing was discontinued. The 20 mJ pulse corresponds to a cavitation bubble radius of approximately 1.5 mm, with a 15 mJ pulse corresponding to approximately 1.3 mm.

No clear extravasation of blood or splattering of blood was noted in the saline filled arteries at any laser pulse energies (n=2).

Discussion

This experiment vividly illustrates that forces due to cavitaion alone, without laser/tissue interaction, can induce perforation. In all cases of blood field laser pulsing, perforation occurred at the same pulse energy. Yet, in the saline field, where laser/tissue interaction would be at a maximum, there was no perforation. We also see that shock waves need not be generated to perforate a vessel wall. In all cases, energies were well below that needed for plasmas initiation.

The occurrence of perforation at a characteristic bubble diameter leads one in the obvious direction of a vessel diameter dependent perforation threshold. The link to perforation established, we are left to determine which associated feature of cavitation causes perforation. Preceding and following a cavitation phenomena, as we now know, are two intense acoustic transients. As is detailed in the preceding section, these may possess very high peak pressures, upwards of 300 bar 1 mm away from the cavitation bubble foci. Also the radial expansion of the vapor bubble itself may possess more of a force than the wall can maintain. Assuming a very small resistance to motion, calculations imply a transient increase in diameter of over 1mm (approximatley 35%). A third possibility is jet formation from an asymmetric bubble collapse. As cavitation bubbles expand, if one side is impeded relative to the other, an asymmetric expansion culminating in a toroid like jet can ensue. The fluid velocity in this jet

can reach velocities of 30 m/s. A picture of this from Nyborg is shown below.

Also indicative of the trauma inflicted upon a blood vessel, is the high speed ejection of blood that occurs through the vessel wall. This may explain the "blanching" of the myocardium one sees subsequent to coronary laser angioplasty. In this blanching phenomena, contrast agent is impregnated in the myocardium subsequent to laser angioplasty. To the unsuspecting observer, this looks remarkably like extravasation of dye. To put it all together one needs but to remember that contrast dyes have a very high absorption coefficient in the ultraviolet, were most of today's clinical systems operate. Hence, cavitation in a contrast medium may ensue In any case, this forceful ejection of blood, although not yetexplored, is unlikely to be beneficial to the arterial wall.

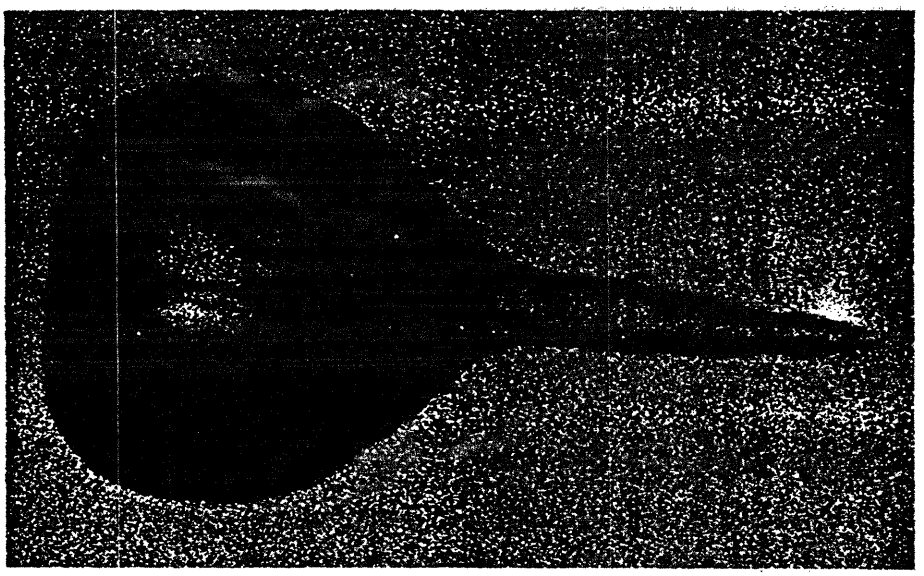

Collapse of a cavity near a solid boundary. The boundary is on the edge of the photograph on the side of the jet. (From Lauterborn, ref 9).

Clinical Suggestions

These studies indicate intravascular cavitation should be minimized. One way of limiting cavitation is to decrease the absorption coefficient of the medium. This can be done by choosing an appropriate wavelength of light or by changing the properties of the medium. Many wavelengths of visible light have absorption coefficients well below the UV absorption coefficients (for blood) and hence decrease cavitation. This approach, however, needs to be evaluated in the context of laser/plaque interaction. Another approach is to change the properties of the medium. As shown, decreasing the Hct would increase the threshold for cavitation. This effect, however, is decreased due to the inhomogeneous medium effect described above. Hence, saline flushing would have to be substantial. If this compromises oxygenation, lysed blood (possibly diluted) could be infused through the central lumen of the catheter. If the blood lysis occurs inside the lumen of the catheter total oxygen delivery is not changed; the inhomogeneity component, however, is decreased.

Multi-fiber delivery systems are also advantageous in that they produce oddly shaped bubbles. These bubbles tend to have less violent collapse than cavitation bubbles produced by single fiber systems.

A third way of decreasing bubble size is to increase optical divergence. By having large cone angles, the dependence of absorption coefficient is magnified. The effect upon ablation would could be controlled by choosing a wavelength with a high absorption

coefficient for plaque, and a lowered absorption coefficient for blood (this usually the case anyways).

Pulse duration could also be adjusted to decrease cavitation. This would decrease the thermal confinement in plaque ablation with short pulsed lasers, especially since pulses longer than the thermal relaxation of a red blood cell, approximately 15 usec, would be needed.

A scheme has been presented to minimize damage done by intravascular cavitation. In the next chapter we will see how intravascular cavitation can result in a beneficial outcome given the appropriate clinical scenario.

INTRODUCTION TO CEREBRAL VASOSPASM

Approximately 100,000 Americans a year are striken by a subarachnoid hemorrhage. These occur most often following rupture of saccular aneurysms or arterio-venous malformations and can have grave consequences. Of the patients that survive (approximately 75% 0 30-40% subsequently develop cerebral vasospasm. Cerebral vasospasm, the most common cause of delayed neurologic deficit following subarachnoid hemorrhage, represents a reduction in the caliber of intracranial arteries. This most often manifests one week after the subarachnoid hemorrhage and can result in wide varying deficits. The severity of these deficits, which can include cerebral infarction and death, is determined by the intensity of the spasm and the distribution of the affected arteries.[20]

Since its arteriographic discovery in the 1950's intracranial vasospasm has been the subject of much research. In the 1960's many believed it was only a matter of time before a pharmacologic solution to the problem would be found.[20,21] The search began with extensive research as to the possible mediators of vasospasm. Prostaglandins, serotonin, and catecholamines were but a few of the agents investigated. This search for a vasoactive mediator, however, has proven futile.[21,22,23,24] All known, vasoactive, blood born substances break down rapidly in vivo and must be present in large concentrations to produce spasm. Despite extensive investigation, a specific cause of cerebral vasospasm has not been identified. The current theory postulates that free oxyhemoglobin collects around a vessel and induces spasm. The associated clot is not only a source of

free hemoglobin but also of other breakdown products with significant spasmogenic properties.[25] The induced spasm is subsequently prolonged by the inability of nutrients in the cerebrospinal fluid to reach the adventitial aspect of the arteries. Since these vessels have no vasa vasorum, the cerebral spinal fluid is their only source of nourishment. Many believe the inability to supply nutrients, and subsequent ATP loss, causes a state analogous to rigor mortis.[20]

Therapeutic measures have also proven futile. Many agents, such as reserpine, aminophylline, nitroprusside, intracisternal papaverine, and calcium channel blockers have not been effective. Some have even attempted balloon angioplasty, with very limited results. Nimodipine, a calcium channel blocker once thought to hold promise for treatment, has had equivocal results at best.[26,27,28] Hence, the state of the field; a very grave phenomena with no true therapeutic alternatives.

LASER INDUCED VASODILATATION

The first observation of pulsed laser induced vasodilation came serendipitously during laser angioplasty studies on the rabbit femoral artery. Gregory et al noticed that while using a 480 nm, 1 usec, pulsed dye laser they would often get transitory vasodilation.[29] In this model, intended to study laser/tissue interaction, the laser fiber, a 320 um quartz fiber, was brought in via a side branch of the femoral artery and placed perpendicular to and in contact with the vessel wall. A train of up to 20 pulses were then delivered at varying energy levels. The vasodilation, usually occurring between 2.5 and 7.5 mJ/pulse was erratic with respect to the degree of dilatation (the increase in diameter) and the extent of dilatation (the length of artery dilated). Furthermore, perforation often occurred prior to vasodilation. This finding presented many unanswered questions: was pulsed laser induced vasodilation due to a light/tissue interaction or a light/blood interaction; was this technique applicable to vasospasm induced by means other than trauma to the artery; and could this be harnessed into a feasible modality for the treatment of cerebral vasospasm. It soon became apparent, as will be documented below, that laser induced cavitation was responsible for the vasodilation observed. Hence, the knowledge of cavitation gained through the investigations presented in the prior two chapters was used to enhance pulsed laser vasodilation and make it a viable tool for the treatment of cerebral vasospasm.

Thus was born the purpose of these investigations :

1) To establish that this phenomena does in fact occur and is not an artifact of the experimental procedure.
2) To determine which of the sequlae of laser/blood or laser/tissue interaction is(are) responsible for this effect
3) To establish the validity of this treatment within the context of a cerebral vasospasm model.
4) To generate a laser catheter design and optimize that design so as to cause vasodilation while avoiding perforation.

In this chapter I will deal with the four goals stated above. I begin by addressing the issue of pulsed laser/tissue interaction and pulsed laser/blood interaction. This was done using an in vitro investigation as delineated below. The applicability of this to a vasospasm model was then addressed using both in-vivo and in-vitro techniques. The last section sets out to determine which of the characteristics of pulsed laser induced cavitation is responsible for this vasodilation. This knowledge was then used to harness cavitation within the context of a new medical device that dilates vessels in spasm without exposing the vessel to other untoward effects.

Laser/Blood interaction as the mechanism in laser induced vasodilation: In-vitro treatment of a dog basilar artery in spasm.

Methods

Eight mongrel dogs were sacrificed by exsanguination under thiamylal sodium anesthesia and their basilar arteries subsequently harvested. All side branches were then ligated using 10/0 nylon suture. The vessels were then mounted in the in- vitro apparatus pictured in figure 4.1 using blunt 19G needles. The arteries were

perfused at a constant pressure of 120 mmHg using a modified Krebs solution containing: NaCl,118mM; KCl, 4.1mM; NaH2PO4, 1.54mM; NaHCO3, 24.9mM; MgSO4, 1.19mM; CaCl2, 2.54mM; glucose 5mM. The perfusate was maintained at 37 degrees C and at a Ph of 7.4 (by bubbling 5% CO2/ 20% O2/ balance N2 gas).

Upon mounting in the apparatus, autologous red blood cells were added to the luminal perfusate of six vessels in order to achieve an hematocrit of 40%. In the other two vessels, no autologous red cells were added and the vessels were continuously perfused with the modified Krebs solution. All vessels were simultaneously superfused with the modified Krebs solution and allowed to equilibrate for 20-30 minutes at which point the resting diameter was measured. Measurements were made using pictures obtained by a 35mm Nikon N2000 camera attached to an operating microscope. A high speed video camera was often used via the operating microscope to record the experiment.

Supernatant hemolysate (ultracentrifugation was carried out to remove cell debris) was then added to the Krebs solution to achieve a hemoglobin concentration equivalent to 0.5 OD units at 575 nm. This lysate solution was then used to superfuse the vessel with resultant vasoconstriction. After allowing 20-30 min for equilibration, spasm diameter was measured.

At this point a Dymed Spectrum Series 30310 pulsed dye laser of wavelength 480nm , pulse duration 1-2 usec, and a repetition rate of 1-2 Hz was used to deliver a calibrated laser pulse through a 320 micron quartz fiber. The distal end of the laser fiber consisted of a flat, fire-polished tip without convergent or divergent properties.

Pulse energy calibrations were done pre and post laser treatment using a Molectron power meter and a Tektronix 7934 oscilloscope. The fiber was placed coaxially within the lumen of the vessel with the distal end approximately at the midpoint of the vessel. Laser pulses were then given in a progressive fashion beginning with 2.5 mJ and advancing to 5.0 mJ, 7.5 mJ, 10.0 mJ, and 15.0 mJ if dilation had not been observed after 20 pulses at a given energy level. In the case of incomplete dilation the treatment was repeated without advancement of the energy level and the diameter reevaluated post treatment.

After treatment, arteries were observed for up to five hours. Following this period, the artery was perfused in situ with 1.5% glutaraldehyde and sent for histologic examination.

Results

Significant vasospasm was achieved with addition of lysate superfusate. Mean diameter was seen to decrease from 1.1mm (range 1.01-1.26mm) to 0.77 mm (constriction to 70% of baseline, range 55-84%).

In the two vessels perfused with Krebs solution alone, no dilation was noted.

In vessels perfused with a 40% Hct equivalent, bare fiber vasodilation resulted in a mean diameter increase to 83% of control. Energy required to achieve some degree of vasodilation varied from 2.5 mJ to 10 mJ. Vasodilation also varied qualitatively and was comprised of: 1)Partial dilatation, in which dilation was uniform but qualitatively not back to resting diameter; 2) Complete dilatation, in

which dilation was to baseline or suprabaseline levels; 3) Segmental dilatation, in which dilation occurred in specific segments of the artery; and 4) Global dilation, in which dilation to baseline occurred. (see fiqure 4.2). Three vessels were perforated (at energies of 10, 10, and 15mJ) in attempting to achieve global, complete dilation . Table 4.1 details the number of pulses, energies per pulse, and dilation observed. One vessel was challenged with serotonin, 50% K physiologic saline, and substance P following complete dilation. Appropriate vasoactivity was demonstrated in this vessel with adequate vasoconstriction (Vessel # 5). All other vessels were observed for five hours, during which time there was no return of spasm. With global response, vasodilation was seen to progress in a bi-directional stepwise fashion as shown in figure 4.3. It was also observed that responding vessels dilated within the first 5-6 pulses at a given energy. Continued pulse trains, at a given energy, did not result in a diameter change. Light microscopy revealed no damage in treated, non-perforated vessels as compared to control. SEM's showed no endothelial denudation.

Discussion

This study demonstrates the need for laser/blood interaction to produce pulsed laser dilation of vasospasm. As discussed at length in chapter two, this interaction consists of the formation of a cavitation bubble and the sequelae associated with this. Vessels treated in a saline field, maximizing laser tissue interaction, showed no response.

In the six intravascular applications in which a blood field was present, vasodilation was achieved using pulse energy levels of 2.5 to 10 mJ. These pulse energies, in an unconfined environment, correspond to cavitation bubbles of 0.6 and 2 mm, respectively. In these experiments, vasodilation was seen to progress through a stage of partial or segmental dilation at a lower energy level with subsequent complete dilation at a higher energy level. The initial segmental dilation was in the area surrounding the fiber. In most cases dilation progressed bi-directionally away from the fiber tip in a very mechanistic, stepwise fashion. Also, the final state of an artery at a given energy level was usually observed after only 5-6 pulses given at 1.2 to 2 Hz, with subsequent pulses having little vasodilatory effect. Thus an energy dependent dose response was manifested. As bubble dimensions increased, the amount of dilation also increased. Hence in looking for mediators of cavitation, events associated with cavitation need to explored. These include: 1)Acoustic transients; 2)Radial bubble expansion; 3) Hydraulic wave generated from the displaced fluid; 4) Active byproducts generated by blood vaporization. These events will be discussed below.

The high rate of perforation, 50% (3 of 6), within this set of experiments was, however, a great cause for concern. This concern is magnified in the setting of acute subarachnoid hemorrhage with an obviously weakened vessel. Perforation was seen to occur at pulse energies of 10 to 15 mJ. In each case, partial or segmental dilation had been observed prior to perforation, but total dilation had not. Thus, the energy for perforation was found to overlap with the energy for dilation, resulting in a dangerously narrow therapeutic

window. On examination at least one of the perforations occurred at the site of a small side branch whose take-off was situated adjacent to the fiber tip. The etiology of perforation and vasodilation is further discussed in the conclusion.

Vessels were observed for up to five hours with no regression to vasospasm noted. This is important in the setting of cerebral vasospasm which can last for up to several days. To properly evaluate the clinical efficacy of this treatment, a study containing long-term follow-up is necessary.

Post treatment vessels showed no sign of morphologic or pharmacologic compromise. Pharmacologic responsiveness was tested in one vessel demonstrating preserved response to substance p and serotonin. Histologically, no significant evidence of damage as compared to controls was noted. No signs of thermal injury, endothelial denudation, acute thrombosis, or intracellular damage was noted in successfully treated vessels. In vessels perforated secondary to intravascular application, intramural hemorrhage, vacuolization, and scattered tissue carbonization accompanied the transmural disruption.

II. Extravascular application of laser light.

Methods

Two dog basilar arteries were excised and mounted as expressed above. The distal tip of the laser fiber was placed at a controlled distance from the basilar artery and the field filled with saline. Pre and post treatment diameters were measured as

described above for the in-vitro experiments. Video footage was obtained.

Eleven New Zealand white rabbits weighing 2.5-3.5 Kg were subjected to two intra cisternal injections of autologous blood in the "two-hemorrhage" subarachnoid hemorrhage protocol developed by Baker et al. Anesthesia was induced in these animals using 2-4% Halothane by mask with ketamine hydrochloride 40-60 mg/kg im and maintained using 1-2% Halothane GET .

In these animals, as well as three in which SAH was not induced, the basilar artery was transclivally exposed. Anesthesia was maintained during the procedure with pancuronium bromide 0.25-0.5 mg/kg/hr and 1% Halothane/ 70% NO/ balance O2 GET. Ventilation was maintained with a Harvard Apparatus small animal dual phase respirator. End-tidal CO2 was monitored continuously and maintained between 38 and 42 mmHg. The transclival approach consists of placing the animal in a stereotactic head frame and using a dental drill to perform a clivectomy through a ventral midline incision (pharynx and trachea reflected). The 11 animals with induced SAH were irrigated with warm ringers and the clot removed. In the remaining three animals autologous lysate, prepared as described above, was applied to the basilar artery. Six of the SAH rabbits and all of the acute rabbits received laser treatment as described below.

A Dymed pulsed dye laser, 480 nm, 1-2 usec pulse duration, was used to generate a laser pulse into a 320 micron laser fiber calibrated to 2.5 -15.0 mJ. The distal tip of the laser fiber was placed at a controlled distance from the basilar artery and the field filled

with saline. Pre and post treatment diameters were measured as described above for the in-vitro experiments. A train of laser pulses was applied to spasm arteries using the same method as described above. The fiber was not moved unless complete dilation was seen confined to an area of the artery adjacent to the fiber tip. Qualitative determinations as to the form of dilatation (global, segmental, partial) were also made at this time. Number of pulses as well as energy used were recorded as was documentation of any extravasation of blood. Following treatment, the vessels were perfusion fixed using 1.5% glutaraldehyde solution and sent for histological examination.

Results: Extravascular application of laser light.

Acute application of lysate to three in-situ basilar arteries resulted in a mean spasm to 81% of control. Complete dilation without perforation occurred in two of the three animals, at 2.5 and 5.0 mJ per pulse. The third animal was noted to have extravasation of blood at the point of treatment, usually compatible with perforation. On inspection, however, extravasation was not seen and it was felt to have originated from a very small side branch that had quickly sealed. Treatment resulted in a mean post treatment diameter of 106% of control. All dilatation was global and complete in nature.

Degree of spasm in the rabbit two bleed model was not documented on an individual al basis but was assumed to be approximately 70% of control based on previously published studies

incorporating this model. Complete dilation was observed in all rabbits (6) at 5.0 mJ per pulse, with two rabbits exhibiting partial dilation at 2.5 mJ per pulse. Perforation was seen in three rabbits. In two of the three, placement of the laser fiber within 0.5 mm led to perforation from fiber puncture of an expanding artery. In the third rabbit, perforation occurred secondary to rupture of a small side branch. In two rabbits, initial treatment resulted in segmental dilation. Relocation of the laser fiber with subsequent treatment of the undilated segmented resulted in global dilation. Animals were observed from 1 to 5 hours with no return of spasm noted during this time. No regression of spasm was noted in the control group during a 5 hour observation period. As before, it was observed that responding vessels dilated within the first 5-6 pulses and that continued pulsing, at a given energy, had no further effect. Light microscopy revealed no damage in treated, non-perforated vessels as compared to control. SEM's showed no endothelial denudation.

Discussion

Extravascular application of laser light resulted in an average dilation of 53% over the spasm diameter, again showing the efficacy of pulsed laser induced vasodilation in treating cerebral vasospasm with an established model. Since the thin basilar vessel wall does absorbs little light, effectively transmitting the incident pulse to the blood filled lumen, laser/blood interaction is again evidenced as the key component in this procedure. Extravascular application did result in a more segmental vasodilation with two of the in-situ arteries

requiring a shift in fiber position to achieve global dilatation. Dilation was seen to progress bi-directionally. Stepwise dilation, however, did not occur in these experiments. Unlike the in vitro investigations above, the basilar arteries were covered by connective tissue. Although an attempt was made to remove all of the connective tissue this was not always possible and undissected tissue often remained, impinging upon the artery and possibly inhibiting the progression of dilation.

Of the arteries treated, both of the in-vitro arteries and three of the six in-situ arteries were perforated during the course of treatment. One of the in-situ arteries demonstrated a method of perforation not previously seen. The perforation occurred at a side branch opposite the point of light application. It appeared as if a very high shear force had torn the side branch from its insertion. In at least three of the other four arteries, perforation probably occurred from impalement of the radially expanding artery onto the laser fiber. In these cases, the arterial wall was found tethered the laser fiber. Since dilation of the vessels was not of sufficient magnitude to reach the fiber, one must assume a transient superdilation secondary to the cavitation bubble. In other words, the bubble extended the artery beyond its physiological diameter, reaching and impaling the fiber, and then subsequently collapsed with the artery returning to a dilated but much smaller diameter.

Histologic studies seemed to indicate a different mechanism of perforation than that for intravascular application. Lack of thermal or endothelial injury surrounding the perforation site indicate an

extra to intra vascular perforation. As above, no focal histologic abnormalities were noted.

Summary and Discussion of Bare Fiber Vasodilation

These two investigations demonstrate the validity of using pulsed laser vasodilation to treat cerebral vasospasm. Both animals models use lysed blood to initiate spasm, simulating the clinical scenario. We see that pulsed laser vasodilation is a true and viable phenomenon, which reverses vasospasm induced by lysed blood as well as trauma. Hence, these studies address two of the four goals (1 and 3 below) outlined above:

1) To establish that this phenomena does in fact occur and is not an artifact of the experimental procedure.
2) To determine which of the sequelae of laser/blood or laser/tissue interaction is(are) responsible for this effect
3) To establish its validity in treating vasospasm within the context of a cerebral vasospasm model.
4) To generate a laser catheter design and optimize that design so as to cause vasodilation while avoiding perforation.

Further validation of this treatment came from MacFarlane et al. They investigated bare fiber vasodilation using a carotid artery spasm model (the same model used in the next chapter), and found it to be highly effective in reversing vasospasm. In that study, treatment resulted in dilation to 83% of control (n=40), with applied energy ranging from 5 to 10mJ/pulse. They found perforation to be highly dependent on the proximity of the fiber to the vessel wall, with an average of 4 8mJ pulses causing perforation when the fiber

was in contact and 33 8mJ pulses required when it was in the lumen but lateral to the midline. They also found a very high incidence of post treatment intimal hyperplasia, nearly 100% at 60 days. This study was quite different from previous investigations in that an energy of 10 mJ was set as a maximum regardless of the degree of dilation. While limiting energy was effective for the small range of artery diameters tested, it is not practical to assume it would treat all vessels of any diameter. Hence, MacFarlane et al further established the validity of this treatment, while demonstrating a need to reduce the risk of perforation as well as intimal hyperplasia.

In order to increase the safety of the procedure we must determine which sequelae of cavitation is responsible for dilation, perforation, or both. These include:

1) generated acoustic transients,
2) radial expansion of the cavitation bubble,
3) free radicals generated via blood vaporization,
4) jet formation on bubble collapse,
5) hydraulic wave from the fluid displacement seen in cavitation.

for perforation we can add:

6) Laser/vessel wall interaction.
7) Fiber impalement of the wall

Furchgott first described light induced smooth muscle relaxation over 35 years ago. He found that low levels of continuous light resulted in a slow relaxation lasting as long as the continuous light source remained active. Subsequent studies have shown this phenomena to be heavily dependent on intensity as well as wavelength. This phenomena, however, is quite different from that

observed here. The high absorption coefficient of blood and the coaxial light delivery make light/tissue interaction highly unlikely if not outright impossible. Furthermore, Furchgott's phenomena involves CW laser light, not pulsed, and has completely different temporal characteristics. This, combined with the bi-directional, stepwise propagation of dilatation make direct tissue/light interaction unlikely. This interaction, however, could still play a significant role in perforation. The signs of thermal injury present in perforations occurring with intravascular application of laser light support this link.

The prospect of a free radical mediated vasodilation was also considered. The mechanistic fashion in which dilation occurs as well as its bi-directional spread in the face of a constant unidirectional flow make this an unlikely mediator. Furthermore the volume of blood vaporized is so small, it is difficult to imagine how it could affect such a large area in the time frame considered (microseconds). Ziskind et al, however, investigated this possibility and found that free radical scavengers did not affect the induction or propagation of vasodilatation.[30]

Hence, we are left with cavitation related events as possible mediator(s) of vasodilation. My plan was to isolate the three most likely candidates: radial bubble expansion, acoustic transients, and the hydraulic wave through the use of to prototype devices. These devices would isolate the arterial wall from direct light/tissue interaction, from the fiber tip itself, from the radially expanding bubble and from the fluid jet possibly generated on collapse, respectively. One device, the hydromechanical vasodilator detailed in

the next chapter, generated the hydraulic wave while using distance and a non spherical bubble to diminish the acoustic transient and a catheter to shield the vessel wall. The second device would generate only an acoustic transient. Following highly successful trials with the HVD the second prototype was not tested.

Dog in-vitro	# of pulses	Energy /pulse	Dilation	Notes
1	23	5	C	
2	25	2.5	N	
	25	5.0	N	
	25	10	P, G	
	2 5	15	* *	perforation
3	20	2.5	P	
	10	5.0	C	
4	20	2.5	N	
	20	5.0	P	
	21	7.5	*	
	11	10	* *	perforation
5	20	<1*	N	
	20	1.5*	N	
	21	2.6	P	
	10	5.0	C	challenged
6	21	2.5	N	
	22	5.0	N	
	21	7.5	P,G	
	15	10	* *	perforation

Table 4.1 A summary of the number of pulses applied at each given energy and the affect of these pulses upon the in-vitro mounted dog basilar artery.

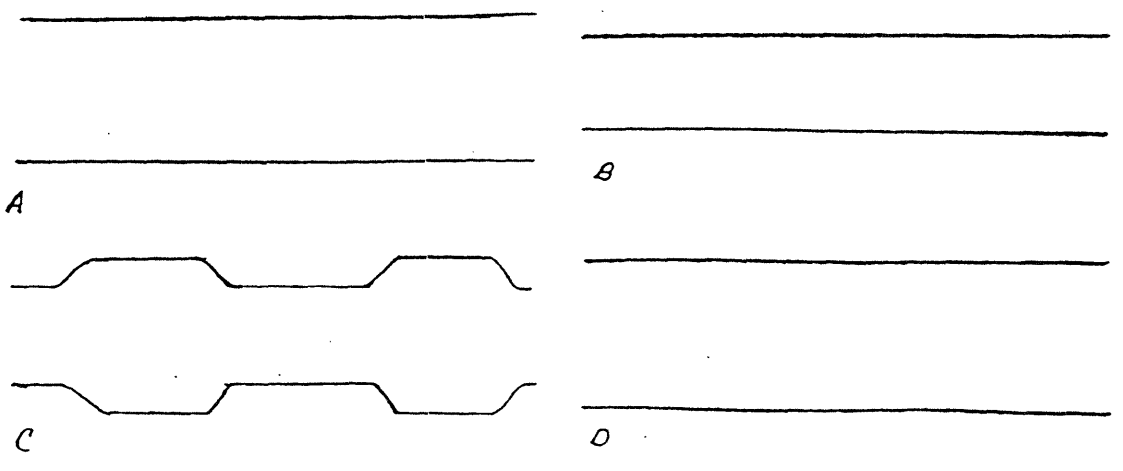

Figure 4.2 Definition of terminology used in qualitative assessments of vasocilation. A, baseline; B, partial; C, segmental; D, global.

HYDROMECHANICAL VASODILATOR

Design

A 200 micron quartz fiber was placed such that the fiber tip was localized 8-30mm within the distal opening of a 3 Fr catheter (Target Therapeutics Tracker-18 with an ID = 1mm). An engineering diagram is shown below. A 1 usec pulsed dye laser was used to create a cavitation bubble of theoretical volume 4.9 mm3. This cavity was used to create a hydraulic wave secondary to the displacement of non vaporized blood within the confines of the catheter. High speed photography was done to document the fluid mechanics of the device.

Method

A 1 usec pulsed dye laser, using 480 nm coumarin dye, was used to deliver a 20 mJ pulse within the confines of a 3 Fr catheter as described above. The lumen of the catheter was filled with heparinized human blood, Hct 46%, obtained from a willing investigator. The field surrounding the catheter was filled with distilled water. To this water, table sugar was added to match the index of refraction of the transparent container. The device described is shown below in figure 4.11. Positive pressure was maintained proximally at the site of blood introduction into the catheter preventing distilled water from entering the device. A photodiode was placed within the laser cavity of the 1 usec laser and the output was used to trigger a Stanford delay generator, model number DG

535. The output from the delay generator triggered a second 1 usec laser with a 588 nm wavelength output. This laser was used as a flash to capture 1 usec frames of varying delays. A wavelength of 588 nm was selected as the flash so as to enhance absorption of blood (peak hemoglobin absorption) and therefore better delineate its distribution and propagation. Delay times were calibrated using dual photodiodes. Pictures were taken with a Pentax, model K1000, camera equipped with a 60mm macro lens and a 2x magnification adapter. A 600 nm bandpass filter (bandwith +/- 40 nm) was placed in front of the camera lens to filter the 480 nm light pulse used to create the cavity.

Results of high speed photography: action of the HMV.

The hydraulic wave consisted of a fluid column, approximately 3 mm in length, propagating from the tip of the catheter. Cavity formation could be visualized within the catheter. At no time did the cavitation bubble exit the catheter. Cavitation bubble volumes were found to be approximately 50% less than predicted. This comes about due to increased work done in moving the fluid within a confined volume. Viscous drag also contributes to the time delay seen with the HMV. With the HMV, peak cavity volume occurs between 400 and 500 usec with peak fluid expulsion occurring at approximately the same time. The single fluid wave propagates in an over damped mode with a single oscillation. Fluid dynamic effects of the stream entering a still fluid medium cause the formation of a toroid at the leading edge of the wave. Based on the photographic measurements,

the wave had an average velocity of 5-6 m/s during the expansion. Complete collapse of the wave occurs approximately 1-1.5 ms following initiation. Therefore, if a pulse repetition rate of 2 Hz is used, there is no interaction between subsequent waves. No deformation of the catheter was noted.

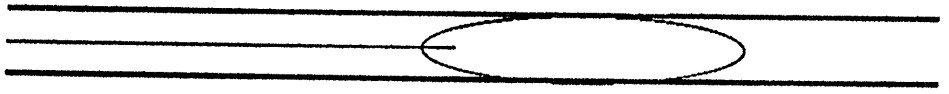

2r

L

Parameters:

1 usec
480 nm
pulsed dye laser

2 R

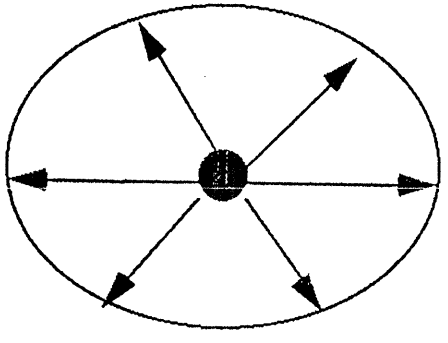

Figure 3.1 Schematic representation of the Hydromechanical vasodilator. Velocity and length of fluid column are given in the lower right hand corner.

Delay=120 usec after 1usec laser pulse.
Note cavity contained inside of catheter

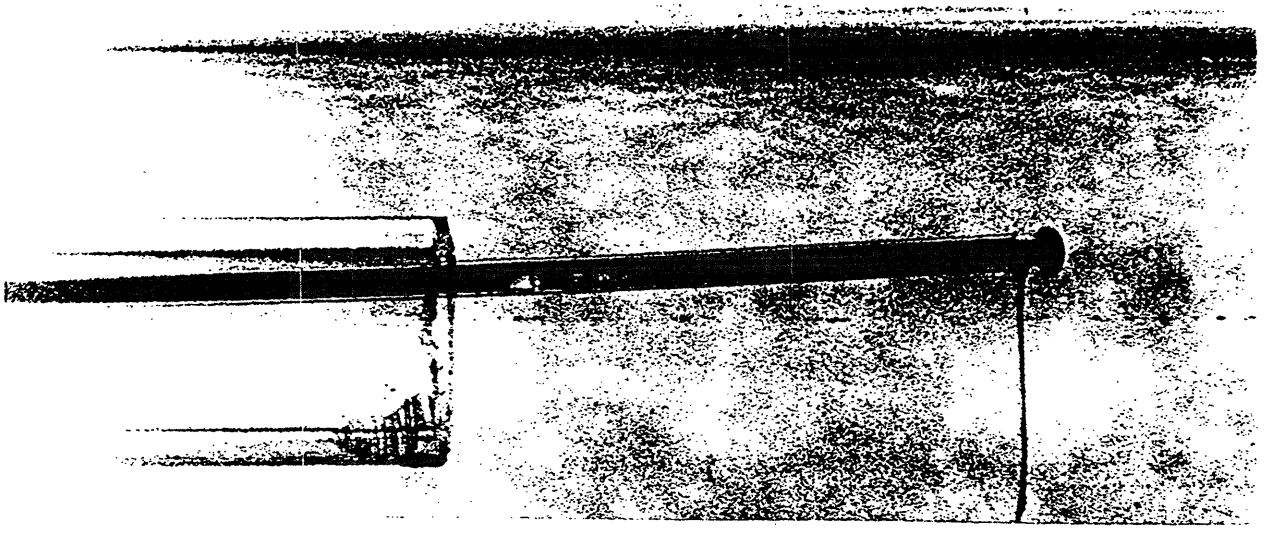

Delay=300 usec after 1usec laser pulse.

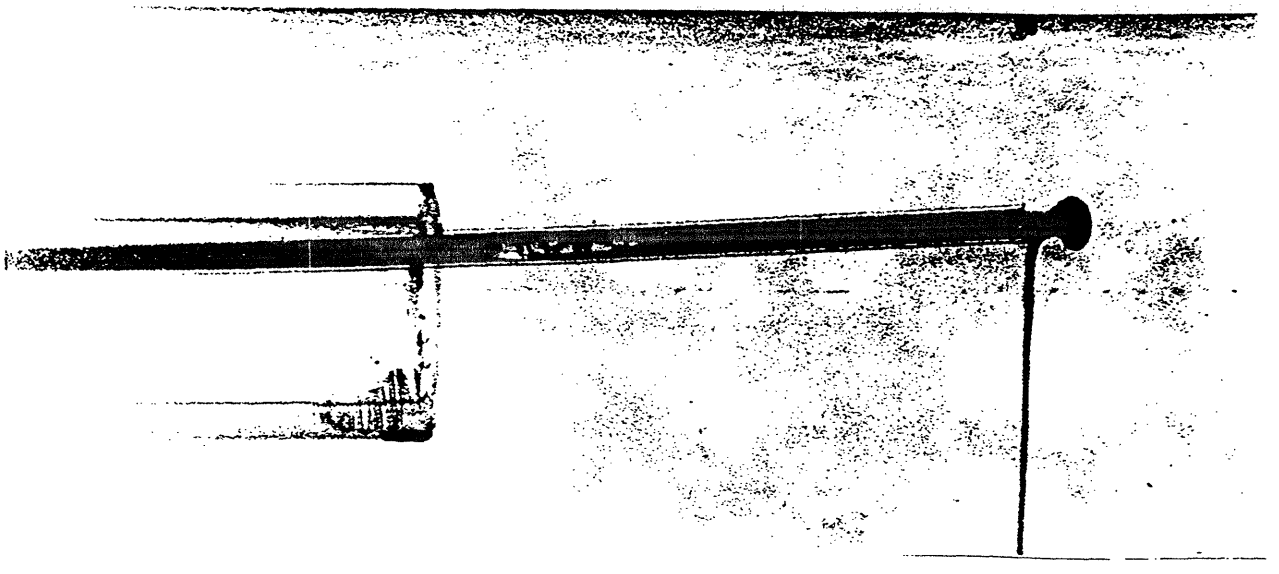

Delay=220 usec after 1usec laser pulse.

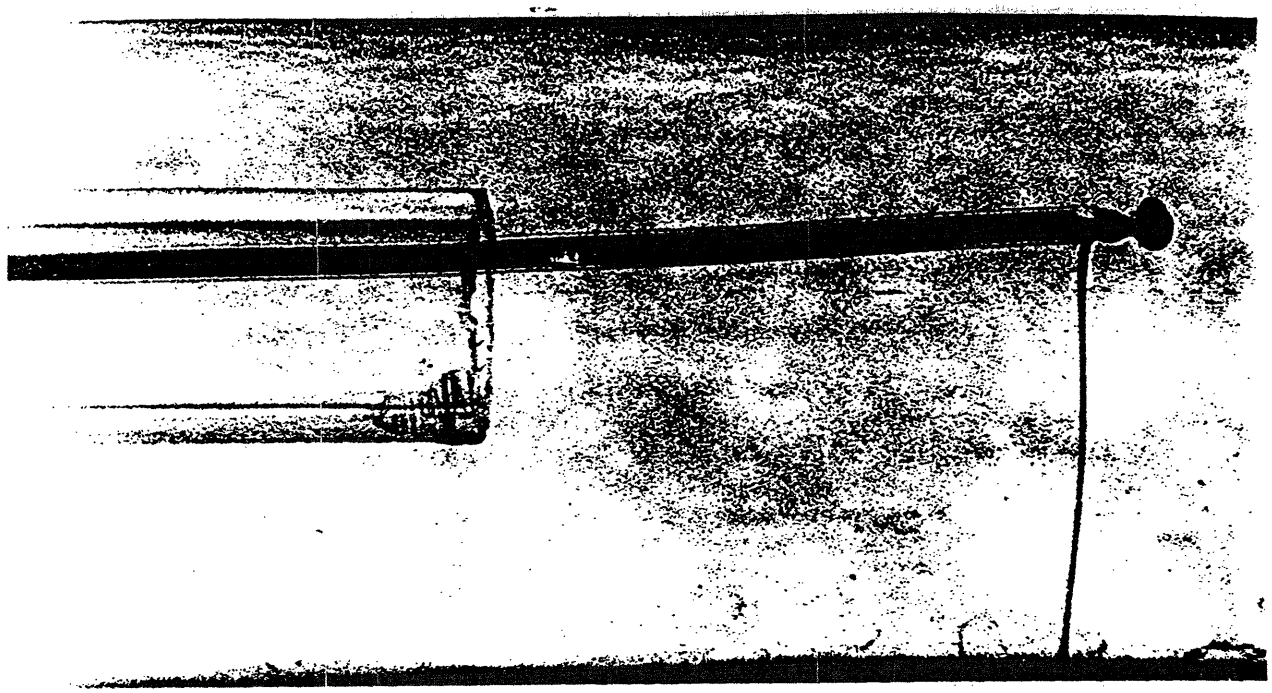

Delay=500 usec after 1usec laser pulse.

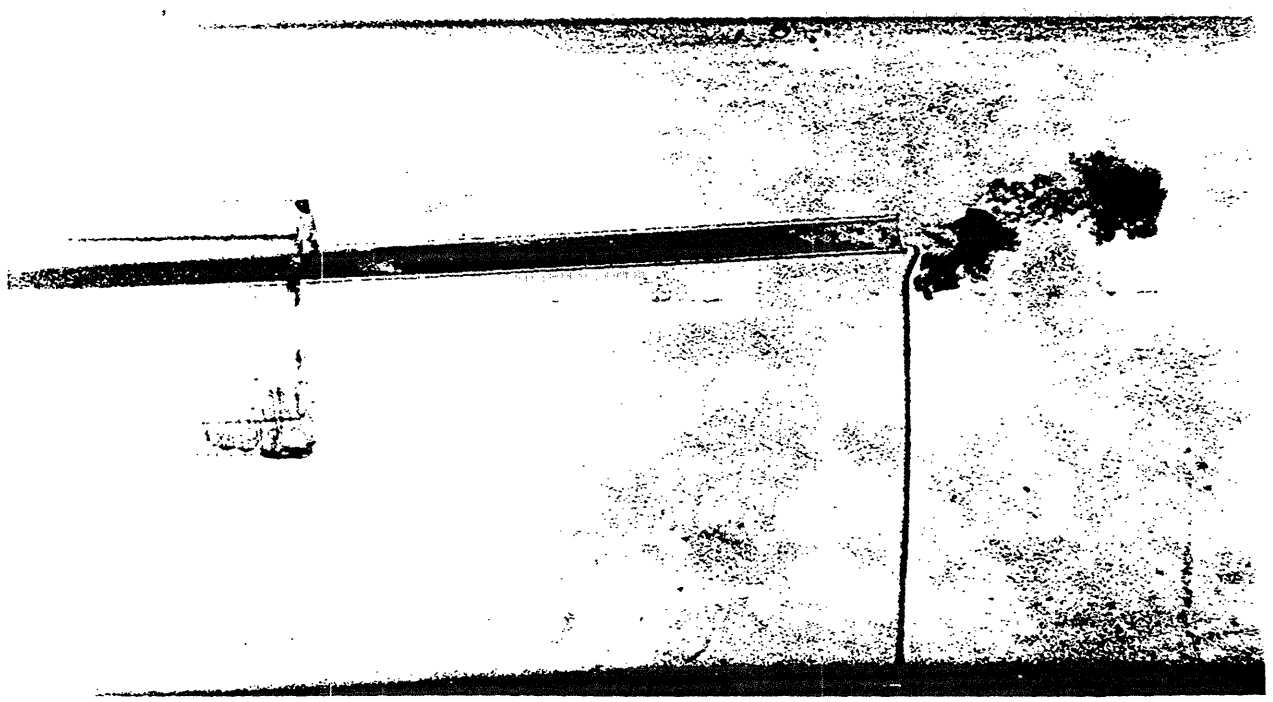

Delay= 2000 usec after 1usec laser pulse.

III. Vasodilation using the Hydromechanical Vasodilator

Methods

Ten New Zealand White Rabbits weighing 2.5-3.5 kg were anaesthetized using 4% Halothane mask and ketamine hydrochloride 30 mg/kg IM. Anesthesia was then maintained using 1-2% Halothane by inhalation. End tidal CO2 was monitored as above and maintained between 35-45 mmHg. Using a femoral cut-down under sterile conditions, a Target Therapeutics Tracker-18 catheter was inserted into the femoral artery and advanced fluoroscopically into the right common carotid artery. Selective carotid angiography was done using Renograffin-60 iodinated contrast dye. Angiography was then repeated, if possible, for the left common carotid artery. The catheter was subsequently withdrawn and the artery ligated. A ventral midline incision was then used to expose both common carotid arteries. All loose areolar tissue investing the vessel was cautiously removed. A three cm long strip of Dow Corning silicone tubing with an internal diameter of 2.6 mm was then placed around each common carotid artery. Copper wire, serving as an angiographic marker, was then placed at each end of the tubing. The space between artery and cuff was then filled with fresh non-heparinized investigator's blood (human). The animal was then allowed to recover.

The following day rabbits were anaesthetized as described above and recatheterized from the femoral stump. Angiographic evidence of spasm was obtained at this time. The prototype hydromechanical vasodilator (HVD) was then inserted via the

femoral artery and advanced fluoroscopically distal to the area of spasm. The HVD was then engaged at a repetition rate of 2 Hz and withdrawn through the area of spasm at a rate of approximately 1mm/s. After having passed the proximal copper wire marker (viewed under fluoroscopy) the HVD was disengaged and withdrawn. Repeat angiography was then performed.

Animals were then sacrificed using sodium pentobarbital overdose and the common carotid arteries excised after in-situ 1% glutaraldehyde perfusion via the ascending aorta. Specimens were then submitted to scanning and/or transmission electron microscopy.

Controls for this protocol were well delineated in a recent paper by MacFarlane et al and not repeated here. This is included in the appendix.

Results: Vasodilation using the HVD

Application of non-heparinized human blood within the silicone cuff resulted in an average decrease of 37.5% in lumenal diameter in 7 of the 10 carotid arteries. Three carotid arteries were found not to be in spasm. Following delivery of the hydraulic waves, arterial diameter increased by 48% over spasm diameter. Hydraulic waves delivered to the three vessels not in spasm had minimal affect on their diameter (mean decrease of 5.3%). (See figure 4.4). Also, the spasm diameter of the vessel was seen to have an inverse relationship with the degree of vasodilation. (see figure 4.5) Scanning electron microscopy did not reveal evidence of endothelial damage. No perforations were observed.

In all rabbits vasodilation was attempted using a 20 mJ pulse to create the cavitation phenomena and subsequent hydraulic wave. In four of the animals (rabbits number 6, 7, 9, and 10), a subsequent attempt at vasodilation was carried out using a 30 mJ pulse to create the hydraulic wave. Two of these rabbits (9 and 10) served as non spasm controls. In all but two rabbits, three and four, the cavitation phenomena was created 8 mm from the distal tip of the HVD. In these two rabbits the, the source of the wave was located at 10 and 30 mm, respectively.

Discussion

The HVD uses cavitation to generate a fluid wave. Even if one assumes perfect spherical geometry for bubble expansion and collapse, a highly unlikely assumption, the acoustic transient generated upon collapse would be between one and two orders of magnitude less than that expected from bare fiber vasodilation. As seen in the photographs, the cavity does not leave the catheter. Hence, the HVD protects the arterial wall from the radially expanding bubble, from possible jet formation, and from direct laser/tissue interaction. Using the HVD, we were able to achieve vasodilation without any perforations while varying the energy. In one rabbit, not included in the study, the power was continuously increased in an attempt to perforate the vessel. In this case, the fiber was ablated but the artery was not damaged. The HVD also has the added advantage of a more maneuverable distal tip as compared to the laser fiber. We are currently investigating other methods of

generating this hydraulic wave, such as ultrasound and spark gap technology.

As above, histologic studies have revealed no significant endothelial denudation or intracellular damage as compared to controls. One theory is that the HVD functions by mechanically disrupting the smooth muscle cells that are engaged in constriction. If one assumes a subset of irritable smooth muscle cells as the cause of cerebral vasospasm, we have a plausible explanation. No evidence of smooth muscle cell disruption, however, has been seen.

With the Hydromechanical vasodilator we achieve the last two goals of these studies: To determine which of the sequelae of cavitation is responsible for vasodilation, and to generate a laser catheter design and optimize that design to produce vasodilation while avoiding perforation. Since the completion of this work, a second HMV, with an outer diameter of 0.6mm (less than 2Fr), has been used to treat vasospam. This catheter size has enabled us to begin a 20 dog, two bleed subarachnoid hemorrhage model which involves catheterizing and treating the spasm basilar artery of a dog and long-term follow up to 60 days. If initial results are indicative of outcome, the HMV will be in limited clinical trials within a year.

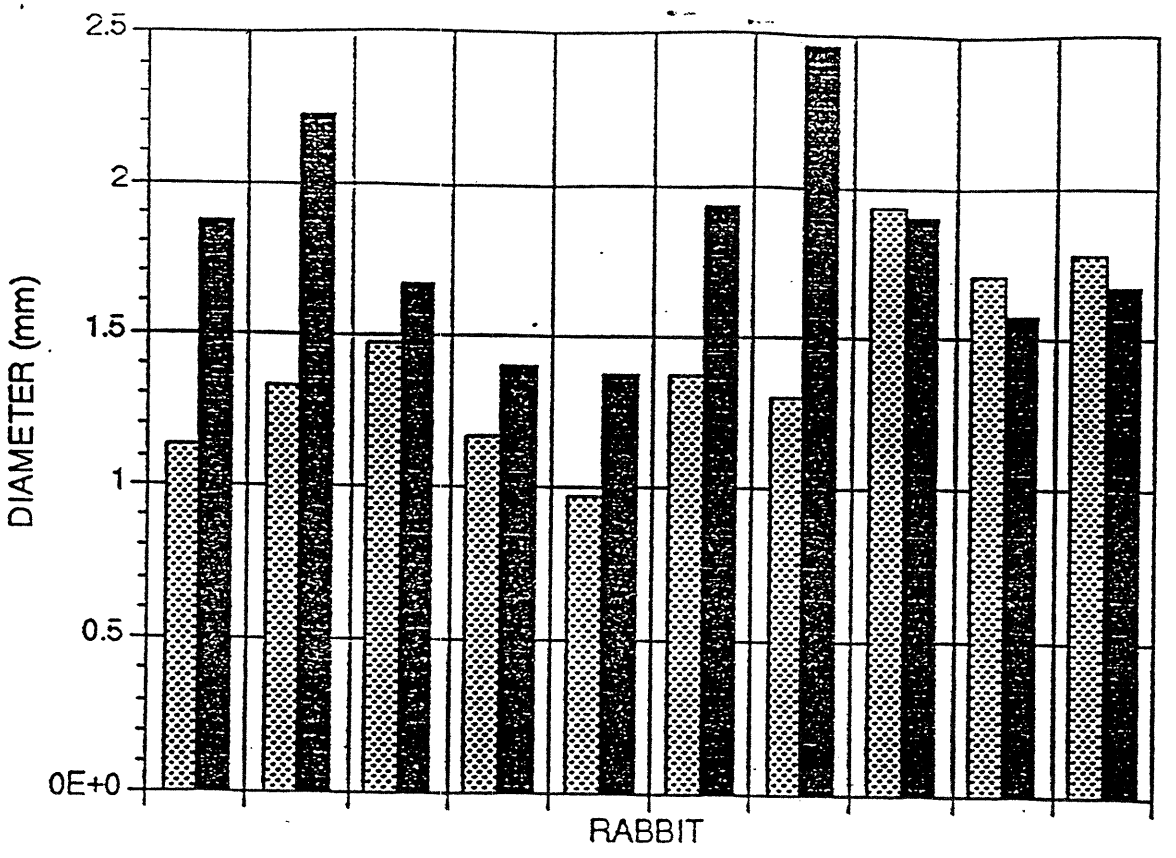

Figure 4.4 A per rabbit account of the results obtained using the Hydromechanical vasodilator. Speckled bar represents spasm diameter, solid represents post treatment diameter.

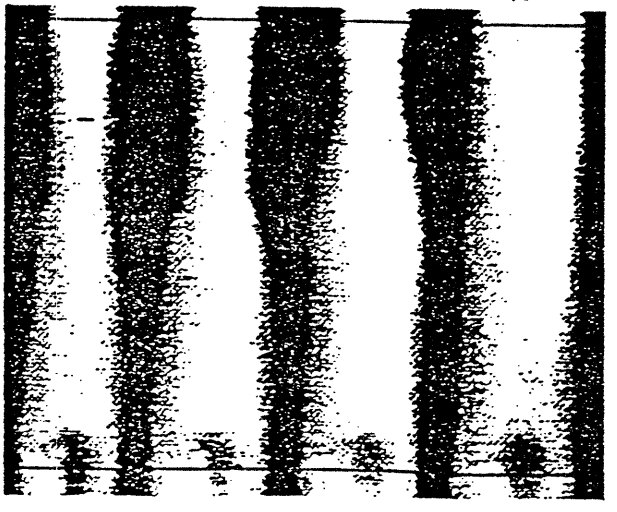

Figure 4.3 Pictured are four consecutive pulses applied to the dog in-vitro basilar artery. Note the stepwise progression of dilatation on a per pulse basis.

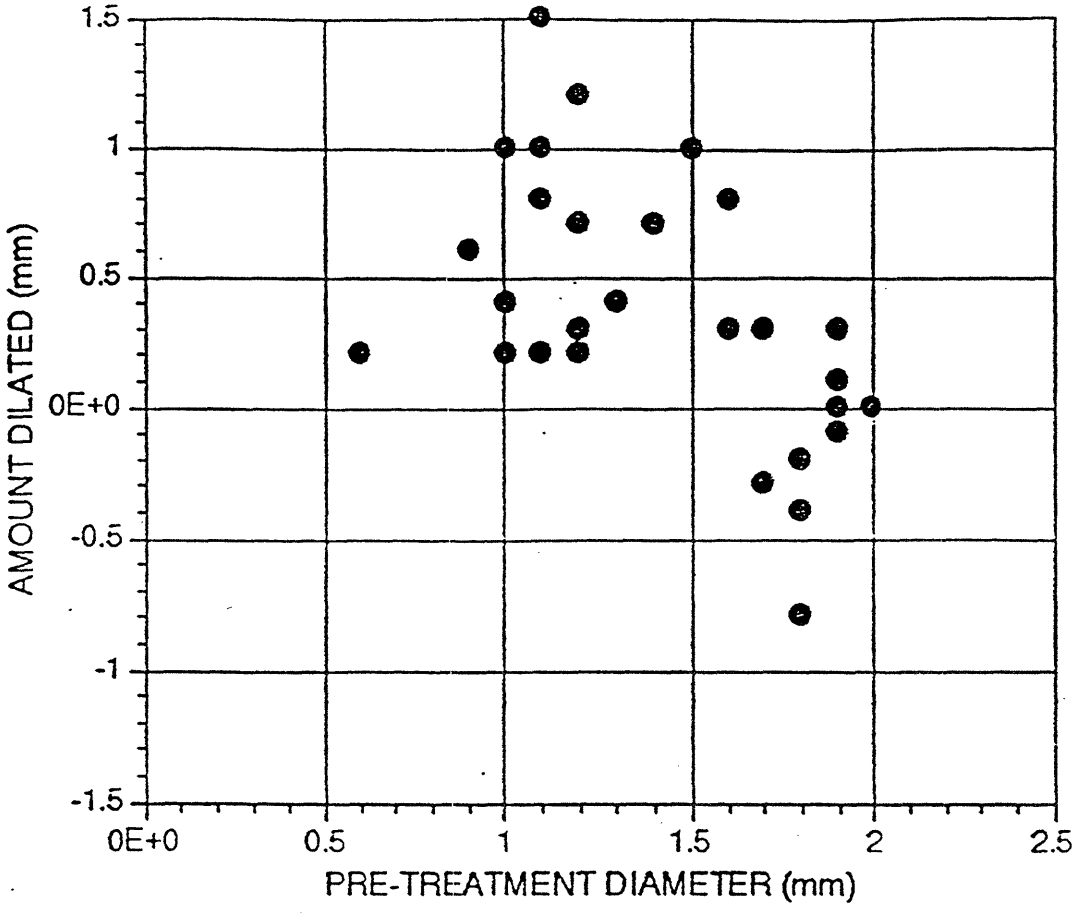

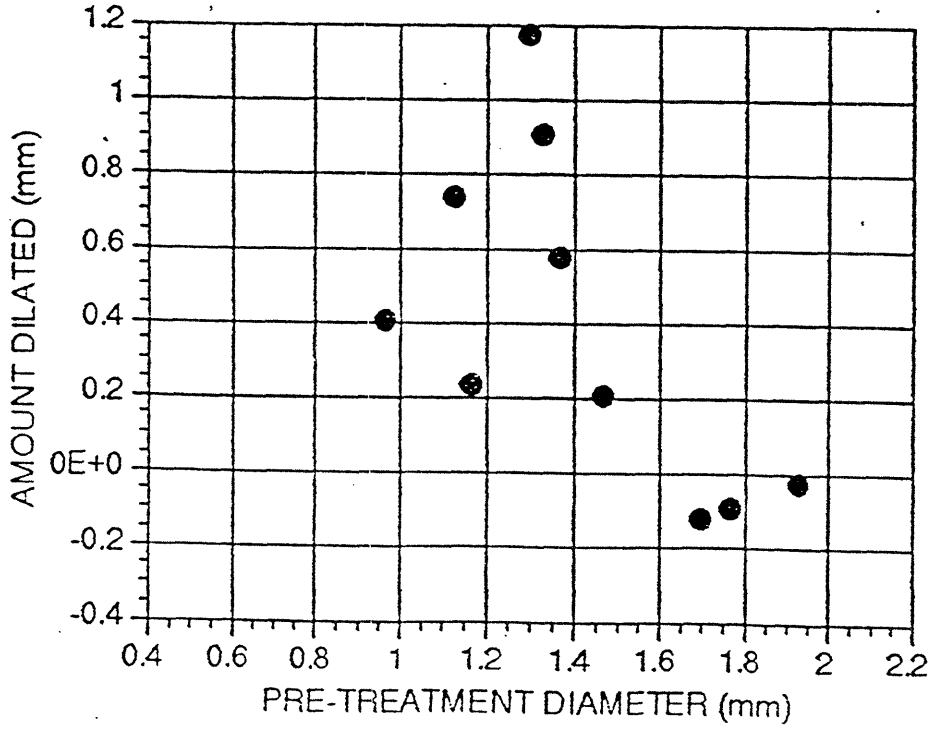

Figure 4.5 Degree of dilatation versus spasm diameter for arteries treated with the Hydromechanical vasodilator. Top plot represents all points measured on all arteries, bottom plot represents average per artery of all measured points.

1. Gruntzig, A, et al, *Non operative dilation of Coronary-Artery Stenosis.* N Engl J Med, 301, 1979.

2. Abela, G, Normann, S, et al., *Laser recanalization of Occluded Atherosclerotic Arteries in vivo and in v itro,* Circulation, 71, 1985.

3. Walsh,J, Flotte, T, Anderson, R, Deutsch, T, *Pulsed CO2 Laser Tissue Ablation: Effect of Tissue Type and Pulse Duration on Thermal Damage,* Lasers Surg. Med., 8, 1988.

4. Grundfest, W, White, R, (ed). Lasers in Cardiovascular Disease, Clinical Applications, Alternative Angioplasty Devices, and Guidance Systems. Year Book Medical Pub., Chicago, 1989.

5.Vogel et al, *Cavitation Bubble Dynamics and Acoustic Transient Generation in Ocular Surgery with Pulsed Neodynium:YAG Lasers.* Ophthalmology. Oct, 1986

6 A.G. Doukas, A.D. Zweig, et al. *Non-invasive determination of shock wave pressures generated by optical breakdown.* Appl. Phys. B53, 237-245, 1991

7.Newton,I. Optiks, Dover Publications, New York, 1952

8.Young, F. Cavitation. McGraw-Hill Book Co., 1989.

9. Lauterborn, W (Ed). *Introduction.* Cavitation and Inhomogeneities in Underwater Acoustics, Springer-Verlag, 1980.

10. Reynolds, O., *Trans. Inst. Naval Arch. V14 Sci Papers,* 1, 1873.

11. A.G. Doukas, R.Birngruber, et al, *Determination of shock wave pressures generated by laser-induced breakdown in water,* In: Laser-Tissue interactions, Proc. SPIE 1202, 61-62, 1990.

12. Vogel, A, Lauterborn,W, *Acoustic transient Generation by Laser-produced Cavitation Near Solid Boundariess,* J. Acoutic Soc. Am., Aug, 1988

13. Flynn, H.G., Physical Acoustics, Vol. 1B, W.P. Mason (ed), Academice Press, Chap. 9, 1964.

14. Rayleigh, L, *On the Pressure Developed During the Collapse Phase of a Spherical Cavity,* Phil. Mag., 34, 1917.

15. Gradshteyn,I, Ryzhik, I, Table of Integrals, Series, and Products. Academic Press, New York, 1980

16. Anderson, R, Selective Thermal Damage from Pulsed Laser Sources. MIT Arch. 1984

17. Carslaw, H, Jaeger, J, Conduction of Heat in Solids. Oxford Science Publications, 1986.

18. Teslenko, Experimental Investigations of Bubble Collapse at Laser-induced Breakdown in Liquids, Lauterborn, W (Ed). Cavitation and Inhomogeneities in Underwater Acoustics, Springer-Verlag, 1980.

19. Grundfest, W, White, R, (ed). Lasers in Cardiovascular Disease. Clinical Applications. Alternative Angioplasty Devices, and Guidance Systems. Year Book Medical Pub., Chicago, 1989.

20. Braunwald, E, et al (ed). Principles of Internal Medicine, McGraw-Hill Inc, 1987.

21. Macdonald, R, Weir,B, *A Review of Hemoglobin and the Pathogenesis of Cerebral Vasospasm.* Stroke, 22,1991

22Heros, R, Zervas,N, *Cerebral Vasospasm after Subarachnoid Hemorrhage: An Update.* Ann Neurol, 14, 1983.

23. Miyaoki,M, Nonaka,T, et al. *Etiology and Treatment of Prolonged Vasospasm: Experimental and Clinical Studies.* Neurol Med Chir (Tokyo), 16, 1976

24. Sonobe,M, Suzuki,J, *Vasospasmogenic Substances produced Following Subarachnoid Hemorrhage.* Acta Neurochir, 44, 1978.

25. Weir, B, Aneurysms Affecting the Nervous System. Williams and Williams,Co, Baltimore, 1987.

26. Jan, M, Buchheit, F, et al, *Therapeutic Trial of Intravenous Nimodipine in Patients with Established Cerebral Vasospasm After Rupture of Intracranial Aneurysms,* Neurosurgery, vol 23, 1988

27. Heros, R. Comments. Neurosurgery, vol 23, 1988.

28. Allen, G, Ahn, G, et al , *Cerebral Vasospasm-a controlled trial of Nimodipine in Patients with Subarachnoid Hemorrhage.* N Engl J Med, 308, 1983.

29. Gregory, K, et al. *Pulsed Laser Induced Vasodilation and Vasospasm.* Circulation Supplement, Abst. Vol 80, 1988.

30. Chaudry,H, Light Dependent Relaxation of Smooth Muscle, MIT Arch., 1991.

RELATED WORKS:

PATENTS

Hydromechanical Vasodilator. Ralph de la Torre, Kenton Gregory, MD. Patent Pending. (Patent rights controlled by Massachusetts General Hospital, # 0504.0)

ORIGINAL WORKS

Teramura, A, Macfarlane, R, Owen, C, de la Torre, R, Gregory, K, Parrish, J, Peterson, J, Zervas, N. *Application of 1us Pulsed Dye Laser to the Treatment of Experimental Cerebral Vasospasm.* Journal of Neurosurgery, vol 75: 271-6, August,1991.

MacFarlane, R, Teramura, A, Owen, C, de la Torre, R, Gregory, K, Peterson, J, Parrish, J, Zervas, N. *480 nm Pulsed Dye Laser Treatment of Vasospasm.* Journal of Neurosurgery. (accepted)

de la Torre, R, Gregory, K, Birngruber, R, Block, P, Anderson, R. *Intravascular Cavitation Bubble and Acoustic Transient Formation in Clinical Laser Angioplasty.* (to be submitted : Journal of the American College of Cardiology).

Gregory, K, de la Torre, R, Buckley, L. *Photomechanical Effects of Laser Angioplasty.* Optical Fibers in Medicine. Press of the Society of Professional Industrial Engineers. January, 1992.

de la Torre, R, Gregory, K, MacFarlane, R, Anderson, R. *Hydromechanical treatment of arterial vasospasm.* (Submission pending patent).

ABSTRACTS

Teramura, A, Zervas, N, Macfarlane, R, Owen, C, de la Torre, R, Gregory, K, Parrish, J, Uemura, K. *Photoacoustic Vasodilation by Pulsed Dye Laser.* Journal of Neurosurgery. February, 1990. VOL 72 , Num. 2.

Teramura, A, Macfarlane, R, de la Torre, R, Gregory, K, Peterson, J.W., Parrish, J, Zervas, N. *Pulsed Dye Laser Treatment of Experimental Vasospasm.* Proceedings of International Conference of Vasospasm. Tokyo, Japan. August, 1990.

de la Torre, R, Gregory, K, MacFarlane, R,. *Dilatation of Arterial Vasospasm Using an Intraluminal Hydraulic Wave.* Circulation Supplement. October, 1991.

de la Torre, R, Gregory,K, Block,P. *Cavitation Bubble and Acoustic Transient Production Due to Blood Absorption of Pulsed Laser Energy.* Journal of the American College of Cardiology. February, 1992.

APPENDIX

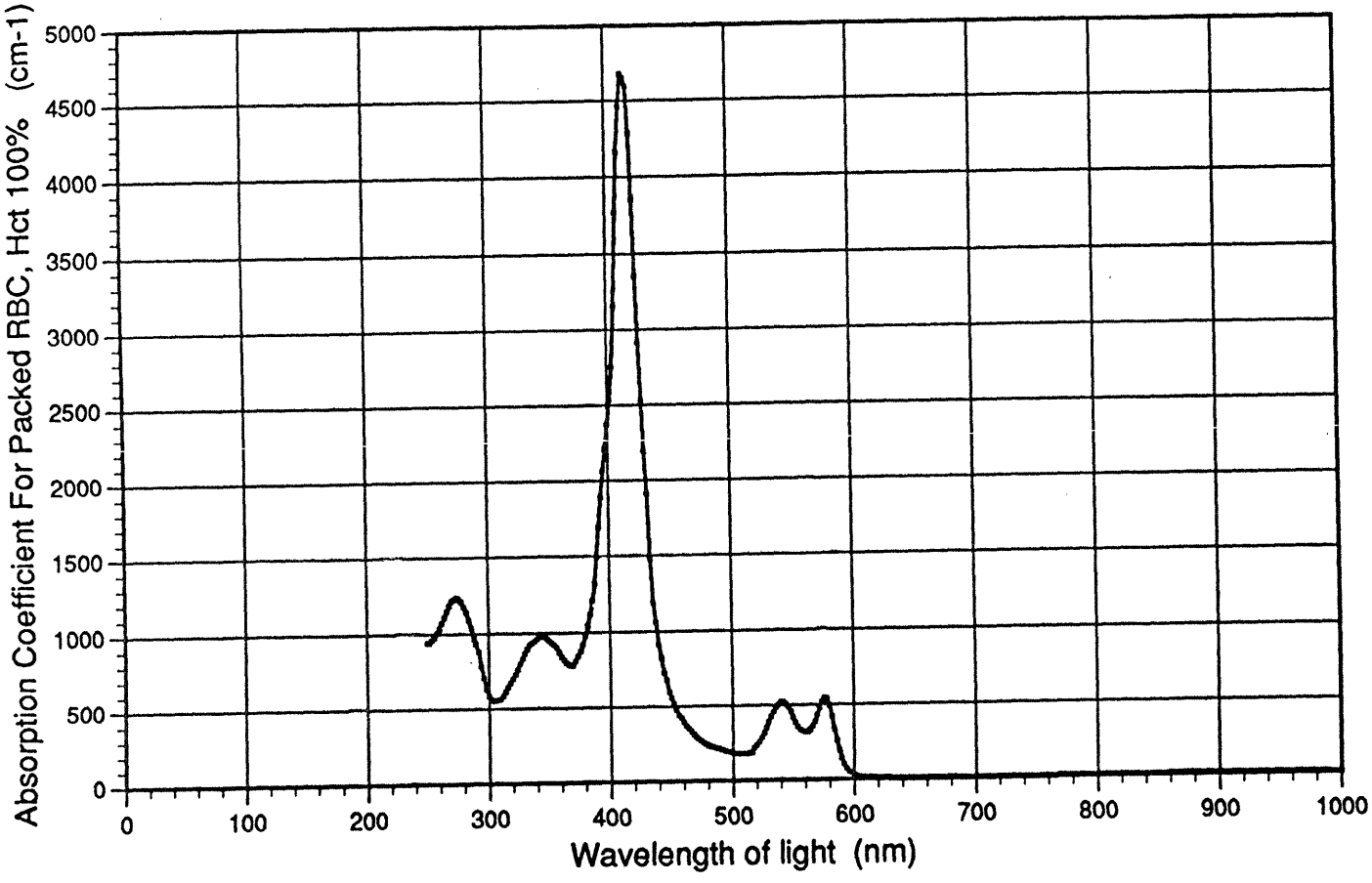

Absorption coefficient of packed Red Blood Cells. Subsequent absorption coefficents can found by dividing by the appropriate dilution. From Scot Prahl, PhD, unpublished data.

J Neurosurg 75:613–622, 1991

Treatment of vasospasm with a 480-nm pulsed-dye laser

ROBERT MACFARLANE, F.R.C.S., ATSUSHI TERAMURA, M.D., CHRISTOPHER J. OWEN, B.Sc., SCOTT CHASE, B.Sc., RALPH DE LA TORRE, B.S.E., KENTON W. GREGORY, M.D., JOHN W. PETERSON, PH.D., REGINALD BIRNGRUBER, PH.D., JOHN A. PARRISH, M.D., AND NICHOLAS T. ZERVAS, M.D.

Neurosurgical Service and Wellman Laboratories of Photomedicine, Massachusetts General Hospital, Harvard Medical School, Boston, Massachusetts, and Department of Neurological Surgery, Addenbrooke's Hospital, Cambridge, England

✓ Laser energy at a wavelength of 480 nm was applied in 1-μsec pulses of 3 to 10 mJ to two models of vasospasm. Rabbit common carotid arteries (CCA's) were constricted chronically by the application of human blood within a silicone sheath. Peak vasospasm developed 24 to 48 hours later, and persisted for up to 6 days. Endovascular laser treatment was delivered to 40 CCA's via a 200-μm diameter silica quartz fiber introduced through the femoral artery. The CCA caliber increased from 60% of the pre-vasospasm control diameter to a minimum post-laser diameter of 83% of control. No instances of laser-induced perforation or of arterial thrombosis were observed for up to 60 days after treatment. Prophylactic laser application to nine normal vessels was able to attenuate the development of vasospasm if blood was applied immediately thereafter (88% vs. 59% of control diameter, $p < 0.02$), but not if blood was applied 7 days later. Studies in 16 normal CCA's established that there was a considerable margin between the laser energy required to induce dilatation and that which caused perforation, providing that the fiber remained relatively central within the artery. Morphological examination demonstrated focal loss of endothelial cells immediately after laser application, followed approximately 7 days later by the development of areas of intimal hyperplasia. Only minimal changes were observed in the medial or adventitial layers.

In a second study, the basilar artery of seven dogs was constricted chronically by two intracisternal injections of autologous blood 3 days apart. Five dogs received endovascular laser treatment 7 or 10 days after the first injection, when basilar artery diameter was reduced to a mean of 61% and 77% of control, respectively. Immediately following treatment, basilar artery diameter increased to 104% and 102% of resting diameter, respectively. Both untreated and laser-treated arteries were smaller than the control diameter at 30 days (80% and 82%, respectively), but in each group the vasodilatory response to hypercapnia was preserved.

These findings indicate that 1-μsec laser pulses are well tolerated by systemic and cerebral arteries in two different animal models, and suggest that the 480-nm pulsed-dye laser may have an application for the treatment or prophylaxis of cerebral vasospasm.

KEY WORDS • pulsed-dye laser • vasospasm • common carotid artery • basilar artery • subarachnoid hemorrhage • rabbit • dog

PULSED-DYE lasers have been used increasingly to treat a variety of medical conditions. These include the eradication of port-wine stains,[2,5] the fragmentation of urinary calculi,[18] the ablation of atheromatous plaques,[13,14] and thrombolysis following experimental myocardial infarction.[8] This type of laser has several important features. First, depending upon the dye selected, laser emission can be varied throughout the visible spectrum and matched to the absorption peak of the target tissue. Second, energy can be delivered by single optical fibers. Third, because the pulse duration is generally shorter than the thermal relaxation time of neighboring tissues, heat-induced injury to surrounding structures is minimized.[1]

Recent reports from our laboratory have demonstrated that the pulsed-dye laser may be of benefit in the treatment of vasospasm. Intravascular delivery of low pulse energies induces sustained dilatation in rabbit femoral arteries constricted acutely by a variety of pharmacological agents,[7] and in isolated dog basilar artery segments constricted by superfusion with hemolysate.[16] Extravascular irradiation of rabbit basilar

artery constricted *in vivo* either by superfusion with hemolysate, or by a "two-hemorrhage" subarachnoid hemorrhage (SAH) protocol, is similarly effective.[16] However, our previous studies have not permitted us to assess the duration of dilatation or to determine long-term effects on the arterial wall.

Intracranial arteries differ fundamentally in structure from extracerebral vessels, principally because they have no more than a rudimentary adventitia. A chronic model of cerebral vasospasm clearly would be the most appropriate manner in which to study the long-term effects of laser treatment on vasospasm. Unfortunately, the smallest laser fiber available to us initially was slightly too large and inflexible to permit catheterization of an intracranial artery in spasm. For this reason we elected first to undertake a pilot study using an extracerebral vessel.

Materials and Methods

Chronic Vasospasm in Rabbit Common Carotid Artery

New Zealand White rabbits of either sex, each weighing 2 to 3 kg, were anesthetized with ketamine hydrochloride, 30 mg/kg, and 4% halothane by inhalation. Following endotracheal intubation, anesthesia was maintained with 1% to 2% halothane. End-tidal CO_2 was maintained between 35 and 45 mm Hg. Systemic blood pressure was monitored in selected animals via a brachial or femoral artery catheter. Bilateral common carotid artery (CCA) angiography was obtained with Renografin-60 as the contrast material following selective catheterization via a Tracker-18 catheter introduced via the femoral artery.* The Tracker catheter was then removed and the femoral artery ligated.

Both CCA's were exposed through a midline cervical incision. All loose areolar tissue investing the vessels was excised. Silicone tubing with an internal diameter of 2.6 mm was divided into 3-cm lengths and copper wire markers were attached to each end. The sleeves were stored in 70% isopropanol until use; one sleeve was placed around each CCA. The space between the artery and the tube was filled with fresh nonheparinized human blood, after which the animals were allowed to recover.

The rabbits were reanesthetized 24 to 48 hours later, and angiography was repeated as before. In the rare event that spasm was not evident, blood application was repeated and the animals were reassessed 24 hours later. The rabbits were divided into five groups: a control group, a laser-treated group; a sham-treated group; a group with laser prophylaxis; and a group with laser vessel perforation.

Control Group. The time course of untreated vasospasm was established by serial angiography in 15 CCA's from 13 rabbits. The silicone sleeves were removed after 7 days. In nine animals, the left CCA was excised at the time of cuff removal, and angiography was then repeated 30 and 60 days later.

The ability of vessels with vasospasm to relax in the presence of a vasodilator was assessed angiographically in a further six CCA's 24 hours after blood application. Papaverine, 30 mg, was diluted to 2 ml with saline, and warmed to 37°C. Following carotid angiography, papaverine was infused continuously via the Tracker catheter over a 5-minute period, and angiography was repeated 10 minutes later.

Laser Treatment Group. Twenty-four to 48 hours after the induction of spasm, 40 CCA's from 32 rabbits received endovascular laser therapy from a 1-μsec pulsed-dye laser at a wavelength of 480 nm.† The tip of the Tracker-18 catheter was positioned in the proximal CCA. A polytetrafluoroethylene (PTFE)-coated fused silica quartz fiber with a 200-μm diameter and a fire-polished ball tip (spot size 0.6 to 1.1 mm) was inserted into the Tracker-18 catheter and advanced coaxially under fluoroscopic control to the most distal extent of the spasm. Laser light was delivered to the quartz fiber at a range of pulse energies between 4.7 and 10 mJ (pulse–pulse variation $< 10\%$) and a repetition rate of 2 Hz. The fiber was withdrawn progressively into the catheter during treatment, at a rate of approximately 1 mm/sec, until the entire area under the cuff was irradiated. Angiography was then repeated. If no dilatation was observed, treatment was repeated at a higher pulse energy. If only modest enlargement was seen, laser treatment was repeated using the same parameters.

Animals were allowed to recover after laser treatment. The silicone cuffs remained *in situ* for the first 7 days. Serial angiography was performed as before at intervals for up to 60 days. In seven rabbits the contralateral CCA was excised shortly after laser dilatation, and angiograms were obtained 30 and 60 days later.

Sham-Treated Group. The effect of Tracker catheter and laser fiber insertion was determined in five vessels. Angiograms and morphological studies were obtained immediately after 200-μm fiber insertion, and at varying intervals thereafter.

Laser Prophylaxis Group. In nine rabbits, laser energy of 7 to 10 mJ (20 to 50 pulses/cm of vessel) was applied unilaterally to a 4-cm length of normal CCA. Silicone sheaths and human blood were applied to the irradiated region either immediately thereafter (five vessels) or 7 days later (four vessels). Angiography was obtained simultaneously from left and right CCA's 24 hours after blood application, via a catheter placed in the aortic arch.

* Tracker-18 catheter manufactured by Target Therapeutics, San Jose, California.

† Dymed Spectrum Series 3010 pulsed-dye laser manufactured by Dymed Corp., Marlborough, Massachusetts.

Perforation Study Group. The threshold for laser perforation was determined in 16 normal CCA's. The vessels were exposed and kept moist by intermittent irrigation with Ringer's solution. A 200-μm diameter quartz fiber was inserted into the artery as before, but was kept static within the vessel so that laser energy was applied to a single focus. The threshold for perforation was established at varying pulse energies when the fiber tip was placed either centrally within the vessel, adjacent to but not touching the wall, or indenting the artery. The position of the ball tip was verified by observation through an operating microscope. Irradiation was discontinued if perforation had not occurred by the 200th pulse.

Rabbits were sacrificed by pentobarbital sodium overdose. The brains were removed, sectioned at 5-mm intervals, and stained with 4% 2-3-5 triphenyltetrazolium chloride (TTC). The CCA's were excised after *in situ* perfusion through the ascending aorta with 1% glutaraldehyde solution containing 100 mM sodium cacodylate buffer at a pH of 7.4. The arteries were subjected to light microscopy (after hematoxylin and eosin and/or elastin staining) and/or transmission electron microscopy.

Dog "Two-Hemorrhage" SAH Model

Seven adult mongrel dogs, each weighing 20 to 35 kg, were anesthetized with 2.5% thiamylal sodium and ventilated mechanically with a dual-phase respirator.‡ End-tidal CO_2 was maintained at 40 mm Hg.§ The head was fixed in a stereotactic frame and left vertebral angiography was obtained via a No. 6.5 French catheter introduced from the femoral artery.‖ The dogs were subjected to a "two-hemorrhage" SAH protocol as described previously.[17] In brief, the occipitonuchal area was shaved and the head flexed acutely. The cisterna magna was punctured with a No. 19 needle. After withdrawal of 3 ml clear cerebrospinal fluid, 3 ml of fresh autologous nonheparinized blood was injected slowly into the subarachnoid space over 1 to 2 minutes. The stereotactic frame was removed and the animal was placed 30° head down for 20 minutes to promote pooling of blood in the basal cistern. Three days later a second hemorrhage was induced in a manner similar to the first.

In two animals, the time course of untreated vasospasm was established for up to 30 days by serial angiography. The remaining five dogs received endovascular laser treatment either 7 or 10 days after the first SAH. Following vertebral angiography, the left anterior spinal artery was catheterized with a Tracker-18 catheter. The tip was positioned, where possible, as far as the bifurcation of the anterior spinal artery. A 125-μ bare fused silica quartz fiber (spot size 0.6 to 0.7 mm), with a platinum marker at the tip, was inserted into the catheter and manipulated as far into the basilar artery as possible. The catheter was then withdrawn into the vertebral artery, leaving the fiber *in situ*. An energy of 3 mJ was applied to the quartz fiber at a repetition rate of 2 Hz. Approximately 20 pulses/cm were applied to the basilar and anterior spinal arteries as the fiber was withdrawn progressively into the vertebral artery. Angiography was repeated immediately after treatment and at intervals for up to 60 days.

The animals were sacrificed by exsanguination under anesthesia, and perfusion through the left vertebral artery with buffered 1% glutaraldehyde solution at pH 7.4. The basilar artery was excised for morphological examination.

Data Collection and Analysis

All vessel diameters were measured angiographically using a × 7 magnifying loupe. The x-ray source and film were kept at a fixed distance from the animal. The diameter of the rabbit CCA was measured at five points in the region under the silicone sleeve, while the diameter of the dog basilar arteries was measured at eight points throughout the laser-treated area (or equivalent area in the case of the two control studies).

Values are expressed as mean ± standard deviation. Student's t-test, paired or unpaired as appropriate, was used to determine statistical significance. P values of < 0.05 were considered significant.

Results

Rabbit Common Carotid Artery Model

Control Group. The CCA diameter was uniform throughout the segment under study (mean diameter 1.93 ± 0.2 mm). The induction of bilateral CCA spasm was tolerated well, with a mortality rate of less than 8%. Vasospasm developed within 24 hours in more than 94% of the CCA's, and was generally more severe in younger animals. Arterial constriction reached a maximum at 24 and 48 hours, when vessel caliber was reduced to a minimum of 60% (1.15 ± 0.2 mm) and 53% (1.15 ± 0.2 mm) of control diameter, respectively. Vessel caliber enlarged progressively thereafter, was 80% (1.54 ± 0.4 mm) of control by 72 hours, and had returned to near-normal diameter 6 days after blood application.

Intracarotid injection of 30 mg papaverine over 5 minutes resulted in transient hypotension, but blood pressure in every case was normal at the time of repeat angiography. Arterial diameter increased by 11% in the segment of the artery in spasm (1.54 ± 0.2 mm vs. 1.33 ± 0.2 mm) and by 14% in normal CCA proximal to the segment in spasm (2.06 ± 0.2 mm vs. 1.8 ± 0.1 mm).

Carotid arteries in spasm exhibited the morphological characteristics of vasculopathy. An acute inflammatory

‡ Dual-phase respirator manufactured by Harvard Apparatus, South Natick, Massachusetts.

§ CO_2 monitor manufactured by Accucap, Datascope Corp, Paramus, New Jersey.

‖ Catheter manufactured by Cook Co., Bloomington, Indiana.

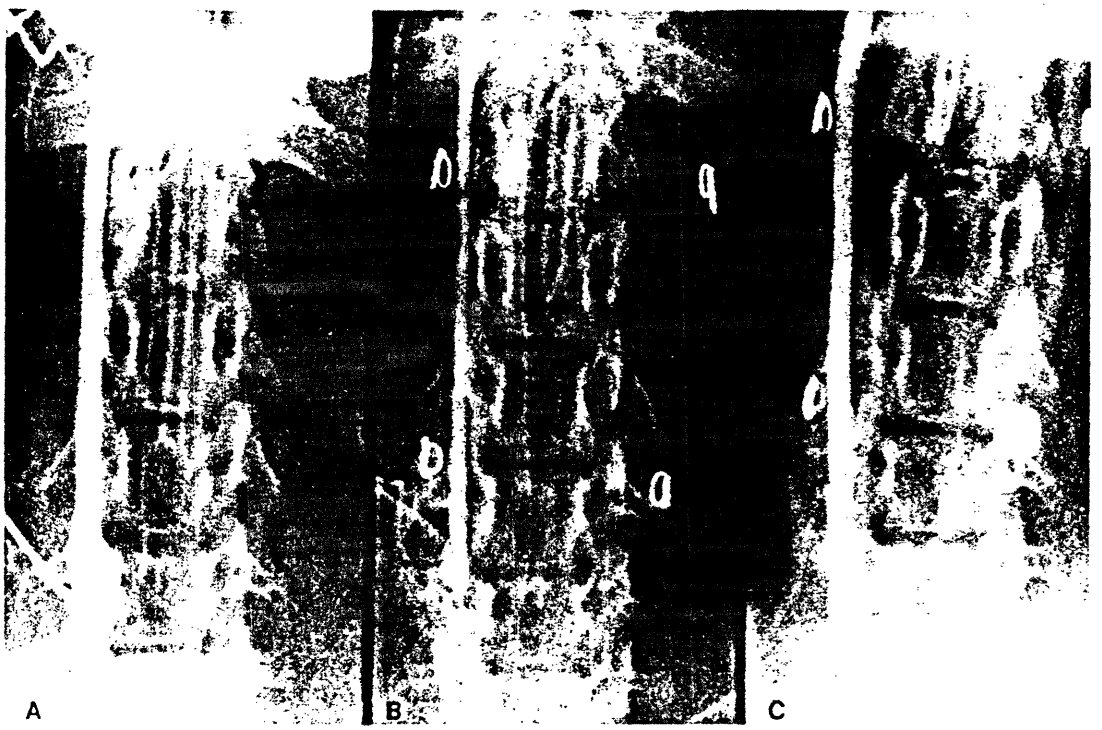

FIG. 1. Rabbit right common carotid artery arteriograms. A: Control group artery. B: Artery 24 hours after induction of vasospasm. The ends of the silicone sleeves are marked with copper wire. C: Artery immediately after laser treatment.

infiltrate was present in almost all cases within 24 to 48 hours of blood application, but the arteries appeared normal at 30 days. Erythrocytes were seen routinely within the adventitia of constricted vessels.

After ligation of the contralateral vessel, CCA diameter increased by 22% over a period of 60 days (2.37 ± 0.2 mm vs. 1.95 ± 0.2 mm), but no histological abnormalities were seen in these arteries.

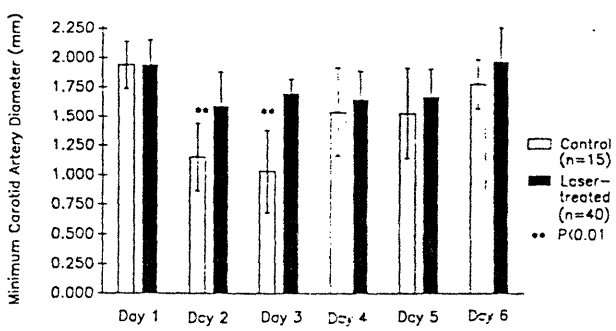

FIG. 2. Time course of treated and untreated vasospasm in rabbit common carotid arteries constricted chronically by the application of human blood within a silicone sleeve impregnated with 70% isopropanol. *Open bars* represent untreated vessels and *solid bars* indicate vessels treated on Day 2 with endovascular therapy from a 1-μsec pulsed-dye laser (480 nm). Minimum arterial caliber in the region under the sleeve is given in both groups. Data are expressed as mean ± standard deviation. n = number of arteries.

Laser Treatment Group. Intravascular pulsed-dye laser irradiation dilated the constricted CCA's in all 40 experiments. In one additional case (the fourth in the series), the CCA was perforated during insertion of the quartz fiber. In the remainder, between 15 and 64 pulses/cm of vessel at an energy ranging from 4.7 to 10 mJ were required to increase caliber from a peak spasm diameter of 60% of control (1.15 ± 0.29 mm) to a minimum post-laser diameter of 83% of control (1.59 ± 0.29 mm, $p < 0.001$) (Fig. 1). No more than three treatments were required for any single artery. The time course of treated and untreated vasospasm is shown in Fig. 2. Some return of constriction was observed in 50% of CCA's 48 to 72 hours after treatment, although at each stage vessels remained larger than in the untreated control group. Repeat constriction was seen only in arteries in which complete dilatation was not achieved initially. There were no instances of laser-induced perforation or of arterial thrombosis. Sixty days after laser treatment, the CCA diameter was a maximum of 11% larger than the untreated areas of the same vessel. Even after ligation of the contralateral CCA, there was no excessive dilatation of the laser-treated segment (maximum 6% larger than the untreated portion of the same artery: 2.6 ± 0.03 mm vs. 2.45 ± 0.02 mm).

Light microscopic examination of paraffin-embedded transverse sections, stained with hematoxylin and eosin or elastin, demonstrated that laser treatment was

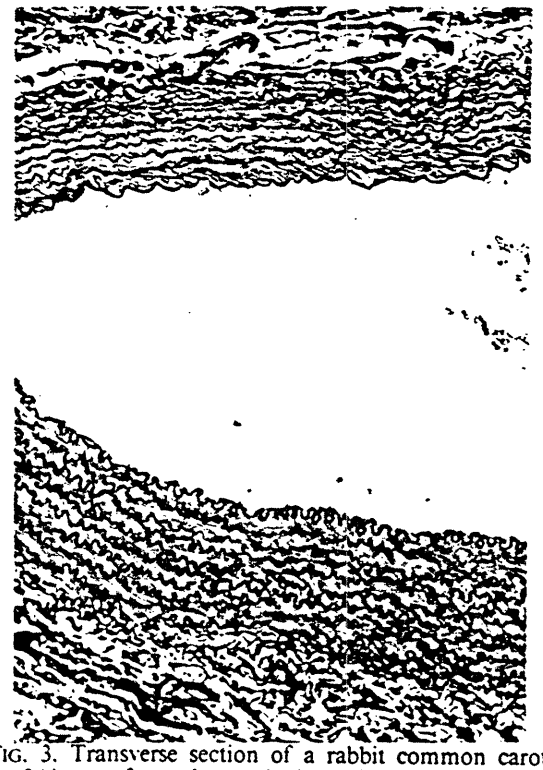

FIG. 3. Transverse section of a rabbit common carotid artery 24 hours after endovascular laser dilatation. While some parts of the vessel wall (top) exhibit loss of endothelial cells and stretching of the media and adventitia, other parts of the artery appear normal (bottom). Elastin, × 115.

asymmetrical in every case. Large segments of the vessel circumference were often little different from control, while in other areas there was loss of endothelial cells immediately after treatment (Fig. 3). No disruption of the medial or adventitial cell layers was observed, although patchy loss of smooth-muscle cell nuclei was seen occasionally a few days after treatment. Intramural

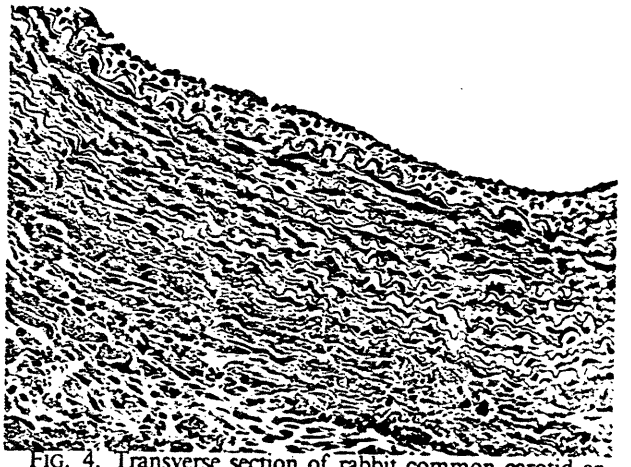

FIG. 4. Transverse section of rabbit common carotid artery 60 days after laser dilatation. Intimal hyperplasia is evident in this segment of vessel, although the majority of the artery appeared normal. H & E, × 120.

hematomas and dissections did not occur. Small patches of intimal hyperplasia, up to five cells in thickness, developed approximately 5 to 7 days after treatment and were present in almost all specimens by 60 days (Fig. 4). Regenerated endothelial cells were often cuboidal rather than flat, and were associated with intimal smooth-muscle proliferation. Similar findings were seen by electron microscopy. While in some areas there was complete loss of endothelial cells after dilatation, the opposite side of the vessel at the same point usually appeared normal (Fig. 5). Surprisingly, few platelets and erythrocytes were adherent to denuded areas.

A solitary laser-induced complication occurred when the quartz fiber became unbonded from its PTFE sheath. During treatment, only the PTFE covering was withdrawn into the Tracker catheter, while the fiber itself remained static within the artery. The entire dose

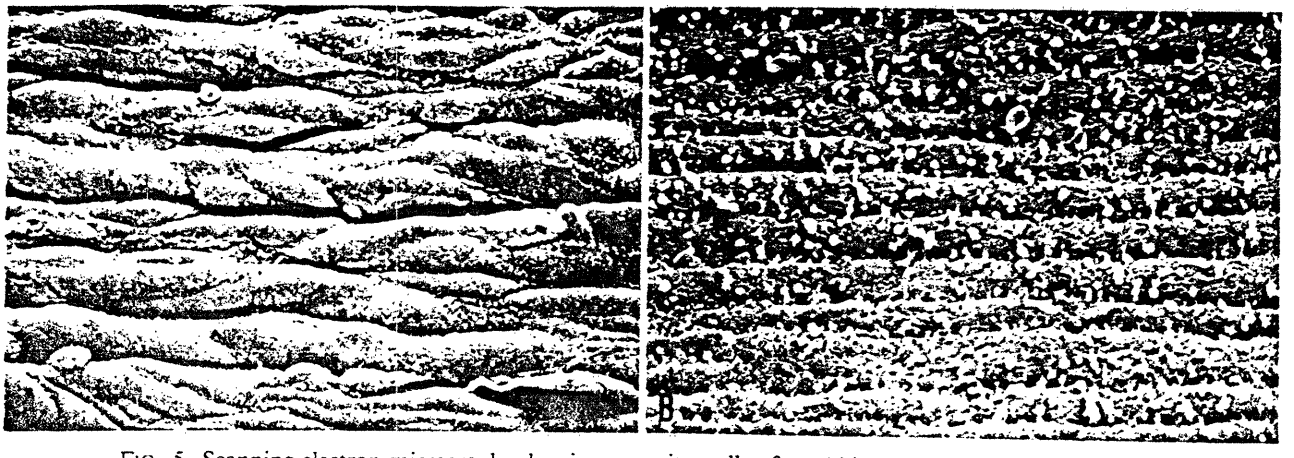

FIG. 5. Scanning electron micrographs showing opposite walls of a rabbit common carotid artery immediately after laser dilatation. *Bar* = 10 μm. A: Normal endothelium. B: There is a loss of endothelial cells, with platelet adhesion to the internal elastic lamina.

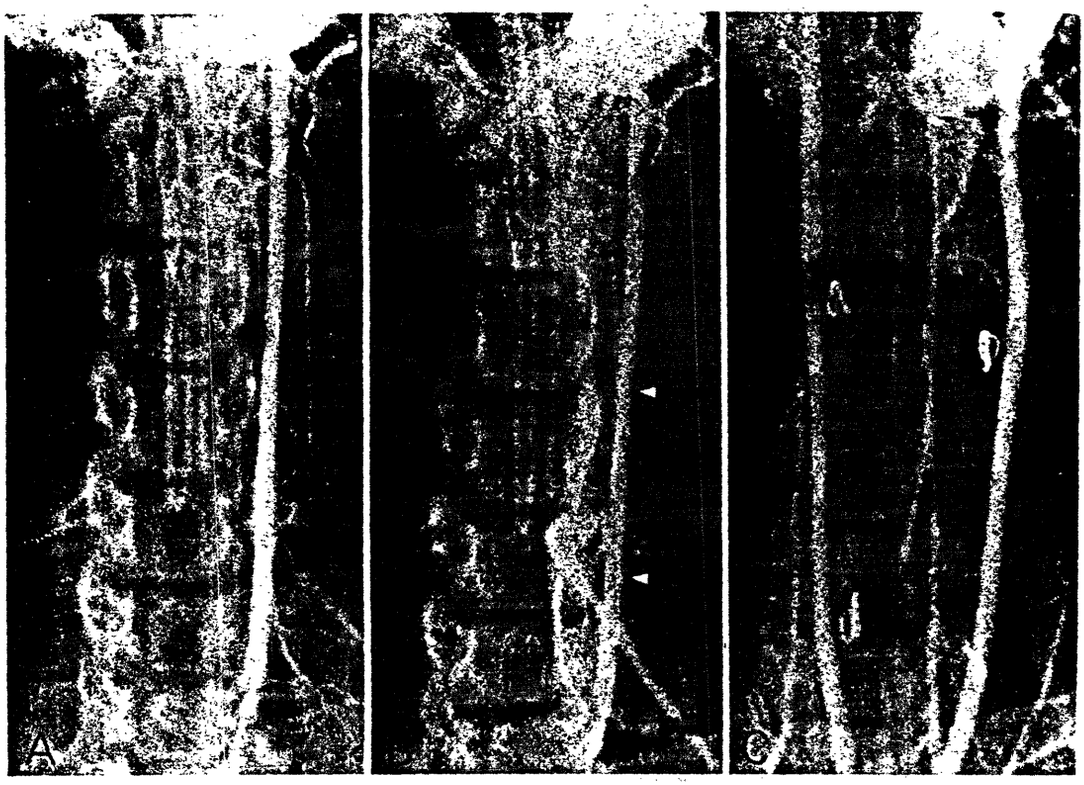

FIG. 6. Angiograms showing results of laser prophylaxis. A: Control vessels. The common carotid arteries (CCA's) were of the same caliber, therefore only the left is shown. B: Immediately after laser irradiation of the left CCA to the area marked by *arrows*. Silicone sleeves and blood were applied immediately. C: Arch aortogram 24 hours later showing considerably more spasm on the untreated side.

for the 3.5-cm segment of vessel was delivered to a focal point (spot size approximately 1 mm). A small saccular aneurysm (0.6 mm in diameter) developed immediately in the vessel, but did not enlarge over the ensuing 60 days.

No neurological complications attributable to laser treatment were seen, and no infarcts were visible in brains serially sectioned and stained with TTC. However, two control and three laser-treated rabbits were sacrificed prematurely because of the development of foot drop related to multiple femoral artery cannulations.

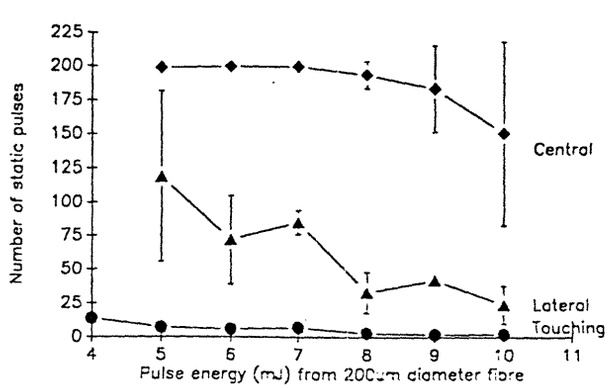

FIG. 7. Results of perforation studies in 16 normal rabbit common carotid arteries. Varying pulse energies were applied via a 200-μm fiber which was fixed either centrally within the artery, adjacent to but not touching the wall, or indenting the vessel. Application was discontinued if perforation had not occurred by the 200th pulse. Results are expressed as the mean ± standard deviation.

Sham-Treated Group. Sham laser treatment of five CCA's increased spasm immediately by an average of 15%, but this resolved within 20 minutes and subsequent caliber did not differ significantly from control arteries. In no instance was dilatation seen after insertion of the fiber or Tracker catheter. Scanning electron microscopic examination of these arteries demonstrated some immediate asymmetrical loss of endothelial cells but, unlike laser-treated vessels, intimal hyperplasia did not develop later.

Laser Prophylaxis Group. Laser irradiation of normal CCA's (7 to 10 mJ, 20 to 50 pulses/cm of vessel) did not alter the angiographic appearance of the vessel. The severity of vasospasm was significantly less in arteries in which blood was applied immediately after laser pretreatment (88% vs. 59% of control diameter; $p < 0.02$) (Fig. 6). However, laser pretreatment had no significant effect on the severity of spasm if blood was applied 1 week later.

Perforation Study Group. Because laser-induced perforations usually bled only momentarily, it was pos-

sible in most cases to perform multiple studies on different segments of the same artery. The threshold for perforation was dependent on both the pulse energy and the relationship between the fiber tip and the arterial wall. While at an energy of 8 mJ, 200 pulses rarely caused perforation if the fiber was centrally placed; lateral placement at the same pulse energy required an average of 33 ± 15 pulses to cause perforation, and if the fiber indented the artery only four ± one pulses. The results of these studies are shown in Fig. 7.

Intravascular Treatment of Dog Basilar Artery

The "two-hemorrhage" protocol resulted in severe vasospasm in all dogs. Basilar artery diameter was reduced to 61% ± 10% of control at 7 days, and 77% ± 8% at 10 days. Laser treatment was attempted 7 days after induction of spasm in three dogs. In one it was possible to insert the quartz fiber tip to the mid-basilar region, while in the other two only the junction of the anterior spinal and basilar arteries was reached. The final two dogs were catheterized 10 days after the first SAH and, in both, the fiber was inserted to within 1 cm of the basilar apex. Laser treatment increased mean basilar and/or anterior spinal artery diameter to 104% ± 2% and 102% ± 2% of control at 7 and 10 days, respectively (Fig. 8).

Two dogs died immediately after laser dilatation; one was sacrificed electively and the other did not recover from anesthesia and died 2 hours later. In the second animal, which was treated 7 days after induction of vasospasm, great difficulty was encountered in negotiating the bifurcation of the anterior spinal artery to enter the basilar artery. Catheterization failed on one side of "the diamond," but was successful on the other. At postmortem examination, it was found that the entire laser-treated segment had dilated uniformly, but that the side of failed catheterization had perforated about 0.5 cm from the bifurcation.

No neurological deficit was apparent in the three surviving laser-treated dogs. In these animals, and in both controls, the basilar artery diameter at 30 days was smaller than the pre-vasospasm state (80% ± 6% and 82% ± 0.5%, respectively). However, in both groups, the vasodilatory response to hypercapnia ($PaCO_2$ 70 mm Hg) was preserved (104% and 90% of basal diameter, respectively) (Fig. 9).

Morphological examination of the basilar artery immediately after laser treatment showed uniform loss of endothelial cells but, as with the rabbit model, there was little adhesion of red cells or platelets to denuded areas and no injury to smooth muscle. Sixty days after dilatation, vessels appeared normal throughout and, in particular, there was no evidence of intimal hyperplasia.

Discussion

This study demonstrates that the 480-nm 1-μsec pulsed-dye laser is able to dilate both systemic and cerebral arteries in chronic spasm. Immediately after laser application the diameter of rabbit CCA's was increased from 60% to 83% of control values, and dog basilar artery from 61% to 104%. Arteries remained larger than untreated control vessels for as long as vasospasm persisted. Laser pretreatment of normal rabbit CCA's attenuated the development of immediate vasospasm (88% vs. 59%), but not if spasm was induced 7 days later. Dilatation was well tolerated by both types of artery. There were no instances of laser-induced perforation, arterial thrombosis, or embolic complications. The only aneurysm to develop in experiments on 40 rabbit CCA's and five dog basilar arteries followed an accidental over-treatment.

Morphological examination has shown that laser dilatation results frequently in patches of endothelial injury. However, the presence of lesser changes in control animals suggests that this occurs in part as a consequence of catheterization. Only minimal injury is caused to the medial and adventitial layers.

Chronic Vasospasm in Rabbit Carotid Artery

Although systemic arteries differ in structure from intracranial vessels, chronic vasospasm still can be induced. Heterologous blood was contained within a silicone sheath to reduce the rate of resorption, and the tubing was impregnated with isopropanol to induce a slow rate of hemolysis. Peak spasm developed 24 to 48 hours later and persisted for up to 6 days. The response to intra-arterial papaverine was almost identical to that reported in dog basilar artery following experimental SAH.[10,17] This model therefore fulfills the basic criteria for vasospasm: namely, chronicity, resistance to pharmacological vasodilators, and evidence of vasculopathy.

Laser Treatment of Systemic Vasospasm

Dilatation followed laser application in all experiments. Although overall the degree of dilatation achieved with the rabbit CCA model was less than that for the dog basilar artery study, this was the result of a different treatment strategy. In early rabbit experiments only the minimum energy necessary to cause any significant dilatation was applied. However, once it became apparent that injury to the vessel wall was minimal, treatment was continued in the remaining experiments until near-normal arterial caliber was restored.

Morphological Studies

Histological examination of CCA's demonstrated that morphological changes were asymmetrical in every case. This is thought due to the rigidity of the 200-μm fiber and the curve at the origin of each CCA, which caused displacement of the fiber tip to one side of the artery. This has two consequences. First, the degree of injury caused to parts of the vessel wall is likely to be greater than necessary to cause complete dilatation. Indeed, in a small number of arteries examined no evidence of endothelial injury was seen, indicating that

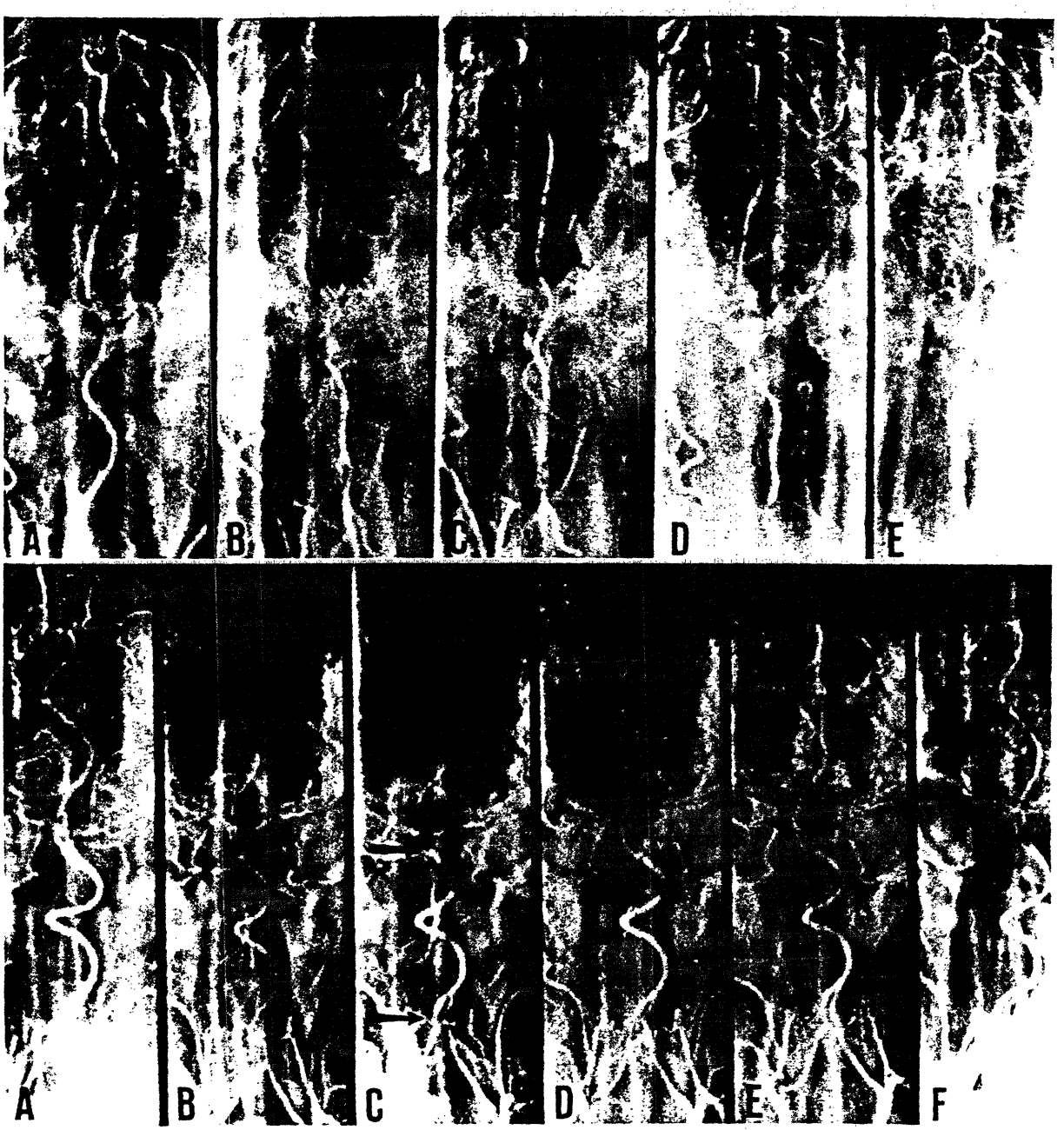

FIG. 8. Serial left vertebral angiograms. *Upper:* Studies in a dog that received endovascular laser treatment to the basilar artery 10 days after induction of vasospasm. A: Control study. B: Study before laser application. C: Study immediately after laser. The distal 1 cm of the basilar artery was not treated for fear that the fiber tip might perforate the basilar apex. D: Study 30 days later, $PaCO_2$ 40 mm Hg. E: Study at the same time as D with a $PaCO_2$ of 70 mm Hg. The vasodilatory response to hypercapnia is preserved. *Lower:* Results of endovascular dilatation of the anterior spinal and proximal basilar artery in a dog 7 days after induction of vasospasm. The caliber of treated and untreated portions of the same vessel is contrasted. A: Control study. B: Study before laser application. C: Study immediately after laser application to area between *arrows*. D: Study 24 hours later. E: Study 48 hours after laser dilatation. F: Study 4 days after treatment.

vascular damage is not an invariable consequence of laser therapy. Possible causes of endothelial cell loss are thermomechanical ablation[6] or cavitation-mediated damage. Second, asymmetrical morphological changes may explain why repeat constriction was observed in some vessels 48 to 72 hours after treatment. This occurred only in cases in which normal vessel caliber was not restored after laser treatment. Morphological examination of one such artery demonstrated that spasm recurred only on the under-treated side of the artery.

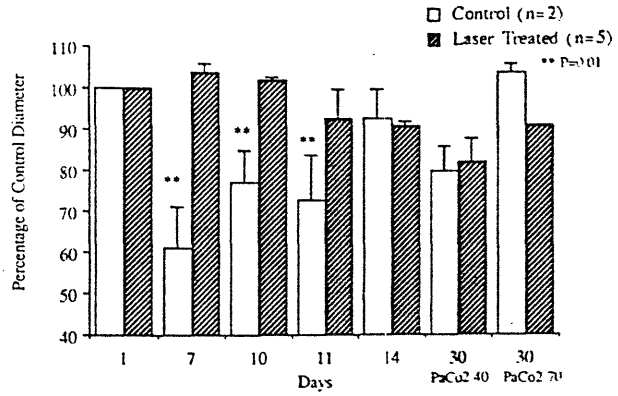

FIG. 9. Time course of untreated vasospasm *(open bars)* and following endovascular laser therapy *(solid bars)* 7 or 10 days after induction of chronic vasospasm in seven dogs by intracisternal injection of autologous blood 3 days apart. Data are expressed as mean ± standard deviation.

Vasospasm Prophylaxis

Laser pretreatment of normal CCA's attenuated the development of immediate vasospasm, but not if spasm was induced 7 days later. This suggests that the laser effect may be relatively short-lived. However, because the artery appeared normal both before and after pretreatment, the laser energy administered was necessarily empirical, and it is possible that administration of a higher dose might have proved more effective.

Perforation Studies

Delivery of excessive energy to the rabbit CCA resulted in endothelial denudation, intramural hemorrhage, thermal debris, dissection, aneurysm formation, or perforation. The risk of perforation was dependent on both the pulse energy and, more important, the distance from the fiber tip to the vessel wall. There was a considerable margin between the energy necessary to induce dilatation and that which caused perforation at pulse energies within the therapeutic range, providing that the fiber was not placed near or touching the arterial wall. The demonstration that only a few pulses are necessary to cause perforation if the fiber indents the arterial wall has important implications for treatment. Laser energy should never be applied during advancement of the fiber, because of the high probability that perforation will occur when a tortuous segment of artery is encountered. For this reason, the fiber was inserted to the most distal extent of spasm, and treatment administered during fiber withdrawal into the catheter.

Laser Treatment of Cerebral Vasospasm

The canine two-hemorrhage SAH model is not ideal to study pulsed-dye laser treatment of vasospasm for two reasons. First, the dog basilar artery is formed not directly from the vertebral arteries but by the union of four anterior spinal arteries, and it is often very tortuous. Second, the smallest catheter that will deliver the laser fiber has an external diameter of 1.3 mm, whereas the dog basilar artery in spasm is only approximately 0.9 mm. Catheterization is necessarily traumatic. In no dog treated 7 days after induction of vasospasm was it possible to insert the fiber to the basilar apex and, in one case, the anterior spinal artery was perforated during the attempt.

Results of laser treatment in the canine model were very similar to those in the rabbit CCA. Laser treatment restored the basilar artery to its prespasm diameter, and no long-term complications were observed. Although the arterial diameter was less than control values 30 and 60 days after treatment, this was true also for the control group, suggesting that this was a consequence of the SAH protocol. In both groups, the vasodilatory response to hypercapnia was preserved.

The morphological appearance of laser-treated dog basilar artery was similar to that of treated rabbit CCA. Focal loss of endothelial cells occurred immediately after treatment, but was not accompanied by large aggregations of platelets or red cells. Damage to the internal elastic lamina and media was negligible. However, the laser effect was much more uniform, and intimal hyperplasia did not occur as a late complication.

Mechanism of Dilatation

While the precise mechanism by which arteries are dilatated has not been established, it is likely to be due to rapid vessel expansion caused by the enlargement and/or subsequent collapse of a cavitation bubble generated by erythrocyte microvaporization.[4] The procedure merits comparison with balloon angioplasty, which has been used with some success in the treatment of cerebral vasospasm.[9,12,20] Endothelial injury is also a complication of this procedure, and may result in progressive intimal smooth-muscle proliferation.[3,19] Persistent and generalized loss of endothelium-dependent relaxation may occur.[19] However, endothelial injury is not universal after pulsed-dye laser dilatation, and the degree of injury and subsequent intimal proliferation seen in rabbit CCA is considerably less than that observed after moderate balloon injury to rabbit iliac artery.[19] The latter may be of importance since experiments have shown that endothelial dysfunction may persist after regrowth.[15,19] Furthermore, lipid accumulates preferentially in areas of intimal thickening covered by regenerated endothelium, and may predispose to atherosclerosis.[11]

Conclusions

These findings suggest that 480-nm 1-μsec laser pulses may be of benefit not only in the treatment of established cerebral vasospasm, but also as a prophylactic measure in patients at high risk of developing this complication after aneurysmal SAH. Further work is required to optimize the delivery of laser energy to the vessel wall, in order to maximize vasodilatation while at the same time minimizing the risk of endothelial injury.

Acknowledgments

The technical assistance of Staci Kerrigan, Lisa Buckley, and Thomas Haw is gratefully acknowledged.

References

1. Anderson RR, Parrish JA: Microvasculature can be selectively damaged using dye lasers: a basic theory and experimental evidence in human skin. **Lasers Surg Med 1**: 263–276, 1981
2. Anderson RR, Parrish JA: Selective photothermolysis: precise microsurgery by selective absorption of pulsed irradiation. **Science 220**:524–527, 1983
3. Clowes AW, Reidy MA, Clowes MM: Kinetics of cellular proliferation after arterial injury: I. Smooth muscle growth in the absence of endothelium. **Lab Invest 49**: 327–333, 1983
4. Gange RW, Jaenicke KF, Anderson RR, et al: Effect of preirradiation tissue target temperature upon selective vascular damage induced by 577-nm tunable dye laser pulses. **Microvasc Res 28**:125–130, 1984
5. Garden JM, Polla LL, Tan OT: The treatment of port-wine stains by the pulsed-dye laser. Analysis of pulse duration and long-term therapy. **Arch Dermatol 124**: 889–896, 1988
6. Garden JM, Tan OT, Kerschmann R, et al: Effect of dye laser pulse duration on selective cutaneous vascular injury. **J Invest Dermatol 87**:653–657, 1986
7. Gregory KW, Berdus BO, Grandaw PC, et al: Pulsed laser-induced vasodilation and vasospasm. **Circulation 78 (Suppl II)**:295, 1988 (Abstract)
8. Gregory KW, Guerrero JL, Girsky M, et al: Coronary artery laser thrombolysis in acute canine myocardial infarction. **Circulation 80 (Suppl II)**:344, 1989 (Abstract)
9. Higashida RT, Halbach VV, Cahan LD, et al: Transluminal angioplasty for treatment of intracranial arterial vasospasm. **J Neurosurg 71**:648–653, 1989
10. Kuwayama A, Zervas NT, Shintani A, et al: Papaverine hydrochloride and experimental hemorrhagic cerebral arterial spasm. **Stroke 3**:27–33, 1972
11. Minick CR, Stemerman MB, Insull W Jr: Effect of regenerated endothelium on lipid accumulation in the arterial wall. **Proc Natl Acad Sci USA 74**:1724–1728, 1977
12. Newell DW, Eskridge JM, Mayberg MR, et al: Angioplasty for the treatment of symptomatic vasospasm following subarachnoid hemorrhage. **J Neurosurg 71**: 654–660, 1989
13. Prince MR, Deutsch TF, Matthews-Roth MM, et al: Preferential light absorption in atheromas *in vitro*. Implications for laser angioplasty. **J Clin Invest 78**:295–302, 1986
14. Prince MR, Deutsch TF, Shapiro AH, et al: Selective ablation of atheromas using a flashlamp-excited dye laser at 465 nm. **Proc Natl Acad Sci USA 83**:7064–7068, 1986
15. Shimokawa H, Aarhus LL, Vanhoutte PM: Porcine coronary arteries with regenerated endothelium have a reduced endothelium-dependent responsiveness to aggregating platelets and serotonin. **Circ Res 61**:256–270, 1987
16. Teramura A, Macfarlane R, Owen CJ, et al: Application of the 1-μsec pulsed-dye laser to the treatment of experimental cerebral vasospasm. **J Neurosurg 75**:271–276, 1991
17. Varsos VG, Liszczak TM, Han DH, et al: Delayed cerebral vasospasm is not reversible by aminophylline, nifedipine, or papaverine in a "two-hemorrhage" canine model. **J Neurosurg 58**:11–17, 1983
18. Watson G, Murray S, Dretler SP, et al: The pulsed-dye laser for fragmenting urinary calculi. **J Urol 138**: 195–198, 1987
19. Weidinger FF, McLenachan JM, Cybulsky MI, et al: Persistent dysfunction of regenerated endothelium after balloon angioplasty of rabbit iliac artery. **Circulation 81**: 1667–1679, 1990
20. Zubkov YN, Nikiforov BM, Shustin VA: Balloon catheter technique for dilatation of constricted cerebral arteries after aneurysmal SAH. **Acta Neurochir 70**:65–79, 1984

Manuscript received February 4, 1991.

This study was supported by National Institutes of Health Grant HL22573, a gift from the Pappas Fund for Neurosurgical Research to Dr. Zervas, and SDIO Contract N00014-86-K-00116 to the Wellman Laboratories of Photomedicine.

Mr. Macfarlane was supported by East Anglian Regional Health Authority.

The 1991 Bayer Neurosurgery Award was presented to Mr. Macfarlane for this work.

Address for Mr. Macfarlane: Department of Neurological Surgery, Addenbrooke's Hospital, Cambridge, England.

Address reprint requests to: Nicholas T. Zervas, M.D., Neurosurgical Service, Massachusetts General Hospital, Boston, Massachusetts 02114.